DESIGN AND APPLICATIONS FOR QUANTUM-ONION-MULTICODE NANOSPHERES AND OTHER LUMINESCENT SEMICONDUCTOR-DERIVED NANOCOMPOSITES

Iván Castelló Serrano

Dipòsit Legal: T.1025-2013

Ph. D. Thesis

Design and applications for Quantum-Onion-Multicode nanospheres and other luminescent semiconductor-derived nanocomposites

Iván Castelló Serrano

Supervised by Dr. Emilio Palomares Gil

(Institut Català d'Investigació Química- Universitat Rovira i Virgili)

Tarragona, June 2013

UNIVERSITAT ROVIRA I VIRGILI

UNIVERSITAT ROVIRA I VIRGILI
DESIGN AND APPLICATIONS FOR QUANTUM-ONION-MULTICODE NANOSPHERES AND OTHER LUMINESCENT SEMICONDUCTOR-DERIVED NANOCOMPOSITES
Iván Castelló Serrano
Dipòsit Legal: T.1025-2013

UNIVERSITAT ROVIRA I VIRGILI
DESIGN AND APPLICATIONS FOR QUANTUM-ONION-MULTICODE NANOSPHERES AND OTHER LUMINESCENT SEMICONDUCTOR-DERIVED NANOCOMPOSITES
Iván Castelló Serrano
Dipòsit Legal: T.1025-2013

UNIVERSITAT ROVIRA I VIRGILI
DESIGN AND APPLICATIONS FOR QUANTUM-ONION-MULTICODE NANOSPHERES AND OTHER LUMINESCENT SEMICONDUCTOR-DERIVED NANOCOMPOSITES
Iván Castelló Serrano
Dipòsit Legal: T.1025-2013

Emilio Palomares Gil, Group Leader at he Institute of Chemical Research of Catalonia (ICIQ) in Tarragona, and Research Professor of the Catalan Institution for Research and Advanced Studies (ICREA) in Barcelona

CERTIFY:

That the present research study, entitled "Design and applications for quantum-onion-multicode nanospheres and other luminescent semiconductor-derived nanocomposites", presented by Iván Castelló Serrano for the award of the degree of Doctor, has been carried out under my supervisión in ICIQ.

Tarragona, June 2013

Prof. Dr. Emilio Palomares Gil

ICIQ
Institut Català d'Investigació Química

UNIVERSITAT ROVIRA I VIRGILI
DEPARTAMENT DE QUIMICA ANALITICA I QUIMICA ORGANICA

UNIVERSITAT ROVIRA I VIRGILI
DESIGN AND APPLICATIONS FOR QUANTUM-ONION-MULTICODE NANOSPHERES AND OTHER LUMINESCENT SEMICONDUCTOR-DERIVED NANOCOMPOSITES
Iván Castelló Serrano
Dipòsit Legal: T.1025-2013

UNIVERSITAT ROVIRA I VIRGILI
DESIGN AND APPLICATIONS FOR QUANTUM-ONION-MULTICODE NANOSPHERES AND OTHER LUMINESCENT SEMICONDUCTOR-DERIVED NANOCOMPOSITES
Iván Castelló Serrano
Dipòsit Legal: T.1025-2013

"The more we learn, the less we know for sure"
Ted Sheridan

UNIVERSITAT ROVIRA I VIRGILI
DESIGN AND APPLICATIONS FOR QUANTUM-ONION-MULTICODE NANOSPHERES AND OTHER LUMINESCENT SEMICONDUCTOR-DERIVED NANOCOMPOSITES
Iván Castelló Serrano
Dipòsit Legal: T.1025-2013

UNIVERSITAT ROVIRA I VIRGILI
DESIGN AND APPLICATIONS FOR QUANTUM-ONION-MULTICODE NANOSPHERES AND OTHER LUMINESCENT SEMICONDUCTOR-DERIVED NANOCOMPOSITES
Iván Castelló Serrano
Dipòsit Legal: T.1025-2013

TABLE OF CONTENTS

UNIVERSITAT ROVIRA I VIRGILI
DESIGN AND APPLICATIONS FOR QUANTUM-ONION-MULTICODE NANOSPHERES AND OTHER LUMINESCENT SEMICONDUCTOR-DERIVED NANOCOMPOSITES
Iván Castelló Serrano
Dipòsit Legal: T.1025-2013

Chapter 1:

General Introduction

The number of nanomaterials available now is vast despite the fact that, just 15 years ago, the chemistry of nanomaterials was an emerging area. One of the key nanomaterials is semiconductor quantum dots: luminescent solid-state structures in a size regime between large clusters and bulk solids, with optical properties that are desirable in a range of disciplines, from photophysics to biomedicine.

TABLE OF CONTENTS

Quantum Dots

Quantum Dots (QDs) are quasi-zero dimension aggregates of atoms - from hundreds to tens of thousands that behave as one- of semiconductor materials that produce a crystalline matrix (nanocrystal) whose size is smaller than the exciton Bohr radius. This three-dimensional quantum confinement confers atomic-like discrete energy spectra that is strongly size dependent.[1]

A natural length scale of electronic excitations in bulk semiconductors is given by the Bohr exciton radius **(**rBohr**),** which is determined by the strength of the electron**-**hole **(**e **-** h**)** Coulomb interaction, which is also called an exciton**.** In QDs, where sizes are comparable to or smaller than the Bohr radius, the dimensions of the nanoparticle itself defines the spatial extent of the e **-** h pair state **(**but not the strength of e **-** h Coulomb coupling**)**, and hence the size of the spatial confinement of electronic wave**-**functions, which is known as "quantum confinement"**.** As the quantum dot size is reduced, the electronic excitations shift to higher energy, and the oscillator strength is concentrated within just a few transitions.[2, 3]

Two peculiar characteristics of semiconductors influence the way in which we think of an ideal semiconductor cluster (QDs). First, it is important to realize that in any material, substantial variation of fundamental electrical and optical properties with reduced size will be observed when the electronic energy level spacing exceeds the temperature. In semiconductors, this transition occurs for a given temperature at a relatively large size compared to metals, insulators, or molecular crystals. This difference can be understood by considering that the bands of a solid are centered about atomic energy levels, with the width of the band related to the strength of the nearest neighbor interactions. In the case of van der Waals or molecular crystals, the nearest neighbor interactions are weak, the bands of the solid are very

narrow, and consequently, not much size variation in optical or electrical properties is expected or observed in the nanocrystal regime. As cluster size increases, the center of a band develops first and the edges last. Thus, in metals, where the Fermi level, which is the hypothetical level of potential energy for an electron inside a crystalline solid, lies in the center of a band, the relevant energy level spacing is small, and at temperatures above a few Kelvin, the electrical and optical properties resemble those of a continuum, even at relatively small sizes (tens or hundreds of atoms).[4, 5] In semiconductors, however, the Fermi levels lies between two bands, such that the edges of the bands dominate the low-energy optical and electrical behavior. Therefore, optical excitations across the gap depend strongly on size for clusters as large as 10.000 atoms. Electrical transport also depends strongly on size, mainly because of the large variation in energy required to add or remove charges on a nanocrystal. As a consequence, many useful size-dependent phenomena are observed in clusters so large that they possess an identifiable interior, structurally identical to the corresponding bulk solid, with a substantial fraction of the total number of atoms in the surface. Clusters of this size are usually called nanocrystals.

A second important characteristic of semiconductor concerns the influence of the surface on optical and electrical properties, and the need to embed semiconductors clusters in a passivating medium. At the surface of a pure tetrahedral inorganic semiconductor, substantial reconstructions in the atomic position occur, invariably leading to energy levels within the energetically forbidden gap of the bulk solid. These surface states trap electrons or holes and degrade the electrical and optical properties of the material. Passivation is the chemical process by which these surface atoms are bonded to another material of a much larger band gap, eliminating all of the energy levels inside of the gap. The ideal termination naturally removes the structural reconstructions, leaving no strain, and simply produces an atomically abrupt jump in the

chemical potential for electrons or holes at the interface. This potential confines electrons or holes inside the cluster.

By using this effect, it is possible to continuously tune the quantum dots energy gap **(**Eg**)**, and so, the optical properties by simply changing the nanocrystal dimensions,[6] as shown in Figure 1A. The change in optical properties as a function of size is one of the most striking properties of semiconductor nanocrystals**.** The shifts in absorption onset in colloidal prepared II **-** VI nanocrystals, such as CdS and CdSe, or CdTe can be a large fraction of the band gap and can result in tuning across a major range of the visible spectrum.[7]

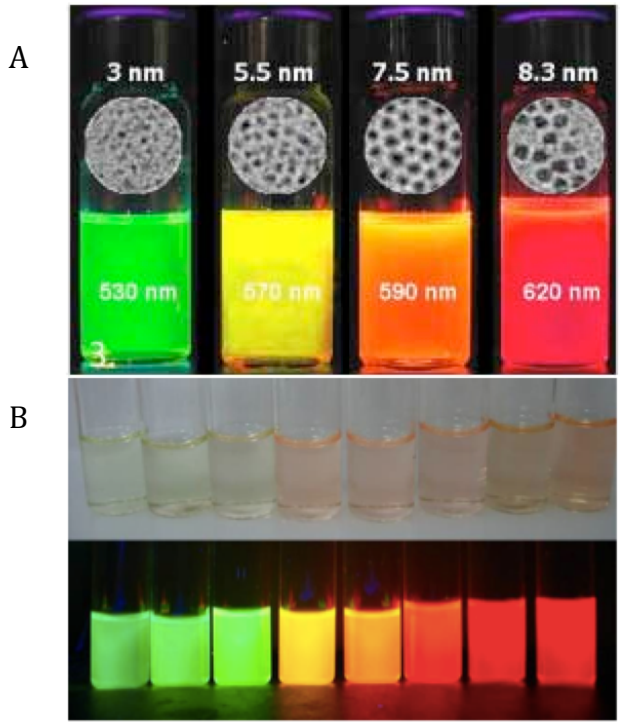

Figure 1. Size-dependent optical properties of QDs (A) and Digital picture of colloidal CdSe QDs prepared at ICIQ with different size under normal light (B, top) and UV light (B, bottom).

In addition to the tunable energy gap, another distinct feature of the quantum dot regime is the development of discrete, well-separated

energy states that replace the continuous energy bands of a bulk semiconductor material.

An important consequence of the strong confinement of the electronic states in quantum dots is a strong enhancement of Coulomb interactions. Not only the exciton binding energy, which provides a measure of the e - h interaction strength, but also the bi-exciton binding energy, which is a measure of the strength of the exciton - exciton interaction. In bulk semiconductors, these energies are inversely proportional to the natural exciton and bi-exciton radius.

In contrast, in semiconductor nanocrystals, the Coulomb interaction energies become size dependent and for spherical nanoparticles approximately as R-1 (R is the quantum dot radius), which leads to a rapid increase of these energies (up to more than 100 meV for exciton) with decreasing nanocrystal size.

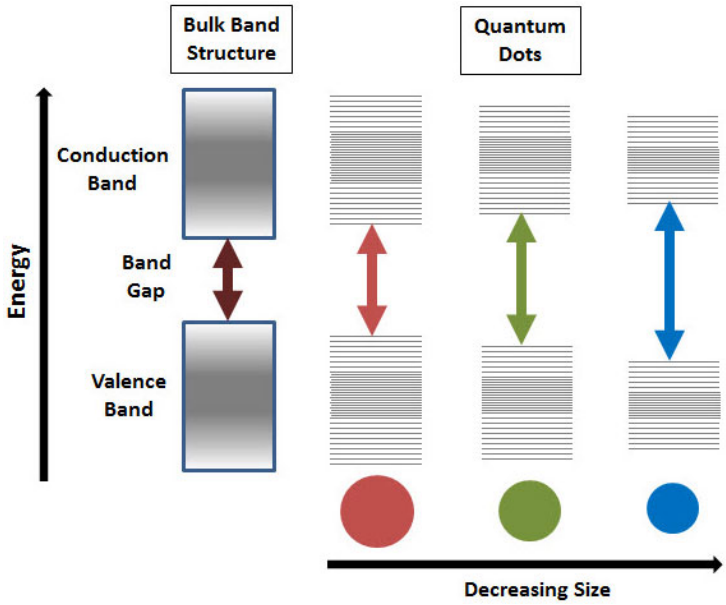

Figure 2. Splitting of energy levels in quantum dots due to the quantum confinement effect; semiconductor band gap increases with decrease in size of the nanocrystal.

Composition, size and shape of this matrix determine their physical characteristics. The properties of nanocrystals vary according to their size, which ranges generally from 1 to 10 nm in diameter;[8] as size is reduced, the electronic excitations shift to higher energy and the oscillator strength is concentrated into just a few transitions, as shown in Figure 2. These basic physical phenomena of quantum confinement arise as a result of changes in the density of electronic states.

Optical properties

Absorption

Absorption of a photon by the nanocrystals occurs if the photon energy exceeds the QD energy gap. Due to quantum confinement, decreasing the particle size results in a blue-shifted absorption onset. A relatively sharp absorption feature near the absorption onset corresponds to the first excitonic peak, which can be correlated to the lowest excited state, as shown in Figure 3. Because of its position depends on the band gap and, consequently, on the particle size, its form and width is strongly influenced by the size distribution, as well as the shape and stoichiometry of the nanocrystals. Therefore, poly-disperse samples typically exhibit only a shoulder in the absorption spectrum at the position of the excitonic transition. Less pronounced absorption features in the shorter wavelength range corresponds to excited states of higher energy. It has been observed that the larger the number of such spectral features and the more distinctly they are resolved in the absorption spectrum, the smaller is the size dispersion of the samples.[3, 9] For non-spherical nanocrystals, the excitons in nanorods and in the arms of branched nanocrystals are confined mostly along the diameter since the length often exceeds the exciton radius by several times. In all cases, quantum confinement can enhance the oscillator strength for absorption.

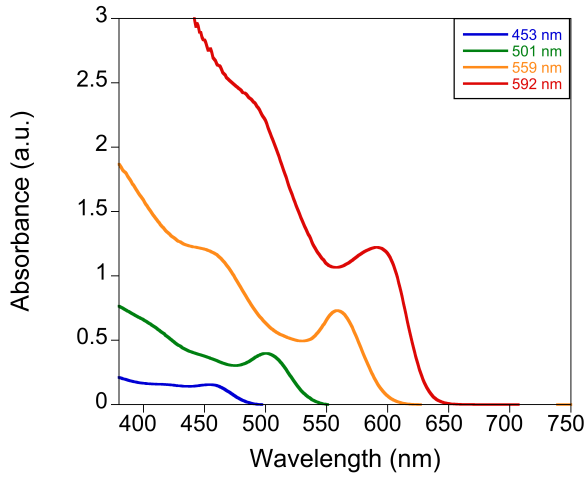

Figure 3. UV-vis absorption spectra of colloidal CdSe QDs prepared at ICIQ. The legend corresponds to the wavelength of the last excitonic peak.

Quantum confinement not only produces size-dependent band gap of nanocrystals, but also size-dependent extinction coefficient (ε), which indicates how much light a material absorbs at a certain wavelength, per mass unit or molar concentration. It is an intrinsic property of the species and can be calculated via the Lambert-Beer law:

$A = \varepsilon \cdot l \cdot c$

Where A is the absorbance of the first exciton absorption peak for a given sample. C is the molar concentration (mol/L) of the nanocrystals of the same sample. L is the path length (cm) of the radiation beam used for recording the absorption spectrum.

Peng et al.[10] found empirical fitting functions of extinction coefficient for several nanocrystals (CdE, E= Te, Se, S).

For CdTe: $\varepsilon = 3450 \cdot \Delta E \cdot (D)^{2.4}$

For CdSe: $\varepsilon = 1600 \cdot \Delta E \cdot (D)^{3}$

For CdS : $\varepsilon = 5500 \cdot \Delta E \cdot (D)^{2.5}$

Where ΔE is the transition energy corresponding to the first excitonic peak in eV, and D is the diameter of the QDs, which can be calculated by the following formulas:

CdTe: $D = (9.8127 \cdot 10^{-7}) \lambda^3 - (1.7147 \cdot 10^{-3}) \lambda^2 + (1.0064) \lambda - (194.84)$

CdSe: $D = (1.6122 \cdot 10^{-9}) \lambda^4 - (2.6575 \cdot 10^{-6}) \lambda^3 + (1.6242 \cdot 10^{-3}) \lambda^2 (0.4277) \lambda + (41.57)$

CdS: $D = (-6.6521 \cdot 10^{-8}) \lambda^3 + (1.9557 \cdot 10^{-4}) \lambda^2 - (9.2352 \cdot 10^{-2}) \lambda + (13.29)$

In the above equations, D (nm) is the size of a given nanocrystal sample, and λ (nm) is the wavelength of the first excitonic absorption peak of the corresponding sample.

The extinction coefficient was found to be independent of the temperature, the photoluminescence quantum yield of the nanocrystals, the solvents, the nature of the capping groups and the synthesis methods.[10]

Photoluminescence

Photoluminescence is a process in which a material absorbs photons (electromagnetic radiation) and then radiates photons at lower energy. There are two forms of photoluminescence: a) fluorescence, in which the emitted photons are of lower energy (red-shifted) than those absorbed, and b) phosphorescence, in which energy from absorbed photons undergoes intersystem crossing into a state of higher spin multiplicity (usually triplet state) where returning by transition is quantum mechanically forbidden, resulting in a slower process of radiative transition return to the singlet state.

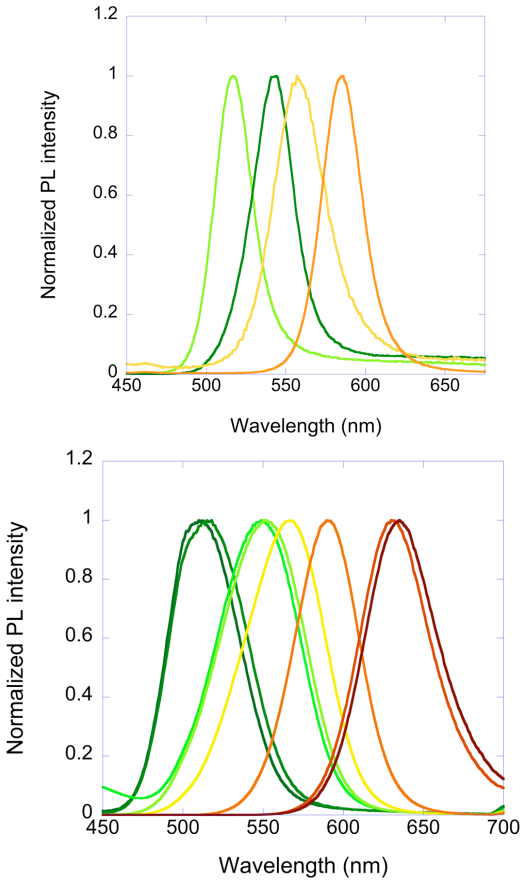

Figure 4. Emission spectra of colloidal CdSe (top) and CdTe (bottom) QDs prepared at ICIQ.

The novel optical property of QDs arises from the so-called “quantum confinement” effect of the semiconductor materials. This refers to the size- and composition-dependence of the semiconductor band gap energy, as shown in Figure 2. For nanocrystals smaller than the so-called Bohr excitation radius (a few nanometers), energy levels are quantized, with values directly related to the size of the nanoparticle. This dependence of light emission on the particle size allows the development of new fluorescence emitters with precisely tuned emission wavelengths. For example, the semiconductor cadmium selenide (CdSe) has a bulk bandgap of 1.7 eV (corresponding to 730

nm light emission). QDs of this material can be tuned to emit between 450–650 nm (Figure 4-top) by changing the nanocrystal diameter from 2 to 7 nm. The composition of the material may also be used as a parameter to alter the band gap of a semiconductor. Materials such as cadmium telluride and indium phosphide potentially allow emission in the far red (up to aprox. 750 nm) (Figure 4-bottom), and cadmium sulfide and zinc selenide give access to the ultraviolet.[11] QDs with a diameter of 5 nm can be tuned to emit between 610–800 nm by changing the composition of the alloy $CdSe_xTe_{1-x}$.[12] This property allows the production of virtually "unlimited" number of fluorophores using the same material, as shown in Figure 4.

The classic and most commonly used QDs consist of a CdSe core and a shell layer made of ZnS or CdS. Fluorescent properties are determined by the core materials and the shell layer removes surface defects and prevent non-radiative decay, leading to a significant improvement in the particle stability and fluorescent quantum yields (QY).

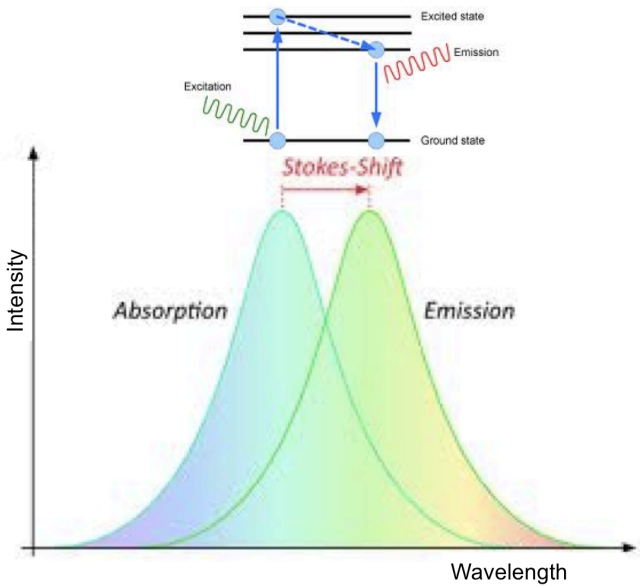

Figure 5. Scheme demonstrating the concept of Stokes-shift.

The capping ligands can also affect the surface properties creating emissive deep traps sites, which quench the emission.[13]

When a molecule or atom absorbs a photon, it gains energy and enters an excited state. One way for the system to relax is to emit a photon, thus losing its energy (another method is the loss by heat energy). When the emitted photon has less energy than the absorbed one, this energy difference is called Stokes shift (Figure 5). In the case of QDs, this phenomenon corresponds to the difference between the last excitonic peak and the emission peak. In a colloidal quantum dot photoluminiscence spectrum, the maximum of the emission peak are red-shifted by ca. 10 - 20 nm as compared to the first excitonic peak in the absorption spectrum.

Photoluminiscence decay dynamics of colloidal quantum dots differ from those of organic dyes in two important ways. On the one hand, extremely long (tens of nanoseconds at room temperature to microseconds at low temperature) lifetimes are observed; on the other hand, the decays exhibit multiexponential dynamics.

The explanation for the origin of multiexponential emission decay of nanocrystal semiconductors in solution has been studied in detail and ascribed to the trapping sites within the nanocrystals. These surface defects give rise to trap states that lie within the bandgap, and are responsible for these characteristic emission dynamics.[14]

The decay curves can be fitted to a biexponential model described by:

$F(t)= A+B_1\exp(-t/\pi_1)+B_2\exp(-t/\pi_2)$

Where π_1 and π_2 represent the time constants and B_1 and B_2 represent the amplitudes of the components, respectively.

The average lifetime π is calculated by the expression[15]:

$\pi=(B_1\pi^2_{1+} B_2\pi^2_2)/ (B_1\pi_{1+} B_2\pi_2)$

The fast component of the PL decay in QDs can be associated with the geminative exciton recombination[16] and the slow component is considered to come from the surface-related emission of QDs, as

shown in Figure 6.

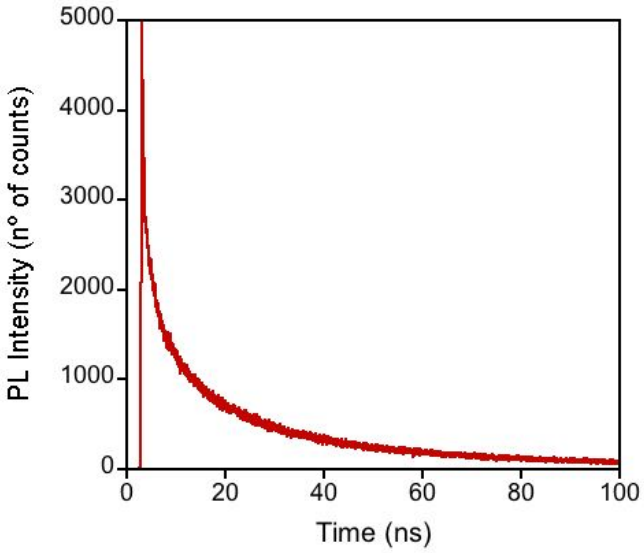

Figure 6. Emission lifetime decay of colloidal CdSe QDs prepared at ICIQ.

Quantum Yield and blinking

Quantum Yield (QY) in fluorescence is defined as the ratio between the number of photons emitted to the number of photons absorbed. As a consequence of the QDs "blinking phenomena", the QY is not close to the theoretical value of 1 since a certain number of nanocrystals are not emitting at the same time as a consequence of charge transfer. Therefore, they are in "off" state. Transitions from "on" to "off" state of the QDs occur by photo-ionisation, which implies catching a charge carrier in the surrounding media. The mechanisms to return to the "on" state are either recapturing the localized charge carrier into the core or capture an opposite charge carrier from traps in the proximity. A reorganization of charge distribution around the nanocrystal can also happen.

Additionally, the QY can be reduced as a result of the quenching process due to surface trap states. These limiting factors are closely related to the quality of the nanocrystal surface and they can be

minimized by passivation/exchange ligands. For instance, passivation can be accomplished by exchanging the capping ligand by molecules with amine functional groups or by growing hetero-epitaxially and organic coating shell around the nanocrystal core. The latter not only improves the QY (reducing the number of surface swinging bonds, which can act as trap states), but also the photo-oxidation resistance. The shell significantly improves the intensity of emission, QY and stability against photo-bleaching, and corresponds to a small red-shift of the last excitonic peak in the UV-vis absorption and photoluminescent peak in the emission spectra (5-10 nm).

Quantum Dots *versus* Organic Dyes

Compared with organic dyes and fluorescent proteins, QDs have several advantages and unique applications[17]. QDs are able to absorb 10–50 times more photons than organic dyes at the same excitation photon flux (that is, the number of incident photons per unit area), leading to a significant improvement in the probe brightness; making them brighter probes under photon-limited *in vivo* conditions (where light is severely attenuated by scattering and absorption). In theory, the emission lifetimes for single QDs are 5–10 times slower than those of single organic dyes because of their longer excited state lifetimes (20–50 ns). In practice, however, fluorescence imaging usually operates under absorption-limited conditions, in which the rate of absorption is the main limiting factor of fluorescence emission (versus the emission rate of the fluorophore). As a result, individual QDs have been found to be 10– 20 times brighter than organic dyes[18]. Secondly, QDs are several thousand times more resistant against photobleaching than organic dyes and are thus well suited for continuous tracking studies over a long period of time (Figure 7). In addition, the longer excited state lifetimes of QDs can be used to separate the QD fluorescence from background fluorescence, in a technique known as time-domain imaging;[19] since QDs emit light slowly enough that most of the

background autofluorescence emission is over by the time when QD emission occurs. Thirdly, the large Stokes shifts of QDs (measured by the distance between the excitation and emission peaks) can be used to further improve the detection sensitivity. The Stokes shifts of semiconductor QDs can be as large as 300–400 nm, depending on the wavelength of the excitation light. Organic dye signals with a small Stokes shift are often buried by strong tissue autofluorescence, whereas QD signals with a large Stokes shift are clearly detectable above the background. A further advantage of QDs is that multicolor QD probes can be used to image and track multiple molecular targets simultaneously. This feature is very desirable because most complex human diseases such as cancer and atherosclerosis involve a number of genes and proteins.

Tracking a panel of molecular markers at the same time will lead to better understanding, classifying and differentiating complex human diseases than a single biomarker each time. Multiple-parameter imaging, however, represents a significant challenge for magnetic resonance imaging, positron emission tomography, and computed X-ray tomography. By contrast, fluorescence optical imaging provides both signal intensity and wavelength information, and multiple wavelengths or colors can be resolved and imaged simultaneously (color imaging). In this regard, QD probes are particularly attractive, because their broad absorption profiles allow simultaneous excitation of multiple colors and their emission wavelengths can be continuously tuned by varying particle size and chemical composition. For organ and vascular imaging in which micrometer-sized particles could be used, optically encoded beads (polymer beads embedded with multicolor QDs at controlled ratios) could allow multiplexed molecular profiling in vivo at high sensitivities.[20, 21]

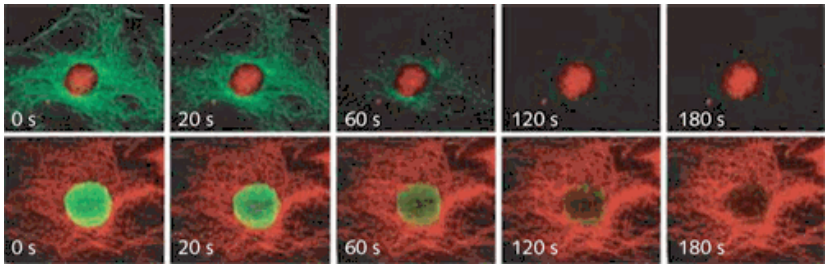

Figure 7. Experimental results show drastically reduced photobleaching in cell imaging with quantum-dot (QD) labels (red) compared to organic dye molecules (green). Images shown are complementary; the nucleus is labeled with QD 630-steptavidin and the periphery labeled with AlexaFluor 488 in the top panel, whereas the inverse labeling scheme is used in the bottom panel. ***(Image courtesy of X.Y. Wu, Quantum Dot Corp.)***

Synthesis of Quantum Dots

Luminescent solid-state structures in a size regime between large clusters and bulk solids, with optical properties that can be tuned with particle size, (or in some cases, the addition of a further shell) and a judicious choice of semiconducting system are now available because this has been an emerging area in the last 15 years.

Development of processing chemistries has resulted in robust materials and advances in synthetic techniques have allowed almost all the families of semiconducting systems to be explored, with a wide range of synthetic pathways being developed, the majority of the most successful ones being based on organometallic or organometallic/inorganic hybrid precursor thermolysis routes.

The capping ligand is a key parameter when preparing nanomaterials by organometallic precursors. The capping agent can be thought of primarily as a stabilizing agent, providing colloidal stability, stopping uncontrolled growth and agglomeration. The passivating ligands are also intimately linked to the nucleation process, tuning the availability of reagents and are important when considering the growth process. The ligands control the rate of growth, particle morphology, reaction pathways and the particle size distribution. At a deeper level, the

electronic structure of the passivating ligands contributes to the overall electronic and optical profile of the nanoparticles, blocking surface states and hence affecting emission yields.

How surfactants interact with nanoparticles is a key concept and is surprisingly complex. To fully understand the role of ligands in semiconducting nanoparticles, we have to examine the evolution of the capping agents. Traditionally, arrested precipitation was used as a method of preparing colloidal QDs.[22, 23] Then a micelle route using bis-2-ethylhexylsulfuccinate (AOT) as a capping agent was reported,[24] including sodium hexametaphosphonate in the reaction, which was further developed using sodium polyphosphate as stabilizer.[25] This use of a well-defined stabilizer became important, as the nanoparticles were then redispersable in water, allowing processing and purification. This can be seen as one of the first reports highlighting a deliberate attempt at including a capping agent in the synthesis of colloidal QDs.

The micelle route was extended producing the first pseudo-organometallic route to nanomaterials,[26] where a microemulsion was prepared and an aqueous solution of cadmium precursor was added and the resulting powders were soluble in hydrocarbons after processing. Addition of cadmium stock solution followed by phenyl(trimethylsilyl) selenide resulted in the first example of monomer passivation of a nanoparticle surface and the particles could be isolated by centrifugation. The phenyl-passivated clusters were soluble in pyridine and insoluble in petroleum ether, becoming one of the first examples of solvent/non-solvent pair, important for QDs purification and size selective precipitation.

Annealing of small particles in a mixture of phosphine oxide capping ligands resulted in further particle growth, and was the basis for further studies, notably in the seminal paper by Murray in 1993,[27] who described the first oganometallic reaction using chain phosphine oxides as capping agents and organometallic precursors originally highlighted by Steigerwald[26] in high temperature inert-atmosphere solution

chemistry. This resulted in trioctylphosphine oxide (TOPO) becoming the standard capping agent for organometallic type synthetic routes towards QDs and also made Murray to be considered the father of the hot-injection procedure.

TOPO

The advantages of using TOPO as surfactant, solvent and capping ligand include the high boiling point, allowing reactions to proceed at 350ºC facilitating high temperature precursor decomposition and nanoparticle annealing unavailable to aqueous based routes, and the compatibility with organic solvents allows a completely inert reaction environment and hence the use of air sensitive precursors. The long alkyl chains impart solubility to the QDs and allow the material to be manipulated like a common organic reagent despite the solvents used must posses a significantly high dielectric constant to overcome the van der Waals attraction between the colloidal particles. The steric properties of the alkyl groups also affect particle growth, controlling shape and morphology.[27, 28] Besides, the ligand blocks the electronic surface trap sites that are normally responsible for broad emission and non-radiative charge carrier recombination, allowing clean, near band edge luminescence.[29] The surfactant additionally plays a key role in the carrier relaxation between excited intraband states, where soft ligands are responsible for slow relaxation rates.[30] In the case of TOPO-capped CdSe, the TOPO binds to the surface of cadmium sites through the lone pairs of electrons on the phosphine oxide moiety, forming dative bonds.[31, 32] It is reported, however, that TOPO does not remain at cadmium sites and can shift to selenium sites under illumination, forming TOPO-Se complexes that are intimately linked to the photobrightening process where the emission quantum yield of the nanoparticles temporarily increases after synthesis.[33] The interaction of surfactant and the nanoparticle surface is a key parameter, as both optical and structural properties are dominated by the interaction

between the interfaces. This was confirmed by a set of ligand transfer experiments, which raised the question of whether dative bonds are enough to stabilize a particle.[34]

Other impurities in TOPO have been identified and examined which play a role in the reproducible growth of certain anisotropic structures.[35] QDs of CdSe with a wurtzite crystalline core are inherently anisotropic and were the focus of the seminal work into anisotropic QDs structures, using dimethylcadmium and trialkylphosphine selenide as precursors.

Alivisatos *et al*. reported the use of pure TOPO was unsuitable as a surfactant for the reproducible synthesis of anisotropic QDs, with growth proceeding too quickly at high precursor concentrations yielding insoluble materials.[36] The use of technical grade TOPO was found to be more suitable, due to the large amount of impurities that strongly coordinated to the precursor ions and retarded the growth. Slow growth in technical grade TOPO resulted in spherical particles, while a fast growth rate resulted in increased growth along the unique *c*-axis. A massive increase in the monomer concentration (kinetic overdrive) also resulted in the formation of elongated nanorods along the *c*-axis, due to the differing growth rates of differing crystal faces. Impurities present in technical grade TOPO included hexyl-phosphonic acid (HPA), which is used as an additive to pure TOPO to controllably regulate the growth of nanorods. The range of shapes observed using high concentrations of HPA was attributed to the isolation of particles in different stages of growth. The particle morphology was tracked from rods to pencils and "pine trees".

TOP

Tri-n-octylphosphine (TOP) is also routinely used as both surfactant and selenium-delivery solvent when in the form of a TOP-Se solution during the preparation of TOPO capped CdSe nanocrystals. TOP is generally thought to coordinate to the surface of the particles along side TOPO (via the selenium sites), supplying a more complete passivation.[31] TOP-

Se has also been shown to bind to surface cadmium sites; the role of TOP in the electronic structure of CdSe QDs is not clear. The deep trap emission observed in CdSe nanoparticles can be attributed to the complex of TOP with the surface selenium sites, leading to a lower energy chemical state.[37] Although, another report has shown that deep trap emission occurs in both TOP passivated and TOP-free nanoparticles and that the lower energy emission states are surface related.[38] The presence of TOP on selenium rich surfaces has also been shown to be the source of enhanced photoluminescence[39] and contributing to the hexagonal crystal character of the CdSe nanoparticles.

TOP has also been found to be a phosphorus source in the synthesis of other materials such as FeP,[40] MnP or NiP.[41] But why TOP acts as a reagent in these reactions and as a simple surfactant in the synthesis of most semiconductor QDs is already unknown.

An examination into synthesis mechanisms of cadmium and lead chalcogenide QDs explores the essential role of the surfactant and highlights that the passivating ligands, TOP in particular, react with the precursor reagents, providing key steps in the nanoparticle synthesis.[42, 43] In brief, the soft acid cationic precursor coordinates to the chalcogenide ion. The phosphine then undergoes nucleophilic attack from either the carboxylic acid/phosphonic acid counter ion or excess TOP in solution, cleaving the P=Se bond. Steckel[41] states the counter ion is from the metal (II) precursor, therefore negating the need for a surfactant interaction. The reaction should therefore proceed from the metal salt and TOP-Se alone, although it is clear from control experiments by Liu *et al.*[43] that the presence of oleic acid or n-octadecylphophinic acid in solution induces P=Se cleavage. Liu[43] therefore states that the surfactants such as oleic acid or n-octadecyl phosphinic acid are responsible for that. Steckel[41] also suggested another competing mechanism based on experimental observations, in which the surfactant (TOP) reduced the metal precursor from M^{2+} to M^{0}, which then reacted with trialkylphosphine selenide, eliminating the

phosphine, which reacted further to provide the phosphine oxide and metal counter ion anhydride. This again highlights the importance of the surfactant as a reagent and not just a simple passivating ligand.

Amines

TOPO and TOP, however, are not ideal solvents; heating TOPO above 300ºC is known to induce decomposition,[44] the product of which is not identified but is known to have luminescence (albeit weakly). This decomposition product emission can in some cases be mistaken for QDs emission, especially where the parent semiconductor exhibits a low emission quantum yield.[45] Long chain amines are found to be more suitable surfactants for II-VI based QDs. Nanoparticles of CdSe prepared using long chain primary amines are generally found to have emission quantum yields around 60% without the need for an inorganic shell.[46, 47] This has been attributed to the closer packing of the ligands on the nanoparticle surface and the etching of surface defects, while amines have also seen shown to contribute to the oxygen etching process.[48] The use of amines as capping ligands on CdSe QDs has similarly been shown to result in a surface reconstruction,[49] especially a lattice contraction during growth, which may contribute to the elevated emission.[50]

It has been reported that primary amines strongly enhance the emission of CdSe QDs, because they have close to 100% coverage of the surface as compared to 30% with TOPO, while secondary and tertiary amines have negligible effect.[51] The addition of primary amine to a solution with colloidal CdSe besides provokes a blue shift in the emission, what was attributed to an electronic contribution from the amine but may moreover come from a slight reduction in particle size due to an etching process which is in agreement with also found blue shift in the absorption.[52] The addition of amides has no effect on the emission intensity due to the poor electron donating properties.

Even post-treatment of TOPO-capped CdSe QDs with primary amines

improved the emission quantum yield by 50% and, again, a blue shift in the absorption was observed, consistent with a small decrease in the particle size.

The mode of bonding is through the lone pair of electrons on the nitrogen atom, and in the case of CdSe, the amine binds to both selenium and cadmium sites.[53]

It has been suggested that the linear shape of some capping ligands allows the oxygen to reach the QDs surface, oxidizing the surface and decreasing the emission quantum yield, while capping ligands with branched structures protect the surface in a more satisfactory way.[54]

Thiols

Long chain thiols are a common surfactant and an excellent capping agent for most semiconducting and metal nanoparticles.[55, 56] Thiols are generally the surfactant for simple routes to inert metal nanoparticles that do not use organomatellic precursors, although the use of thiols in organometallic-based routes is likewise becoming popular.

Thiolated species bond to the QDs metal surface and surface sulfur atoms, although the bond is much weaker.[57] The reactivity of thiol has been used efficiently in aqueous CdTe particles where the thiol group hydrolyses, inducing a thin CdS buffer layer on the CdTe particle resulting in a wide band gap protective shell.[58]

The exposure of CdSe QDs prepared by organometallic routes to thiols is detrimental, resulting in quenching of the luminescence and reducing the stability in solution.[59] A red shift in the emission peak has also been observed upon thiol addition, attributed to an electronic contribution from the adsorbed ligands.[50]

It has been observed that at low concentrations, thiolates provide electrons for the trapping sites, while at higher concentrations, thiolates act as hole traps.[59, 60]

The role of thiols in other systems, such as the II-V, is much more beneficial. As-synthesized InP QDs capped with TOPO have low

quantum yield (below 1% at room temperature), which can be improved by treatment with octanethiol (around 30%).[61]

Carboxylic Acids

The use of carboxylic acids as capping ligands and surfactants predates the organometallic route.[62] Oleic acid is the standard carboxylic acid used as surfactant, the double bond and associated "kink" in the alkyl chain are found to be essential for imparting colloidal stability;[63] the closely related stearic acid does not stabilize magnetic colloids, but is often used in the capping of QDs.

Oleic acid was first used as a stabilizer in the organometallic route in the preparation of iron colloid,[64] but then it was used as a binding ligand in the preparation of cobalt nanoparticles and required the use of a weaker binding co-ligand to control the particle size.[65] The use of oleic acid alone inhibited particle growth.

Interestingly, oleic acid appeared to be able, in some cases, to coordinate to a nanoparticle surface through the double bond, making the nanoparticles soluble in polar rather than non-polar solvents, and allows phase transfer reaction without changing the surfactant.[66] This feature, having an interchangeable binding point, exposing either the alkyl group or the alkyl and carboxylic acid groups makes oleic acid extremely novel amongst most standard capping ligands. The formation of bilayers of oleic acid on particle surface has been reported, where the ligand has double function, *i.e.* capping the particles and phase transfer reagent, respectively. This shows that oleic acid is extremely versatile and can be used effectively with luminescent materials, and is, nowadays, almost unique in its use in both polar and non-polar solvents.[67]

The synthesis of CdTe water-soluble QDs with mercaptopropionic acid as capping ligand will be further detailed in Chapter 2.

Other alternatives

TOP and TOPO are considered toxic[68] and a search for novel solvents is often driven by the need for a phosphine free system. Peng *et al.*[69] demonstrated that non-coordinating solvents could also be used in nanoparticles synthesis, as opposed to thermolysis in TOPO where cadmium oxide and oleic acid were dissolved in octadecene. Elemental sulfur dissolved in octadecene was then injected into the reagents at elevated temperatures forming CdS nanoparticle capped with oleic acid. The delicate balance between forming too many nuclei, which resulted in the defocusing of the size distribution by Ostwald ripening, and too few nuclei, which resulted in growth that was too fast to reach the required size and distribution, was easily achieved by simply altering the concentration of the capping ligand and thus the amount of metal complex available for the reaction. Another advantage is the control over the particle size.

This work was extended to the preparation of CdSe,[38] which was achieved by dissolving the cadmium precursor (cadmium oxide) in a solution of oleic acid and octadecene. It was found that TOP was not essential for the production of high quality CdSe, although the use of octadecene/selenium instead of TOP-Se resulted in poorer nucleation, producing approximately half as many particles. The addition of a phosphonic acid in the synthesis allowed the formation of the wurzite structured crystalline form rather than the zinc blende structured, oleic acid capped CdSe.

Peng *et al.*[69] also reported a study into the preparation of CdTe particles in octadecene, using fatty acids and phosphines as capping ligands, with cadmium oxide and tellurium powder as precursors, where ligand effects were found to have significant role in the development of particle size, size distribution, morphology and crystal phase.

Surfactant Exchange

A key feature of most surfactants is the dynamic character associated with ligands bound to a nanoparticle surface. Most surfactants are interchangeable, importantly allowing the exchange of pendant functionalities or the switch from organic to aqueous phases, or *vice versa*.

The foremost benefit of surfactant exchange is the ability to prepare particles that are suitable for different environments and applications. The obvious example is the use of semiconductor nanoparticles, or QDs, in biological labeling, where particles are required to be water-soluble. Nie *et al.*[70] described the simple reaction of TOPO-capped CdSe/ZnS nanoparticles and mercaptoacetic acid in a chloroform solution, where the resulting mercaptoacetic acid capped QDs were isolated by extraction into water. The particles exhibited significantly reduced emission. The availability of the pendant carboxylic acid functional group provided a simple anchor point for further functionalities to be attached to the luminescent particle, a common starting point for the synthesis of more complex biological labels.[56, 71] In related work, mercaptoundecanoic acid capped QDs have had the terminal carboxylic acid groups cross-linked with lysine, giving a stable hydrophilic shell composed of carboxylic acid and amine functional groups available for further conjugation.[72]

Pendant carboxylic acid groups are not used exclusively; thiols with protonated amine groups have also been used to transfer TOPO capped CdTe to water.[73] An important part of bioconjugation is rendering the particle hydrophilic while maintaining the smallest possible hydrodynamic diameter.[74]

Alivisatos *et al.*[1] also reported the use of thiols in the preparation of water-soluble QDs for labeling applications, however, this work used a thiol, (3-mercaptopropyl)trimethoxysilane, as a primer ligand for a further silica shell[75, 76]. In this case, the thiol surfactant can be considered as a precursor for the final shell of SiO_2, which can be

afterwards functionalized.[77] The emission in silica-passivated particles is partially quenched.

The use of silica capped CdSe/ZnS particle was one of the pivotal nanomaterials used for bio-labelling applications although this has generally been surpassed by simplier methods. In some cases, the use of a capping ligand as a bridge is not always necessary. Direct surfactant exchange for thiolated biological reagents, such as peptides,[78] lipids,[79] neurotransmitters,[80] hormones[81] and DNA[82] has become a common and simple method for bioactivating semiconductor QDs, based on previous studies of gold nanoparticles/DNA interactions.[83, 84]

Quantum Dots@Shell

As quantum dots are very toxic due to the heavy metals they are made of and their reactivity to the environment, such as Reactive Oxidative Species (ROS). A direct way to avoid the possible toxicity of QDs is to coat them with another kind of material, biologically inert, leading to harmless core-shell nanostructures. In this sense, many materials have been employed, such as silica, synthetic polymers or biomolecules to make them water-soluble and less toxic.

Different procedures have been reported to achieve this purpose, summarized in two main groups: (i) direct infiltration of the nanoparticles into materials, or (ii) in situ growth in a layer-by-layer procedure.

Trapping of different color-emitting QDs in materials

Nie and coworkers[85] using polymeric beads first developed this procedure. Dissolving the polymeric beads (in this case polystyrene) in a mixture of chloroform/alcohol QDs solution, the inorganic nanoparticles were embedded into the spheres due to the swelling of the beads. Not only single color QDs were inserted by this method but

also different color QDs in different ratios were combined increasing the number of possible encoding labels.

Nie[85] made use of a mixture of polymeric beads, buthanol and QDs in chloroform. We tried to extrapolate this method to silica beads, but the results were not successful since chloroform does not affect silica in a swell behavior like polystyrene. In contrast, by modifying their protocol (mixing dried silica beads in water with water-soluble CdTe QDs), we were able to infiltrate the QDs into silica beads (Figure 8).

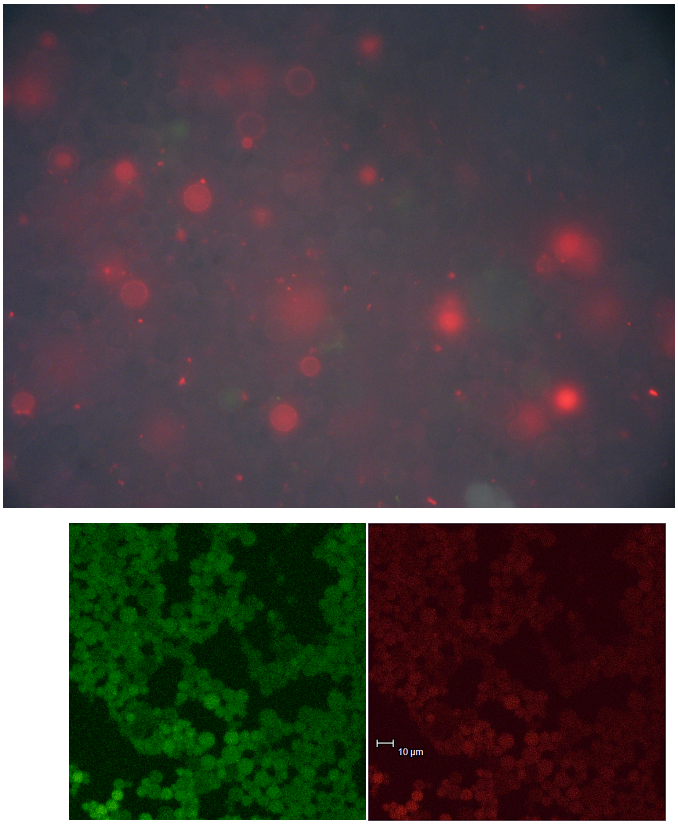

Figure 8. Real fluorescent image of silica bead embedded with green or orange/red CdTe colloidal QDs (top) and confocal images (bottom) of silica bead embedded with both green (left) and orange (right) CdTe colloidal QDs. All the samples were prepared at ICIQ.

Direct in situ encapsulation of QDs

This procedure consists of embedding the nanoparticles into spheres during the polymerization of the beads in a layer-by-layer method.

For this purpose, polymeric materials, such as polyethylene glycol (PEG), polystyrene, etc.; silica, or other materials with different properties, such as iron oxide to get magnetic behavior, have been employed. Nowadays, the principal goal of this procedure is to get hybrid nanostructures combining different properties, e.g. multifunctional nanobeads based on fluorescent material (QDs) and magnetic nanoparticles (using polymer and iron oxide).[86]

A novel procedure consisting of a stepwise encapsulation of QDs into silica multilayers was developed in our group as further explained in Chapter 2.

The similarity of size between nanomaterials provided by this procedure and typical biomolecules makes these nanostructures particularly attractive for intracellular tagging and ideal for conjugation with different functional groups, such as carboxylic, amine, or even through biomolecules like antibodies, proteins, cell-penetrating peptides, etc.

Functionalization of the spheres

Carboxylated silica beads

Vinyl-functionalized silica nanospheres were synthesized according to the literature reported method.[87] VTES, SDBS were added into 30 ml aqueous CdTe QD solution under vigorous stirring for 1 h, then aqueous ammonia solution was added, and the mixture was heated at 50 °C for 48 h. The resulting microspheres were separated by centrifugation and washed several times with deionized water.

2,2'-azobis(2-methylpropionitrile) (AIBN) and mercaptoacetic acid with a molar ratio of 1:1 (thiol:alkene) were added to a ethanol solution containing vinyl-functionalized silica microspheres. After bubbling with

N_2 at 45 °C for 30 min, the solution was heated at 80 °C for additional 24 h for complete reaction.

Besides, microbeads carboxylation was performed with few modifications because the parent material was comercial silica microbead (5-8 μm): commercial silica microbeads, triethoxtvinylsilane (VTEOS) and methanol were mixed in a flask and put in an ultrasound bath for 3 cycles of 30 min. Then the solution was filtered and the powder was dried by dry vacuum at 40ºC for 1 h.[88] A second step was done by mixing dried vinyl silica microbead in ethanol, AIBN and mercaptoacetic acid in a flask under nitrogen stirring at 45ºC for 30 min. Then nitrogen was removed and solution was heated up to 80ºC for 24 h. The product was centrifuged and washed with ethanol 3 times and stored in ethanol.[89]

Aminated silica beads

A mixture of Tergitol NP7 and cyclohexane was prepared in a flask and left to stir for 15 minutes. QDs in chloroform solution and tetraethyl orthosilicate (TEOS) were added to the previous mixture and left to stir for another 30 minutes. From this moment on the reaction was conducted in the dark. Ammonia solution was added to start the hydrolysis and left to stir for 24 hours. Then QDs in chloroform solution were added to the previous mixture and then TEOS was added to the reaction and left for 24 hours.

Next, another color QDs in chloroform solution were added to the reaction for 30 minutes and then TEOS were added to the mixtures and left for 24 hours more.

APTMS and THPM were added to the reaction to functionalize the surface of the beads with amine groups.

Acetone was added to stop the reaction and the mixture was centrifuged 20 minutes with ethanol 3 times at 4500 rpm. Then the samples were stored in PBS (phosphate buffer solution, pH=7.2).

In parallel, previously embedded CdTe@silica microbeads were mixed

with cyclohexane, APTMS and THPM and left for 24 hours at room temperature. Then, the solution was centrifuged, rinsed with ethanol and stored in PBS.

Biofunctionalization with Bovine Serum Albumin (BSA)

We functionalized the carboxylated and aminated beads with Bovine Serum Albumin (BSA) following the next procedure: functionalized silica bead of 5 microns in size stored in PBS were mixed with BSA in PBS (10 mg/mL) and left to stir for 24 hours at room temperature.

References

1. Alivisatos, A. P. Science, 1996, 271, 933.
2. Efros, A. L.; Rosen, M. Annu. Rev. Sci., 2000, 30, 475.
3. Gaponenko, S. V. Optical Properties of Semiconductor Nanocrytals, Cambridge University Press, Cambridge, 1998.
4. Cohen, M. L.; Chou, M. Y.; Knight, W. D.; de Heer, W. A. J. Phys. Chem. 1987. 91, 3141.
5. Ellert, C.; Schmidt, M.; Schmitt, C.; Reiners, T.; Haberland, H. Phys. Rev. Lett. 1995. 75, 1731.
6. Klimov, V. I. Annu. Rev. Phys. Chem., 2007, 58, 635.
7. Norris, D. J.; Sacra, A.; Murray, C. B.; Bawendi, M. G. Phys. Rev. Lett. 1994, 72, 2612.
8. Murra, C. B.; Kagan, C. R.; Bawendi, M. G. Annu Rev Mater Sci 2000, 30:545.
9. Rogach, A. L. Semiconductor Nanocrystal Quantum Dots, SpringerWienNowYork, Wien (Austria), 2008.
10. Yu, W. W.; Qu, L.; Guo, W.; Peng, X. Chem. Mater, 2003, 15, 2854.
11. Hotz, C. Z. Applications of quantum dots in biology, from methods in molecular biology, vol 303: nanobiotechnology protocols, edited by S. J. Rosenthal and D.W Wright.
12. Smith, A. M.; Gao, X.; Nie, S. Photochemistry and Photobiology, 2004, 80, 377.
13. Baker, D. R.; Kamat, P. V. Langmuir, 2010, 26, 11272.
14. Garrett, M. D.; Bowers, M. J.; McBride, J. R.; Orndorff, R. L.; Pennycook, S. J.; Rosenthal, S. J. J. Phys. Chem. C, 2008, 112, 436.
15. Zeng, Q.; J. Phys Chem C, 2008, 112, 2503.
16. Wuister, S.F. Phys. Chem. Chem. Phys. 2003, 5, 1253.
17. Leatherdale, C. A.; Woo, W.K.; Mikulec, F. V.; Bawendi, M. G. J Phys Chem B, 2002, 106, 7619.
18. Gao, X.; Cui, Y.; Levenson, R. M.; Chung, L. W.; Nie, S. Nat Biotechnol. 2004, 22, 969.

19. Dahan, M.; Laurence, T.; Pinaud, F.; Chemla, D. S.; Alivisatos, A.P.; Sauer, M.; Weiss, S. Opt Lett. 2001, 26, 825.
20. Chien, G. L.; Anselone, C. G.; Davis, R. F.; Van Winkle, D. M. Cardiovasc Res. 1995, 30, 405.
21. Han, M.; Gao, X.; Su, J. Z.; Nie, S. Nat Biotechnol, 2001, 19, 631.
22. Kalyanasundaram, K.; Borgarello, E.; Duonghong, D.; Grätzel, M. Angew. Chem. 1981, 20, 987.
23. Rossetti, R.; Brus, L. J. Phys. Chem, 1982, 86, 4470.
24. Meyer, M.; Wallberg, C.; Kurihara, K.; Fendler, J.H. J. Chem Soc Chem Comm, 1984, 90.
25. Weller, H.; Koch, U.; Gutierrez, M.; Henglein, A. Ber. Bunsen-Ges. Phys Chem, 1984, 88, 969.
26. Steigerwald, M. L.; Alivisatos, A. P.; Gibson, J. M. J. Am Chem Soc, 1988, 110, 3046.
27. Murray, C. B.; Norris, D. J.; Bawendi, M. G. J. Am Chem Soc, 1993, 115, 8706.
28. Sun, S.; Murray, C. B. J. App. Phys, 1999, 85, 4325.
29. Guyot-Sionnest, P.; Shim, M.; Matranga, C.; Hines, M. Phys Rev. B, 1999, 60, R2181.
30. Guyot-Sionnest, P.; Wehrenberg, B.; Yu, D. J. Chem. Phys, 2005, 123, 074709.
31. Becerra, L.R.; Murray, C. B.; Griffin, R. G.; Bawendi, M. G. J. Chem Phys, 1994, 100, 3297.
32. Lorenz, J. K.; Ellis, A. B. J. Am Chem Soc, 1998, 120, 10970.
33. Asami, H.; Abe, Y.; Ohtsu, T.; Kamiya, I.; Hara, M. J. Phys Chem B, 2003, 107, 12566.
34. Owen, J. S. J. Am Chem Soc, 2008, 130, 12279.
35. Wang, F.; Tang, R.; Buhro, W. E. Nano Lett, 2008, 8, 3521.
36. Peng, X. Nature, 2000, 404, 59.
37. Kalyuzhny, G.; Murray, R. W. J. Phys, Chem B, 2005, 109, 7012.
38. Jasieniak, J. J. Phys Chem B, 2005, 109, 20665.
39. Jasieniak, J. J. Am Chem Soc, 2007, 129, 2841.
40. Qian, C.; Kim, F.; Ma, L.; Tsui, F.; Yang, P.; Liu, K. J. Am Chem

Soc, 2004, 126, 1195.

41. Wang, J.; Johnston-Peck, A. C.; Tracy, J. B. Chem Mater, 2009, 21, 4462.

42. Steckel, J. S.; Yen, B. K. H.; Oertel, D. C.; Bawendi, M. G. J. Am Chem Soc, 2006, 18, 879.

43. Liu, H.; Owen, J. S.; Alivisatos, A. P. J. Am. Chem Soc, 2007, 129, 305.

44. Micic, O. I.; Sprague, J. R.; Curtis, C. J.; Jones, K. M.; Machol, J. L.; Nozik, A. J.; Giessen, H.; Fluegel, B.; Mohs, G.; Peyghambarian, J. Phis. Chem, 1995, 99, 7754.

45. Furis, M.; Sahoo, Y.; Macrae, D. J.; Manciu, F. S.; Cartwright, A. N.; Prassad, P. N. J. Phys. Chem B, 2003, 107, 11622.

46. Talapin, D. V.; Rogach, A. L.; Mekis, I; Haubold, S.; Kornowski, A.; Haase, M.; Weller, H. Colloids Surf. A, 2002, 202, 145.

47. Talapin, D.V.; Rogach, A.L.; Kornowski, A.; Haase, M.; Weller, H. Nano Lett, 2001, 1, 207.

48. Li, R. J. Am Chem Soc, 2005, 127, 2524.

49. Zhang, J. Y.; Wang, X.Y.; Xiao, M.; Qu. L.; Peng, X. Appl, Phys Lett, 2002, 81, 2076.

50. Qu, L.; Peng, X. J. Am Chem Soc, 2002, 124, 2049.

51. Bullen, C.; Mulvaney, P. Langmuir, 2006, 22, 3007.

52. Woo, PhD Thesis, MIT, 2002.

53. Punzder, A.; Williams, A. J.; Zaitseva, N.; Galli, G.; Manna, L.; Alivisatos, A. P. Nano Lett, 2004, 4, 2361.

54. Yu, W. W.; Wang, Y. A.; Peng, X. Chem. Mater, 2003, 15, 4300.

55. Rajh, T.; Micic, O. I.; Nozik, A. J. J. Phys Chem, 1993, 97, 11999.

56. Medintz,I.; Uyeda, H. T.; Goldman, E. R.; Mattoussi, H. Nat, Mater, 2005, 4, 435.

57. Pong, B. K.; Trout, B. L.; Lee, J. Y. Langmuir, 2008, 24, 5270.

58. Rogach, A. L.; Franzl, T.; Klar, T. A.; Fieldmann, J.; Gaponik, N.; Lesnyak, J.; Shavel, A.; Eychmüller, A.; Rakovich, Y. P.; Donegan, J. F. J. Phys Chem C, 2007, 111, 14628.

59. Gao, X.; Chan, W. C.; Nie. S. J. Biomed Opt, 2002, 7, 532.
60. Sharma, J.; Seo, D. K.; Yan, H. J. Am Chem Soc, 2007, 129, 6380.
61. Micic, O. I.; Sprague, J.; Lu, Z.; Nozik, J. Appl Phys Lett, 1996, 68, 3150.
62. Khalafalla, S. E.; Reimers, G. W. US Pat, 1973, 3 764 540.
63. Tadmor, R.; Rosensweig, R. E.; Frey, J.; Klein, J. Langmuir, 2000, 16, 9117.
64. Suslick, K.S.; Fang, M.; Hyeon, T. J. Am Chem Soc, 1996, 118, 11960.
65. Sun, S.; Murray, C. B. J. Appl. Phys, 1999, 85, 4325.
66. Bala, T.; Swami, A.; Prasad, B. L. V.; Sastry, M. J. Colloid Interface Sci, 2005, 283, 422.
67. Prakash, A.; Zhu, H.; Jones, C. J.; Benoit, D. N; Ellsworth, A. Z.; Bryant, E. L.; Colvin, V. L. ACS Nano, 2009, 3, 2139.
68. Hoshino, A.; Fujioka, K.; Oku, T.; Suga, M.; Sasaki, Y. F.; Ohta, T.; Yasuhara, M.; Suzuki, K.; Yamamoto, K. Nano Lett, 2004, 4, 2163.
69. Yu, W. W.; Wang, Y. A.; Peng, X. G. Chem Mater, 2003, 15, 4300.
70. Warren, C. W.; Nie, S. Science, 1998, 281, 2016.
71. Jaiswal, J. K.; Goldman, E. R.; Mattoussi, H. Simon, S. M. Nat. Methods, 2004, 1, 73.
72. Jiang, W.; Mardyani, S.; Fischer, H.; Chan, W. C. W. Chem Mater, 2006, 18, 872.
73. Wuister, S. F.; Swart, I.; van Driel, F.; Hickey, S. G.; de Mello, C. Nano Lett, 2003, 3, 503.
74. Liu, W.; Choi, H. S.; Zimmer, J. P.; Tanaka, E.; Frangioni, J. V.; Bawendi, M. J. Am Chem Soc, 2007, 129, 14530.
75. Ma, Q.; Castello, I.; Palomares, E. Chem Comm 2011, 47 (25), 7071.
76. Castello, I.; Ma, Q.; Palomares, E. J. Mater. Chem 2011, 21, 17673.
77. Gerion, D.; Pinaud, F.; Williams, S. C.; Parak, W. J.; Zanchet, D.; Weiss, S.; Alivisatos, A. P. J. Phys Chem B, 2001, 105, 8861.
78. Akerman, M. E.; Chan, W. C.; Laakkonen, P.; Bhatia, S. N.; Ruoslahti, E. Proc, Natl. Acad. Sci U.S.A. 2002, 99, 12617.

79. Murcia, M. J.; Minner, D. E. Mustata, G. M.; Ritchie, K.; Naumann, C. J. Am Chem Soc, 2008, 130, 15054.
80. Rosenthal, S. J.; Tomlinson, I.; Adkins, E. M.; Schroeter, S.; Adams, S.; Swafford, L.; McBride, J.; Wang, Y.; DeFelice, L.J.; Blakely, R. D. J. Am Chem Soc, 2002, 124, 4586.
81. Tomlinson, D.; Kippeny, T.; Swafford, L.; Siddiqui, N. H.; Rosenthal, S. J. J. Chem Res Synop, 2002, 5, 204.
82. Mitchell, G. P.; Mirkin, C. A.; Letsinger, R. L. J. Am Chem Soc, 1999, 121, 98122.
83. Alivisatos, A. P.; Johnsson, K. P.; Peng, X.; Wilson, T. E.; Loweth, C. J.; Bruchez, M. P.; Schultz, P. G. Nature, 1996, 382, 609.
84. Mirkin, C. A.; Letsinger, R. L.; Mucic, R. C.; Storhoff, J. J. Nature, 1996, 382, 607.
85. Han, M.; Gao, X.; Su, J.; Nie, S. Nature Biotechnol, 2001, 19, 631.
86. Di Corato, R.; Bigall, N.; Ragusa, A.; Dorf, D.; Genovese, A.; Marotta, R.; Manna, L.; Pellegrino, T. ACS Nano, 2011, 5 (2), 1109.
87. Shen, Z. Y.; Li, L. Y.; Li, Y.; Wang, C. C. J. Colloid Interface Sci, 2011, 354 (1), 196-201.
86. Jia et al. *European Polymer Journal*. **2007**, 43, 1123-1131.
87. Wang et al. *Journal of Colloid and Interface Science*. **2011**, 354, 196-201.

Thesis aims

The work described in this thesis focuses on the *design of highly stable non-toxic core-shell QDs-based materials for application in bio-medicine as imaging tools as well as sensors*. Considering the well-known toxicity of QDs, biologically inert structures are required for these powerful luminescent nanoparticles to be used without any restrictions.

In the first part of the thesis, a nanostructured material, which can solve the drawbacks of QDs in terms of toxicity and susceptibility from environmental conditions, was developed. For this purpose, combined efforts in the group led to the development of a novel layer-by layer (LbL) method (Chapter 2) in which QDs are used as seeds to grow the silica layers around them *in situ*. Silica proved to be an efficient barrier for leaching processes of the QDs as it was observed in the case of polystyrene (PS) microbeads. Embedding QDs into polystyrene (PS) microbeads it is a facile process taking advantage of the swelling behavior of this polymer in organic solvents, such as chloroform, which is a common solvent for the colloidal nanoparticles. Nevertheless, polystyrene beads undergo leaking of the nanocrystals, a negative point if we want to use this material for biomedical purposes. Besides, this procedure does not allow an accurate control of the amount of particles embedded. We solved these problems by using silica shells, by both the LbL and the embedding procedures, respectively, as will be further explained in Chapter 2. Multiplexed color encoded nanospheres (MENs) encapsulating layers of different color quantum dots were reported for the first time. Aspects regarding the dispersity of the nanospheres, as well as photostability and luminescent properties will be presented. Additionally, the QDs loading in the beads can be tuned by varying the number of QDs layers deposited, thus allowing control of the

luminescence intensity of the beads. The approach permits the formation of a new class of QDs encoded beads with high potential application in barcoding biotechnology. Besides, by biofunctionalizing the silica surface, multiplexed assays can be conducted in a very controllable way.

The new strategy described in Chapter 2 not only allows embedding the different color QDs in well-separated spaces in the beads, but also enables tuning their intensities. We took advantage of this characteristic in Chapter 3 to design Quantum Dot-‘‘Onion’’-Multi- code (QOM) structures as pH sensors. It is known that QDs are sensitive to chemicals in the surrounding environment such as acids, bases, ions and proteins. However, under dynamic conditions such as QD endocytosis and exocytosis, it would be very difficult to correlate pH values with absolute QD fluorescence. The silica matrix used plays an important role in making them water-soluble and protecting them from photoluminescence quenching, at least in the pH range useful for biological applications (between pH 4 and pH 8). The influence of the silica layer thickness or of the number of layers will be discussed.

The use of core-shell-like nanostructures in bio-medicine requires in almost all cases a surface functionalization as an intermediate step for the final goal. However, that is not the case if layered double hydroxides (LDHs) or hydrotalcite-like materials are employed as the shell since they are biocompatible with the cell membranes. LDHs were highly exploited as gene or drug delivery systems. Therefore, in Chapter 4, we went one step further using Mg-Al hydrotalcite as host material for our quantum dots nanocrystals. The synthetic procedures of QDs embedment will be explained in detail. Besides, the uptake was monitored in time. The novel composite nanomaterials were extensively characterized by X-ray diffraction, thermogravimetry, infrared spectroscopy, transmission electron microscopy, true color fluorescence

microscopy, photoluminescence, and nitrogen adsorption. Since we envisage using these materials in the biomedical field, high attention was devoted to the stability studies in mimicking physiological media such as saline serum (pH 5.5) and PBS (pH 7.2). Although they are very stable, a slight quantum dot release from the solid structure was noted in both media. In order to prevent the leaking of quantum dots, we have developed a novel strategy which consists on using tailor made double layered hydrotalcites as protecting shells for quantum dots embedded into silica nanospheres. Very interesting optical processes were observed during this study, as I will discuss later in the thesis. In addition, the role of silica will also be highlighted.

Moreover, we observed that this layered delivery system could be used to carry other emitting nanoparticles such as quantum nanorods, as detailed in Chapter 5. The results show that the two different starting materials, i.e. hydrotalcite and nanorods, can be heterogeneously integrated as functional components. Of particular interest are the changes in the fluorescence emission lifetime of the LDH-nanorods nanohybrid depending on the starting form of the host hydrotalcite (as-such or delaminated). These observations will be reasoned in parallel with QD-LDH. The most relevant aspect of this research line relates to the enhanced photoluminescence of the composite LDH-nanorods. This is translated finally in a reduced concentration of CdSe@CdS quantum nanorods, a requisite for their biological use as markers.

Once the materials were well characterized, my next goal was to explore their potential application in the biomedical area. The second part of the thesis focuses on the use of luminescent nanoparticles as labeling agent in bioimaging of cell cultures (Chapter 6) and the use core-shell QDs@silica nanospheres (QOM) for the study of enzymatic processes, namely trypsin, involved in cystic fibrosis (Chapter 7).
In Chapter 6, the incubation of a cell culture with the hybrid materials detailed in bot Chapter 4 and Chapter 5, was used to demonstrate the

potential use of these kind of materials as bioimaging agents. We observed a dependency of diameter of the nanoparticles used and the good quality of the samples as labelling tool. Further studies are required to clarify if this correlation is true or other reasons like the structure of the carrier material are involved.

In Chapter 7, the QD-FRET sensors were used to test the enzymatic activity of trypsin in solution based on FRET signal changes, between luminescent green QDs that serve as donors (l_{em} = 540 nm) and TAMRA acceptors (l_{em} = 575 nm) that are immobilized to the QD@silica surface through peptide linkers. When a second QD nanocrystal (red QD, l_{em} = 660 nm) was used, the qualitative system was improved and served for quantitative determinations as well, the red QDs becoming the reference in the QD_{540}/QD_{660} ratiometric nanosensor. These changes resulted from the release of TAMRA dye from the surface of the QDs@silica due to enzymatic cleavage of the peptide molecules as explained later in Chapter 6. Using the quantum dot-based assay described therein, we were able to detect, for the first time to the best of our knowledge, the trypsin activity at levels that are clinically relevant for determination of cystic fibrosis prognosis. Model dual emitting quantum dot@silica nanostructures represent a fast, non-invasive, highly specific and sensitive potential platform for high-throughput detection of the cystic fibrosis.

Finally, the summary and outlook of the thesis are put in perspective in Chapter 8.

Chapter 1-

Chapter 2:

Multiplexed color encoded silica nanospheres prepared by stepwise encapsulating quantum dot/SiO_2 multilayers.

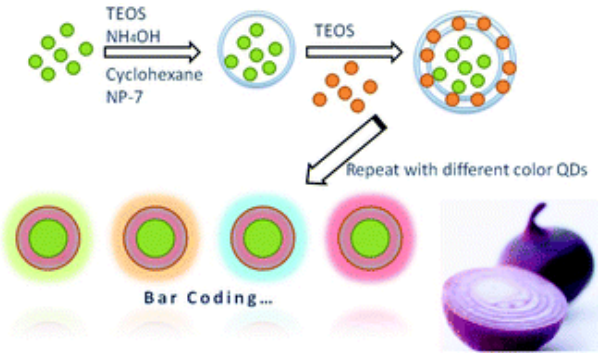

We present a flexible method for Multiplexed color Encoded Nanospheres (MENs) encapsulating layers of different color quantum dots. Our method results in highly efficient photoluminescent nanospheres with monodisperse, photostable, and excellent luminescence properties. Due to their “Onion” character, we have called this system Quantum-Onion-Multicode (QOM).

TABLE OF CONTENTS

Introduction

Semiconductor quantum dots (QDs) have attracted great attention in biotechnological applications as desirable fluorescent labels. In contrast with organic dyes, QDs possess excellent optical properties, such as continuous absorption profiles, robust signal intensity, and narrow emission spectra.[1-3] Moreover, an other advantage of QDs is that the emission wavelength can be finely tuned by changing the size of the QD particles. Due to all the mentioned properties above, and detailed in Chapter 1, QDs have been utilized in ultrasensitive high-throughput analytical detection. In fact, the development of QDs@ spheres as biomolecular probes can provide new insights that overcome several limitations of individual QDs as biological markers, for example: better photostability of the embedded QDs in the bead matrix, more available surface for chemical reactions, higher binding capacity of the spheres, and easier manipulation providing much faster reaction kinetics in homogeneous solution.[4, 5]

Water-soluble QDs are very toxic and harmful and a recover or coating layer is needed to avoid cadmium or selenium toxicity. Many forms of making water-soluble QDs@spheres can be performed in order to be used in bioapplications. Herein I will explain the procedure we performed to get multiplexed color encoded nanospheres.

In 2001 pioneering work by Nie et al. incorporated multicolor QD in polystyrene microspheres based on a swelling procedure.[6] Fuelled by this work, during the last ten years, many methods have been developed for preparing QD-tagged microspheres. Reproducible methods for preparing uniform QD-tagged microspheres can be classified in three basic technologies: (i) embedding QDs directly into the bead; (ii) loading QDs into the beads during the bead synthesis; (iii) the formation of a shell of QDs onto the surface of a bead using layer-by-layer (LBL) assembly techniques.[4,5] In theory, one million biomolecules could be labelled by using 5 different QD sizes in

combination with six different intensity levels.[6] It should be mentioned that although there are a lot of studies on beads encoded with QDs, the encoding procedures to ensemble multicolor QDs are complex. There are lots of limitations alike the variation in the bead size, precise code control, leaching of QDs, bead aggregation and energy transfer processes between different QDs resulting in a deviation of the designed ratios.[4-6] In order to overcome these limitations, the QDs-spheres prepared by LBL deposition have been shown to be one of the best suited methods for multiplexed studies.[5]

In this chapter, we report a facile procedure for stepwise encapsulating QDs multilayers via reverse microemulsion methodology and prepare Quantum-"Onion" Multicode (QOM).

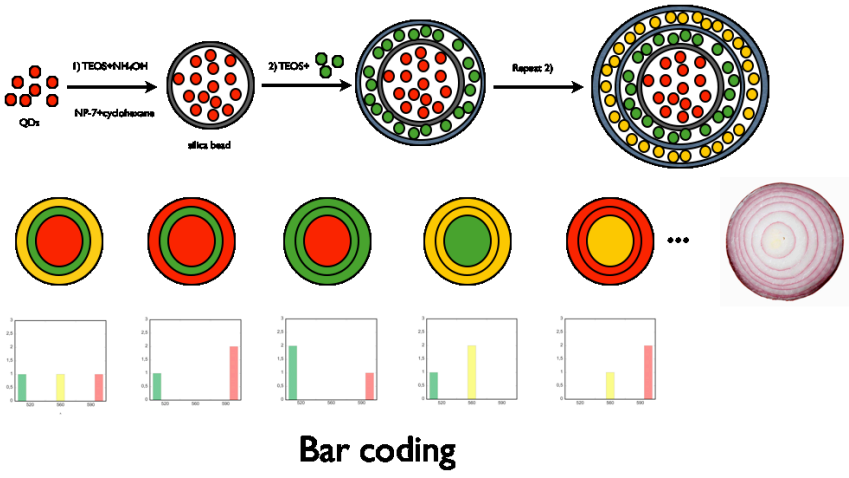

Scheme 1 Illustration of the procedure used to prepare of multiplexed colour encoded silica nanospheres encapsulating QDs multilayers.

Many attempts have been reported on the scientific literature to achieve Multiplexed encoded microspheres (MEMs).[7-9] However, because the water-soluble nature of these methods, lower emission quantum yield and poorer stability is usually observed. Moreover, these methods cannot satisfy the requirements of multi-color encoded microspheres and single color spheres are obtained. Other authors have incorporated

the QDs onto the surface of the micro-spheres[10,11] limiting the amount of QDs that can be used.

Herein we employed a reverse microemulsion method and hydrophobic QDs bridging together the best properties reported for MEMs. To the best of our knowledge, it is the first time that multi-CdSe QDs encoded beads using QDs@SiO_2 nanospheres coating multi-QDs/SiO_2 layers have been reported. The synthetic process is depicted in Scheme 1. The main general features of this novel procedure are: (i) it presents a facile straightforward method, avoiding more elaborate chemical reactions that may quench the CdSe QDs luminescence; (ii) the QD loading and composition can be controlled simply through the number of QD/TEOS encapsulating cycles and the QDs selection, respectively, thereby providing a means to tune the bead optical properties; (iii) silica is one of the proper inert materials for coating QDs to impede the leakage of heavy metal ions (e.g. Cd, Pb) into the environment and, moreover, enhances the chemical stability of CdSe QDs. The silica is also an ideal platform for bioapplications.

Experimental

Materials

CdSe QDs. This type of QDs were synthesized using two different methods both based on the first hot-injection report described by Murray,[12] with some modifications.

One of the way of synthesizing CdSe QDs was using oleic acid as capping ligand.[13] A selenium solution was prepared by mixing 30 mg of selenium poder, 5 mL of 1-octadecene and 0.4 mL of TOP. 13 mg of cadmium oxide, 0.6 mL of oleic acid and 10 mL of 1-octadecene were placed in a round-bottoned flask and heated to 225ºC. The solution was

purged under argon during the hole reaction. When the mixture reached 225ºC, 1 mL of selenium solution was quickly injected into the reaction vessel through a rubber septum and the resulting solution was cooled to room temperature. The size of the QDs is tuned by the time the solution is mantained at a determinated temperatura, 225ºC in this case.. The CdSe QDs were precipitated with copious amounts of chloroform/metanol (1:1)(vol:vol) solution and collected by centrifugation and decanting. The precipitated QDs were recovered by adding a small amount of chloroform metanol solution and re-precipitated with metanol. This purification process was repeated three times. Last time the CdSe QDs were resuspended and stored in chloroform.

The second procedure to obtain CdSe QDs was using TOPO-TOP as capping ligand.[14] A selenium solution was prepared by mixing 0.4 g of selenium poder, 10 mL of TOP and 0.2 mL of anhydrous toluene and stirred under argon. A mixture of 20 g of TOPO and 0.25 g of cadmium acetate dihydrate were placed in a round-bottoned flask, stirred and heated to 150ºC under argon and the temperatura was increased to 320ºC. When the mixture reached 320ºC the selenium solution was quickly injected and then cooled to 270ºC. The reaction was run for a specific time (depending on the size of the QDs that we expected to achieve). After stopping the reaction, samples were cooled and whased with etanol and acetone three times and stored in chloroform.

$Zn_xCd_{1-x}S$ QDs. Due to the difficulty of getting well-formed blue QDs using with CdSe (CdSe has a determinated emission range from 490 to 640 nm in wavelength) we looked for another materials in order to get blue-coloured QDs. We got well-synthesized blue QDs following the Han et al.[15] report with a few modifications.
For a typical preparation of $Zn_xCd_{1-x}S$, (x = 0.10), a mixture of 0.0032 g of CdO, 0.0041 g of ZnO, 2.5 mL of oleic acid, and 20 mL of octadecene was heated to 80 °C and degassed under argon for 20 min. The reaction vessel was then filled with argon, and its temperature was

increased to 310 °C. After the CdO and ZnO precursors were dissolved completely to form a clear colorless solution, the temperature was lowered to 300 °C. A solution of 0.016 g of sulfur in 5 mL of octadecene was quickly injected into this hot solution, and the reaction mixture was kept at 300 °C for the subsequent growth and annealing of the resulting nanocrystals. Aliquots of the sample were taken at different time intervals, and UV−vis and PL spectra were recorded for each aliquot. These sampling aliquots were quenched in cold chloroform (25 °C) to terminate growth of the particles immediately.

ZnS coating of the CdSe QDs. The CdSe QDs were coated with ZnS following a similar method previously described with some minor modifications.[16] A mixture of 5 mL of QDs in chloroform, 0.02373 of sulfur, 0.1866 g of zinc acetate dihydrate and 50 mL of paraffin oil was prepared in round-bottoned flask and heated to 80ºC for 20 minutes. When the mixture appeared homogeneous it was heated to 145ºC and kept this temperatura for 50 minutes. The solution was then removed and cooled to room temperatura. The CdSe/ZnS (core/shell) was precipitated with copious amounts of metanol and collected by centrifugation and decanting. The CdSe/ZnS was thenresuspended in chloroform. The coating procedure was repeated several times and in the final step of centrifugation and decanting the CdSe/ZnS was resuspended and stored in chloroform solution.

QOM nanospheres. The first step in the fabrication of the QDs encoded silica nanospheres involved the synthesis of a primer QDs@SiO2 by the reverse microemulsion method. Under vigorous stirring, 0.8mL QDs and 0.64mL TEOS were introduced into a liquid system containing 15mL of cyclohexane and 2.6 mL nonionic surfactant NP-7. After 30 min, 0.2mL ammonia was injected. Then the microemulsion was stirred for 24 hour. Because the hydrolyzed TEOS and NP-7 molecules replaced the original hydrophobic ligands of CdSe QDs in this reverse microemulsion system, silica growth can around the hydrophobic QDs smoothly. It

resulted in good monodisperse silica bead and high luminescence with QDs in the core.Then, an addition of QDs and TEOS to the liquid system subsequently condenses to form a thin shell of QDs/silica around the beads. In each case utilizing the hydrolysis of TEOS for layer formation, more different CdSe QDs can be encapsulated with a number of silica layers. During different Cdse QDs were separated with silica layers, the deposition of silica layers between QDs can result in more uniform QDS coatings.

Results and discussion

The QDs were successfully synthesized as can be seen in Figure 1, where the emission spectra of CdSe and $Zn_xCd_{1-x}S$, respectively, are shown and well-defined absorption peaks and sharp full width at half maximum (FWHM) are observed, indicating a rather uniform and narrow size distribution. In the case of the emission spectra of blue QDs a small shoulder is observed (green circle) which may be due to imperfections and gaps on the QD surface that can result in the trapping of electrons.[17]

Emission spectra of coated CdSe/ZnS QDs are shown in Figure 1. The shoulder in the blue CdSe-oleic acid QDs surface disappears after coating (green circle), due to capping ligand that makes the surface more homogeneous and the imperfections and gaps have disappeared. The emission wavelength peaks are shifted to the red after the coating due to the increase in size due to the added layers of ZnS. The smaller the core the larger the increase in the shift, in emission peak, after coating (Table 1). As coating adds the same thickness to each QD regardless of size the impact of the addition to a smaller core is greater than in larger samples.

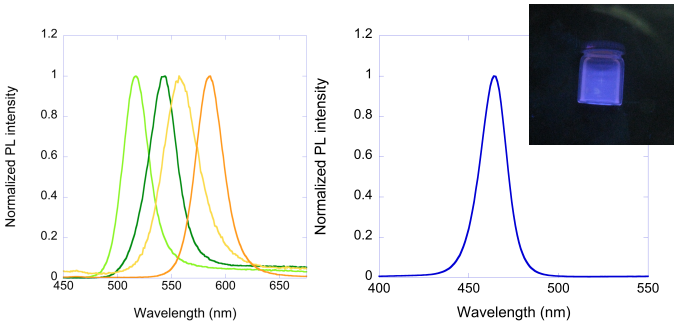

Figure 1. Normalized emission spectra of CdSe-TOPO QDs (whose size is indicated by the colour of each curve) (Left) and $Zn_xCd_{1-x}S$ blue QDs (Em=474 nm) (Right). Inset shows the real-color emission of the colloidal solution under UV-light.

Coating with ZnS layer avoids nanoparticle aggregation and makes them more stable. Without this coating, the colloidal solutions lose their homogeneity in less than a week due to aggregation and precipitation of the QDs.

A higher quantum yield of 22 % is obtained for the CdSe/ZnS nanocrystals because the ZnS shell prohibits the re-absorption of a photon, which is one of the processes reducing the emission intensity of nanocrystals. The organic ligands do not make trap energy levels on the surface of CdSe in the core/shell structured nanocrystals because of the surface coatings of ZnS.[18]

Table 1. Estimated and observed sizes as well as extinction coefficients calculated from the last excitonic peak for the synthesized CdSe and CdSe/ZnS (core/shell) QDs. Samples are named by their emission peaks and composition. ES= estimated size; OS= observed size.

SAMPLE	ES (nm)	OS (nm)	ε (mol^{-1}-cm^{-1})
488 CdSe	1.973	----------	33600
502 CdSe/ZnS	2.255	2.324±0.11	46100
515 CdSe	2.354	----------	51650
538 CdSe/ZnS	2.639	2.663±0.21	73900
570 CdSe	3.216	----------	118000
576 CdSe/ZnS	3.462	3.507±0.16	144900
635 CdSe	4.249	----------	291100
638 CdSe/ZnS	4.557	4.484±0.14	312500

The formation of the multi QDs/silica layers on the beads was directly visualized by transmission electron microscopy (TEM). Figure 2 shows TEM micrographs of the QDs@SiO_2 beads coated with different QDs/silica layers. The surface of silica beads is rather uniform with narrow size distribution, and no aggregation of the beads was observed. The thickness of the multilayer shell can be varied depending on the number of layers deposited and the amount of hydrolysis of the TEOS precursor. For a typical synthesis, the single color QDs@SiO_2 beads can be provided with 50 nm in diameter. When the QDs@SiO_2 beads were coated with one QDs/silica layer, the size of bead increased to 100nm. The thickness of QDs@SiO_2 beads with $(QDs/silica)_2$ layer were about 150 nm. The silica layer thickness was more than 10 nm, limiting the chances to observe energy transfer processes between two different kinds of QDs.

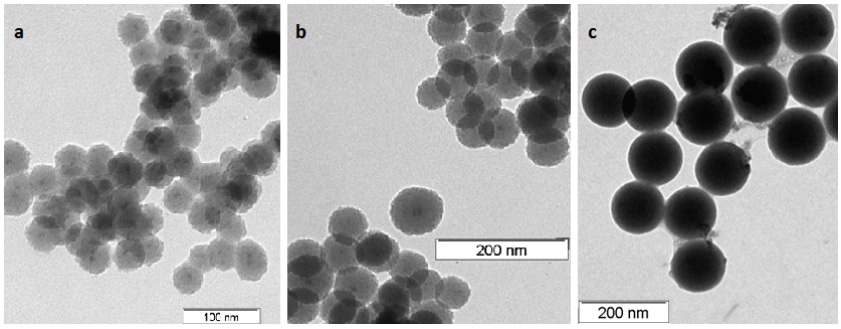

Figure 2. TEM micrographs of QDs@silica beads (a), QDs@silica beads coated with (QDs/SiO_2) layer (b), and QDs@silica beads coated with $(QDs/SiO_2)_2$ layer (c).

Once the QOMs were obtained, we investigate the optical characteristics of the beads, and demonstrate that the QD loading and luminescence intensity of each bead can be controlled through stepwise QDs layers.

Figure 3 shows the optical properties of hydrophobic QDs and QDs@SiO_2 beads according to the current synthesis. The QDs@SiO_2 beads showed a strong photoluminescence. The luminescence

spectrum of the beads has a maximum at 530 nm, corresponding to the emission of the CdSe QDs. It is interesting to notice a blue shift in the peak emission of the CdSe QDs @silica beads when compared with the CdSe QDs in solution (535 nm). Previously, a similar blue shift has been also reported by Caruso with hydrophilic QDs.[19] Moreover, the photoluminescence of CdSe QD@SiO_2 beads under UV light was strong enough to be seen by the naked eye.

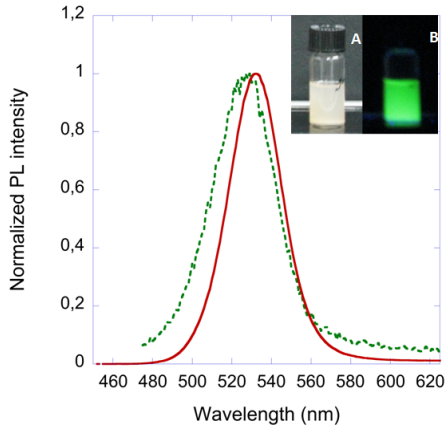

Figure 3. The PL emission spectra of CdSe QDs (solid line) and CdSe@SiO_2 microbeads (dashed line).Insets: The photographs of CdTe@SiO_2 beads under daylight (A) and UV light (B).

The luminescence spectra of QDs and QDs@SiO_2 beads corroborated our initial hypothesis about the successful growth of silica beads where hydrophobic QDs have to undergo a spontaneous phase transfer in the reaction. It was necessary to ensure that QDs capping ligands allowed chemical compatibility and solubility with both; the microemulsion system and the silica matrix. This is achieved by capping ligand-exchange of the native tri-n-octylphosphine oxide (TOPO) ligands on the QDs surface with the hydrolyzed TEOS and the nonionic surfactant (NP-7) molecules. It is also reported by Nann[20, 21] and Koole[22] that hydrolyzed TEOS has higher affinity for the QD surface and replaces the hydrophobic amine ligands, which enables the transfer of the QDs

to the hydrophilic interior of the micelles where the silica growth takes place.

Further investigation for the optical properties of the hydrophobic QDs@silica beads was provided by Visible absorption spectra and luminescence decay curves as shown in Figure 4.

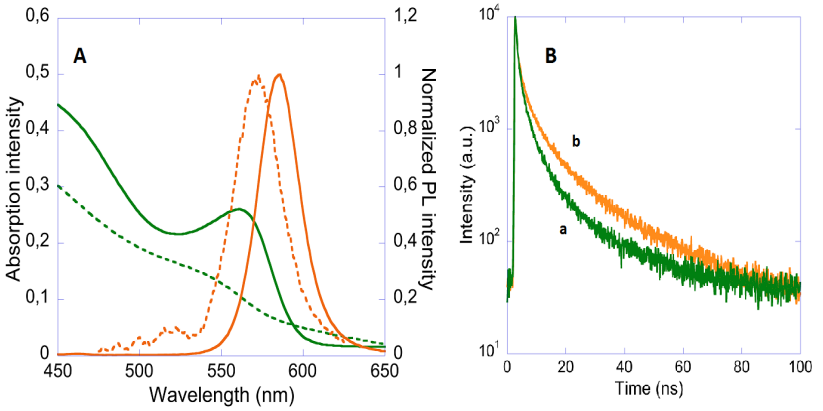

Figure 4. (A) Absorption and PL spectra of QDs (solid lines) and QDs@SiO_2 beads (dashed lines), and (B) Luminescence decay curves of QDs (a) and QDs@SiO_2 beads (b).

The Figure 4A shows a typical absorption spectrum for CdSe QDs and CdSe QDs@SiO_2 beads. The absorbance shoulder at 550 nm is assigned to the CdSe QDs absorption. The Silica beads contain the spectroscopic signature of CdSe QDs, confirming the presence of CdSeQDs. The Figure 3B shows the luminescence decay curves (measured at the emission peak maximum) of QDs and QDs@SiO_2 beads. The decay curves can be fitted to a biexponential model[23] described in Chapter 1. The fitted parameters B_1, B_2, τ_1, τ_2, and τ are summarized in Table 2. The fast component of the PL decay in QDs can be associated with the geminative exciton recombination.[24] The slow component is considered to originate from the surface-related emission of QDs. Comparing with QDs, the fast component (B_1) of PL decay for the bead increased while the slow component (B_2) decreased. The average luminescence lifetime of CdSe QDs and emitting SiO_2 beads are 17.01 and 13.10 ns, respectively. These tendencies are

ascribed to the surface modification of QDs due to the SiO_2 coating. Either the steady-state PL or the luminescence decay dynamics indicate that the hydrophobic CdSe QDs keep the optical properties after the SiO_2 coating.

Table 2. Time constants τ_1, and τ_2, components B_1, and B_2, and average lifetime τ of CdSe QDs and CdSe QDs@SiO_2 beads

Sample	B_1(%)	τ_1(ns)	B_2 (%)	τ_2(ns)	π(ns)
CdSe QDs	48.90	4.30	51.10	19.67	17.01
CdSeQDs@SiO_2	67.31	3.79	32.69	17.30	13.10

In addition to single color-encoded nanospheres, differently colour QDs can also be loaded into both the core and the shell of silica bead, which were rendered with distinguishable emission colours. Figure 5 shows the luminescence spectra taken from the CdSeQDs@SiO_2 beads with $(QDs/silica)_2$ layer with three different ratios related to the different emission peaks.

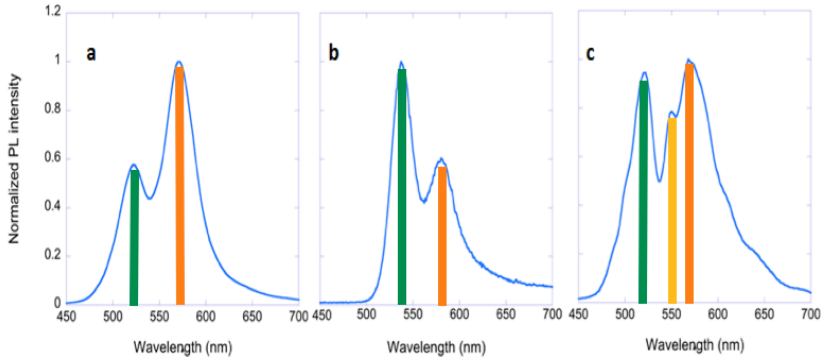

Figure 5. Photoluminescence spectra of multi-coloured QD-tagged silica microbeads with precisely controlled code: 6:10, 10:6, and 10:8:10.

As shown in Figure 5a, the intensity ratios of two emission peaks of silica beads were basically consistent with the designed original ratios, QDs with a peak at 530nm in the core and two silica layers with QDs at 575nm emission on the shell. This result suggests that the QDs are not

aggregated, and likely are evenly distributed throughout the bead. The different ratio can be easy provided with QDs_{530nm} in the core, one silica layer with QDs_{530nm} and another layer with QDs_{575nm} on the shell as shown in Figure 5b. The Figure 5c shows the photoluminescence of triple-color beads, which were designed as $QDs_{520nm}@SiO_2$ beads with (QDs_{550nm}/silica/QDs_{570nm}/silica) layer. Moreover, more different silica beads encapsulating different QDs/silica layers have been synthesized, as shown in Figure 6.

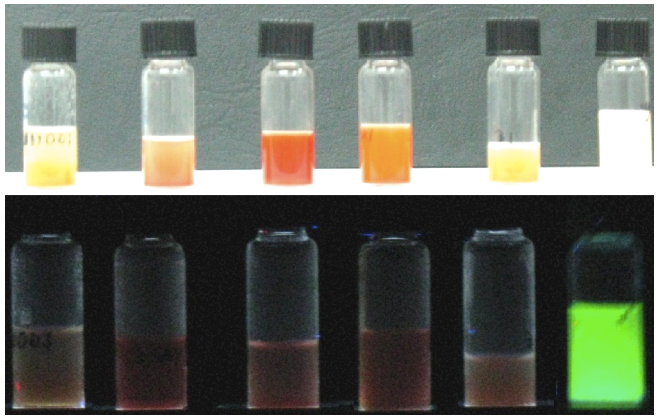

Figure 6. Photographs of serials of multiplexed optical encode silica bead based on one or two different colour QDs under daylight (above) and under UV light (below), respectively.

Conclusions

In summary, we have fabricated $QDs@SiO_2$ nanospheres encapsulating multi CdSe QDs/SiO_2layers, which we called Quantum-"Onion"-Multicode silica nanospheres. The approach permits the formation of a new class of QDs encoded beads for application in biotechnology. The QDs loading on the beads can be tuned by varying the number of QDs layers deposited, thus allowing control of the luminescence intensity of the beads.

In contrast to previously reported multi-QDs encoded beads, these QOM nanospheres with multi QDs/SiO_2layers are not only highly

uniform and show strong luminescence, but also encapsulated QDs throughout the bead (from the core to the shell). Furthermore, QDs with different colour were separated in the different space of beads, which prevent the potential energy transfer process between QDs and make the precise encoding easier. This procedure is expected to embed or encode a variety of beads with QDs and other nanospecies such as magnetic iron oxide nanoparticles and colloidal metal nanoparticles too.

References

1. Liu, A.; Peng, S.; Soo, J. C.; Kuang, M.; Chen, P.; Duan, J. Anal. Chem, 2011, 83, 1124.

2. Pan, J.; Wan, D.; Gong, J. Chem. Commun, 2011, 47, 3442.

3. Ma, Q.; Su, X. Analyst, 2010, 135, 1867.

4. Ma, Q.; Wang, C.; Su, X. J. Nanosci. Nanotechnol, 2008, 8, 1138.

5. Sukhanova, A.; Nabiev, I. Crit. Rev. Oncol. Hematol, 2008, 68, 39.

6. Yang, M.; Gao, X.; Su, J. Z.; Nie, S. Nat. Biotechnol, 2001, 19, 631.

7. Rogach, A. L.; Nagesha, D.; Ostrander, J. W.; Giersig, M.; Kotov, N. A. Chem. Mater, 2000, 12, 2676.

8. Jing, L.; Yang, C.; Qiao, R.; Niu, M.; Du, M.; Yang, D.; Gao, M. Chem. Mater, 2010, 22, 420.

9. Yang, P.; Ando, M.; Murase, N. J. Colloid Interface Sci., 2007, 316, 420.

10. Chan, Y.; Zimmer, J. P.; Stroh, M.; Steckel, J. S.; Jain, R. K.; Bawendi, M. G. Adv. Mater, 2004, 16, 2092.

11. Cho, M.; Lim, K.; Woo, K. Chem. Commun, 2010, 46, 5584.

12. Murray, C. B.; Norris, D. J.; Bawendi, M. G. J. Am. Chem Soc, 1993, 115 (19) 8706.

13. Yu, W. W.; Peng, X. Ange Chem Int Ed, 2002, 41 (13), 2368.

14. Lee, H. Y.; Yum, J. H.; Leventis, H. C.; Zakeeruddin, S. M.; Haque, S. A.; Chen, P.; Seok, S. I.; Gratzel, M.; Nazeeruddin, K. J. Phys Chem C, 2008, 112, 11600.

15. Zong, X.; Fenf, Y.; Knoll, W.; Han, M. J. Am. Chem. Soc., 2003, 125, 13559

16. Zhu, C. Q.; Wang, P.; Wang, X.; Li, Y. Nanoscale Res Lett, 2008, 3, 213.

17. Kalyuznhy, G.; Murray, R. W. J Phys Chem 2005, 109, 15, 7012.

18. Mi. S.; Kim, H. S. Yang, J Korean Phys Soc, 2010, 56 (1), 467.

19. Wang, D.; Rogach, A. L.; Caruso, F. Nano Lett, 2002, 2, 857.

20. Darbandi, R.; Nann, T. Chem.Mater, 2005, 17, 5720.

21. Nann, T.; Mulvaney, P. Angew. Chem, Int. Ed., 2004, 43, 5393.

22. Koole, R.; v. Schooneveld, M. M.; Hilhorst, J.; DonegaÅL, C. d. M.; Hart, D. C.; v. Blaaderen, A.; Vanmaekelbergh, D.; Meijerink, A. Chem. Mater, 2008, 20, 2503.

23. Zeng, Q.; Kong, X.; Sun, Y.; Zhang, Y.; Tu, L.; Zhao, J.; Zhang, H. J. Phys. Chem. C, 2008, 112, 8587.

24. Wuister, S. F.; v. Driel, F.; Meijerink, A. Phys. Chem. Chem. Phys., 2003, 5, 1253.

Chapter 3:

QD-“Onion”-Multicode silica nanospheres with remarkable stability as pH sensors.

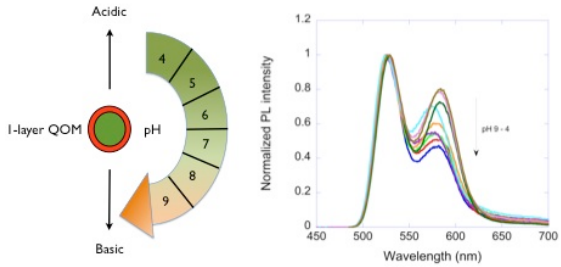

We present a flexible reverse microemulsion using hydrophobic QDs for multiplexed encoded nanobeads encapsulating layers of different coloured quantum dots, called QD-“Onion”-Multicode bead (QOM). This novel system has monodisperse, photostable, and excellent luminescence properties that are stable at different pH values. The protection that the silica layers confer to the QDs allows them to be used as a ratiometric pH sensor by measuring the ratio of PL intensity of QDs from the different layers.

TABLE OF CONTENTS

Introduction

Recent work has used silica beads, in wich are embedded the QDs, to improve the QD fluorescence for the coding signal. Silica is one of the most popular inert materials for surface coating, which has several advantages compared to other materials. Firstly, silica is non-toxic and can be easily modified with functionalized groups that can form covalent bonds with biomolecules. Secondly, degradation can be avoided due to the resistance of silica to both aqueous (except extremely high pH solution) and non-aqueous solvents.[1] Finally, silica nanoparticles are easily separated by centrifugation during preparation, functionalization, and other treatment processes due to its high density.[2] Many atempts have been reported in the scientific literature to achieve multiplexed color encoded silica nanospheres.[3-5] Nevertheless, because of the use of hydrophilic QDs in these methods, lower emission quantum yield and poorer stability is usually observed. Moreover, these methods do not generally satisfy the requirements of multi-color encoded spheres and only single color spheres are obtained. Several authors have incorporated the QDs onto the surface of micro or nanospheres limiting the amount of QDs that can be used.[6, 7]

Herein we employ a reverse microemulsion method for the encapsulation of hydrophobic QDs bringing together the best properties reported for multiplex encoded, using silica nanospheres, that we call Quantum Dots-“Onion”-Multicode (QOM).[8] This novel procedure has several main features. Firstly, it is a facile straightforward, avoiding complex chemical reactions that may quench the CdSe/ZnS QDs luminescence. Secondly, QDs loading and composition can be controlled simply through the number of silica layers and QDs selection respectively, thereby providing a means to tune the nanosphere optical properties. Finally, the use of inert silica for coating QDs avoids the

leakage of heavy metal ions into the environment and enhances the chemical stability of CdSe QDs. Furthermore, the lack of toxicity is also an ideal platform for bioapplications. Look at Scheme 1 in Chapter 2 for the preparation of these QOM silica nanospheres. Previously, a number of groups have built QDs-based pH sensors because QDs are sensitive to chemicals in the surrounding environment such as acids, bases, ions and proteins.[9] However, under dynamic conditions such as QD endocytosis and exocytosis, it would be very difficult to correlate pH values with absolute QD fluorescence. A classier and more robust approach is to use ratiometric measurements such as by using QD-dye FRET pairs, because fluorescence intensity ratios are irrespective of changes in probe quantity, excitation intensity and detector sensitivity.[10, 11] We perform this QOM in order to protect the QDs from the environmental conditions.

Experimental

Materials.

Synthesis of CdSe QDs. A selenium solution was prepared by mixing 0.4 g of selenium poder, 10 mL of TOP and 0.2 mL of anhydrous toluene and stirred under argon. A mixture of 20 g of TOPO and 0.25 g of cadmium acetate dihydrate were placed in a round-bottoned flask, stirred and heated to 150ºC under argon and the temperatura was increased to 320ºC. When the mixture reached 320ºC the selenium solution was quickly injected and then cooled to 270ºC. The reaction was run for a specific time (depending on the size of the QDs that we expected to achieve). After stopping the reaction, samples were cooled and whased with etanol and acetone three times and stored in chloroform.[12]

Synthesis of $Zn_xCd_{1-x}S$ QDs, (x = 0.10), a mixture of 0.0032 g of CdO, 0.0041 g of ZnO, 2.5 mL of oleic acid, and 20 mL of octadecene was heated to 80 °C and degassed under argon for 20 min. The reaction vessel was then filled with argon, and its temperature was increased to 310 °C. After the CdO and ZnO precursors were dissolved completely to form a clear colorless solution, the temperature was lowered to 300 °C. A solution of 0.016 g of sulfur in 5 mL of octadecene was quickly injected into this hot solution, and the reaction mixture was kept at 300 °C for the subsequent growth and annealing of the resulting nanocrystals. Aliquots of the sample were taken at different time intervals, and UV−vis and PL spectra were recorded for each aliquot. These sampling aliquots were quenched in cold chloroform (25 °C) to terminate growth of the particles immediately.[13]

ZnS coating of the CdSe QDs. A mixture of 5 mL of QDs in chloroform, 0.02373 of sulfur, 0.1866 g of zinc acetate dihydrate and 50 mL of paraffin oil was prepared in round-bottoned flask and heated to 80ºC for 20 minutes. When the mixture appeared homogeneous it was heated to 145ºC and kept this temperatura for 50 minutes. The solution was then removed and cooled to room temperatura. The CdSe/ZnS (core/shell) was precipitated with copious amounts of metanol and collected by centrifugation and decanting. The CdSe/ZnS was thenresuspended in chloroform. The coating procedure was repeated several times and in the final step of centrifugation and decanting the CdSe/ZnS was resuspended and stored in chloroform solution.[14]

Synthesis of QOM nanospheres. The encapsulation of QDs into silica beads was performed following our previously reported method.[8] A mixture of 2.6 mL of Tergitol NP7 and 15 mL of cyclohexane was prepared in a flask and left to stir for 15 minutes. To this solution 800 μL of QDs in chloroform solution and 640 μL of TEOS were added to the previous mixture and left to stir for another 30 minutes. From this

moment on the reaction was conducted in the dark. 200 μL of aqueous ammonia solution (30%) were added to start the hydrolysis and left to stir for 24 hours. For the second layer of silica 800 μL of QDs in chloroform solution were then added to the previous mixture and left to stir for 30 minutes. Then 100 μL of TEOS were added to the reaction and left to stir for 24 hours. For the third layer, another 800 μL of QDs in chloroform solution were added to the reaction and left to stir for 30 minutes and 100 μL of TEOS were added to the mixture and left to stir for 24 hours. Acetone was added to stop the reaction and the mixture was centrifuged with ethanol 3 times at 3300 g. The samples were stored in ethanol.

pH sensitivity

1 mL of silica-coated QDs (core) was added to 1 mL of several buffers with different pH values from 2 to 11. They were incubated for 1hour with continuous shaking. The pH stability test was performed following the procedure described above, adding 1 mL of 1-layer QOM to 1 mL of several buffers with different pH values from 4 to 9. The QOM was formed with a core with 590 nm red CdSe/ZnS embedded QDs and an additional layer of silica embedded with 520 nm green CdSe/ZnS QDs. They were incubated for 1 hour with continuous shaking.

Results and discussion

Incorporation of CdSe/ZnS QDs into silica beads forming QOM.

There are two main types of routes to prepare silica spheres, the Stöber method [15-18] and the reverse microemulsion process. The former is hard to apply if the nanoparticles are insoluble in alcohol-water solution. For this reason, ligand exchange is usually required prior to commencing the Stöber process for QDs synthesized by organometallic methods. This exchange is commonly associated with a decrease of fluorescent

efficiency of QDs and it therefore requires more sensitive fluorescence measurements systems. In the case of aqueous QDs, the Stöber method can be directly used to synthesize QDs@SiO_2 to obtain spheres with a controllable thickness of the silica shell over the range from a few nanometers to several micrometers, but multistep procedures[19] are required and the size distribution of QDs/SiO_2 is not very narrow. An alternative method is the reverse microemulsion method that uses water-in-oil microemulsions where the silica spheres are synthesized by the hydrolysis of tetraethoxysilane (TEOS), followed by its condensation in water nanodroplets.[20] Nanocomposites[19, 21] and dye molecules[22] can be encapsulated by the silica spheres as long as they are soluble in water. Recently,[23, 24] a variant reverse micelle-based approach was performed to synthesize silica-coating hydrophobic QDs and other hydrophobic nanoparticles. NP-7 is a surfactant that provokes the microemulsion because of its amphipylic nature and it can also exchange the TOPO from QDs to make them water-soluble to allow the QDs to be inside the mini-pool or bubbles that will be surrounded by TEOS. Ammonia will react with TEOS to become silica via hydrolysis, as shown in Scheme 1. The effects of water and ammonia are complex. Water catalyzes the hydrolysis and increases the nucleation rate of silica particles. Lower water content reduces supersaturation and favors the growth of the QD seed particles over the nucleation fresh silica. This is favoured by solvents with higher dielectric constants (such as water), which favour ionization of silanol groups and enhance electrostatic repulsion between particles. Ammonia is also a catalyst for TEOS hydrolysis. Notwithstanding this the rate of spontaneous nucleation was found to increase as the ammonia concentration was lowered.

The UV-Vis absorption and emission spectra of synthesized CdSe/ZnS and CdSe/ZnS@SiO_2 QDs are presented in Figure 1 and show well-defined absorption peaks and small full width at half maximum (FWHM), indicating a rather uniform and narrow size distribution. Without the silica coating, the colloidal solutions lose their homogeneity in less than a week due to aggregation and precipitation of the QDs. We can

observe a blue shift due to corrosion of CdSe/ZnS during the embedding process in which hydrolysis occurs.

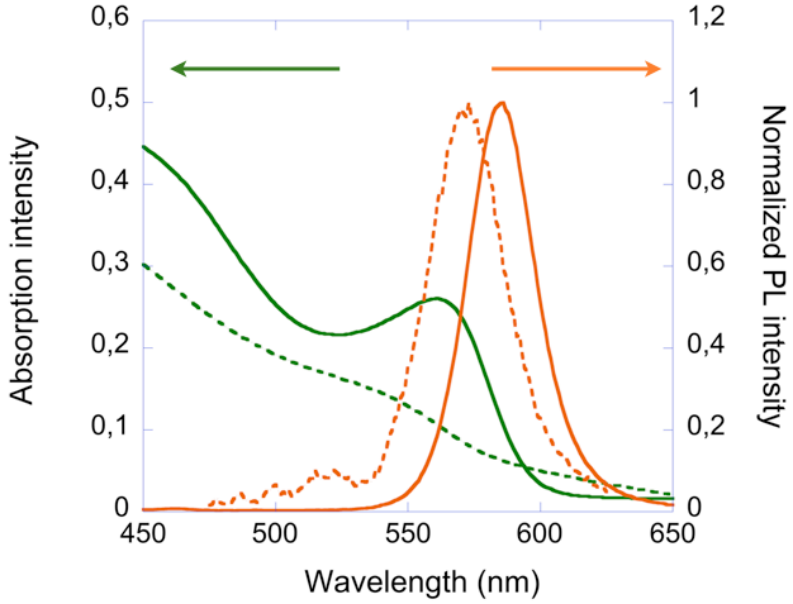

Figure 1. Comparison of the UV-Vis absorption and emission spectra of colloidal CdSe/ZnS QDs (continous line) and the same QDs incorporated into silica bead (dotted line).

The beads were directly visualized by transmission electron microscopy (TEM). In Figure 2 the comparison of the emission spectra of different QOMs is shown. In the case of Figure 2-A, we can see the emission of a 2-layer QOM with a core and an additional layer of silica embedded with green CdSe/ZnS QDs and another silica layer embedded with orange CdSe QDs. In Figure 2-B and C, the emission spectrum belongs to a 2-layer QOM with the inversed code is observed, where the core and an additional layer of silica are embedded with orange CdSe and another silica layer embedded with green QDs. Figure 2-D shows the emission of a 1-layer QOM with orange CdSe/ZnS embedded in the core and an additional layer of silica with blue $Zn_xCd_{1-x}S$ QDs. In Figure 2-E, the emission spectrum of a 2-layer QOM, where the core is embedded with orange CdSe/ZnS QDs, the first silica layer is embedded with green CdSe/ZnS QDs and the second silica layer with

blue $Zn_xCd_{1-x}S$ QDs. The PL intensity is directly related to the ratio of green-orange QDs, playing with different ratios and number of layers we can get many intensities as a bar-code.

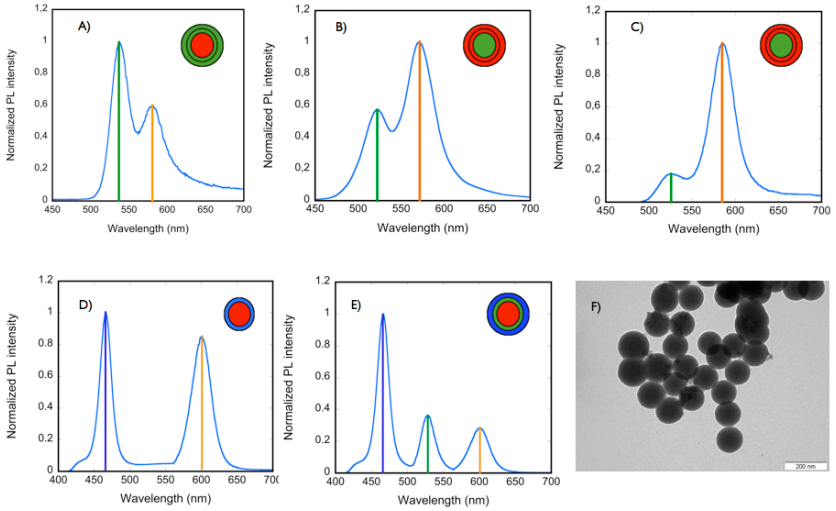

Figure 2. Comparison of the emission spectra and TEM image of multilayer QOMs. A) The QOM code is 10: 6 for the $QDs_{580nm}/QDs_{525nm}/QDs_{525nm}$ (core/shell /shell). B) The QOM code is 6:10 for the $QDs_{525nm}/QDs_{580nm}/QDs_{580nm}$ (core/shell/shell). C) The QOM code is 2:10 for the $QDs_{525nm}/QDs_{580nm}/QDs_{580nm}$ (core/shell/shell). D) The code is 10: 8 (orange: blue) for the QDs_{600nm}/QDs_{465nm} (core/shell). E) The code is 10: 4: 3 for the $QDs_{600nm}/QDs_{525nm}/QDs_{465nm}$ (core/shell/shell). F) TEM image of 2-layer QOM.

Silica protection.

For biological applications, QDs should be at least stable between pH 4 and 8. This is because most bioconjugation reactions are performed at this pH range and pH values found in the human body also fall into this range. TEM images in Figure 3-A and B show samples at different pH values indicating that silica protects the QDs from the different pH environments. Nonetheless, at pH 11, silica becomes unstable (Figure 3-C) and we could not measure the PL intensity directly because the embedded QDs with TOPO are not water-soluble.

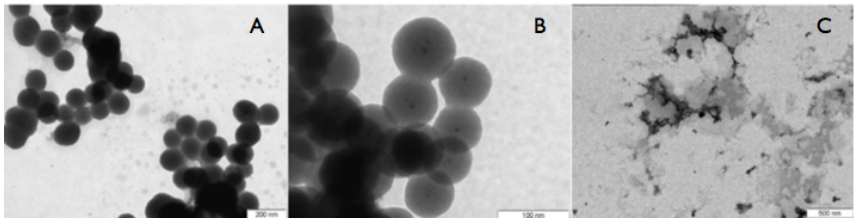

Figure 3. TEM images of QOM after incubation at (A) pH 2, (B) pH 7, and (C) pH 11.

The amount of initially added TEOS was found to be important, irrespective of the composition of the mixture: if the TEOS concentration was high, larger silica particles with multiple QDs were synthesized. The optimal amount of TEOS for our experiments corresponded to silica shell with a thickness of about 10-15 nm. The thickness of the silica shells could be grown by subsequent addition of more TEOS (as discussed below). The higher the amount of TEOS, the higher the protection of the QDs inside the beads. The thickness of the beads were measured by TEM (Figure 4) to be: 60, 130, 180 nm, on average, for the 1x, 2x, 3x TEOS amounts, respectively. So we can conclude that the thicker the silica layer, the more stable the PL intensity of the QDs. We can vary this thickness either by increasing the amount of TEOS during the synthesis or by adding more layers of silica. Figure 5 compares the normalized photoluminescence intensity of the silica beads with different amounts of TEOS used during synthesis. The normalization was done with the PL intensity at pH 7 for all samples.

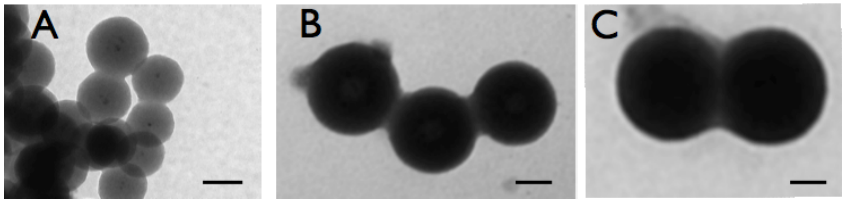

Figure 4. TEM images of QOM with different amounts of TEOS used during synthesis. A) 640 uL of TEOS, B) 1280 uL of TEOS, C) 1920 uL of TEOS. The scale bar corresponds to 50 nm.

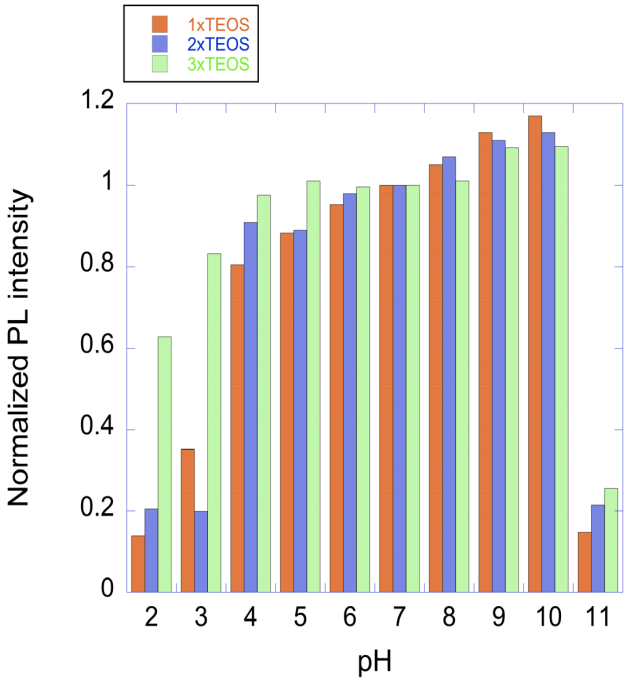

Figure 5. Comparison of normalized PL intensity of different silica beads synthesized with different amount of TEOS (x= 640 μL) at different pH values.

The behaviour of the PL intensities of the silica beads in different pH were measured after different time periods and is shown in Figure 6. The PL intensity is more or less stable in the pH range 4-10, agreeing with the obtained results from Gao et al.[25] All the samples have the same response to the pH, with increasing PL intensity at basic pH and more or less stable from 4-10. However, silica becomes unstable at pH 11 and the QDs are released with an irreversible less of PL. Normalized PL intensity of different silica beads measured as a function of time at different pH values (Figure 7 and Table 1) shows that PL intensity is more or less stable for a full week as silica beads keep at least 60% of the initial PL intensity. This is very attractive for bioapplications where stability is required for up to several hours. In agreement with Gao, a unique silica shell is not enough to protect QDs from acid or chemical-induced quenching, but several shells make them exhibit remarkable

stability for the biological pH range. Although their system shows stability over a wider range, our system is stable enough to be used in bioassays, not only aginst biological pH conditions but also along the time.

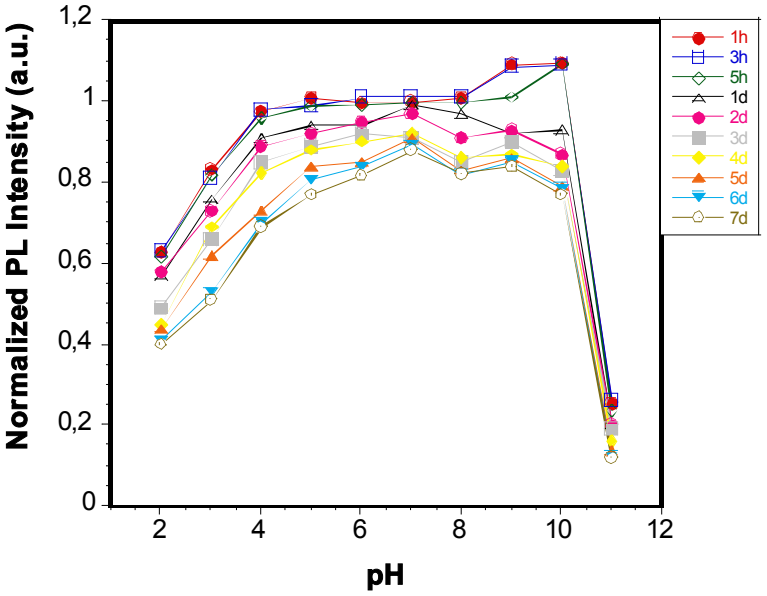

Figure 6. Normalized PL intensity of silica beads as a function of pH monitored after periods of 1h, 3h, 5h, and 1-7 days.

Table 1. Results of the chemical stability at different pH values over time

pH	2	3	4	5	6	7	8	9	10	11
1h	0.628	0.832	0.976	1.010	0.996	1.000	1.010	1.092	1.095	0.255
3h	0.631	0.811	0.980	0.990	1.010	1.010	1.010	1.087	1.091	0.261
5h	0.618	0.820	0.961	0.990	0.992	0.997	0.998	1.011	1.093	0.238
1d	0.570	0.760	0.910	0.940	0.940	0.992	0.970	0.920	0.930	0.201
2d	0.580	0.730	0.890	0.920	0.950	0.970	0.910	0.930	0.870	0.202
3d	0.490	0.660	0.850	0.890	0.920	0.910	0.850	0.900	0.830	0.191
4d	0.450	0.690	0.823	0.881	0.902	0.921	0.861	0.870	0.840	0.163
5d	0.440	0.620	0.730	0.840	0.850	0.910	0.830	0.860	0.790	0.136
6d	0.410	0.530	0.701	0.806	0.839	0.893	0.819	0.853	0.786	0.123
7d	0.400	0.510	0.690	0.770	0.818	0.880	0.822	0.840	0.770	0.120

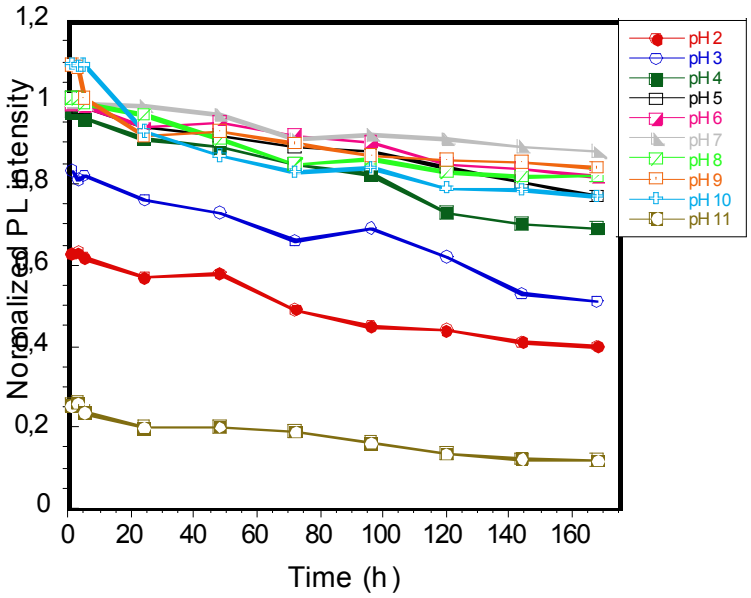

Figure 7. Comparison of normalized PL intensity of different silica beads measured as a function of time at different pH.

pH sensitivity test.

Figure 8 shows a comparison of the emission spectra of different 1-layer QOMs. This system is formed from a core of 590 nm CdSe/ZnS embedded QDs and an additional layer of silica embedded with 520 nm green CdSe/ZnS QDs at different pH values (pH 4-9). As we can see, the more the basic the pH, the more quenched the PL intensity of the orange peak (590 nm). This result is in agreement with our previous results in which we could see that PL intensity increases at higher pH values, at least until pH 10. As sigmoidal behaviour in the ratio between the PL intensity of both peaks is observed (Figure 8, inset), it can be concluded that both acidic or basic conditions affect the PL intensity more or less to the same degree. Therefore, the QOM appears to be functioning as a ratiometric pH sensor and, indeed, a rather stable one.

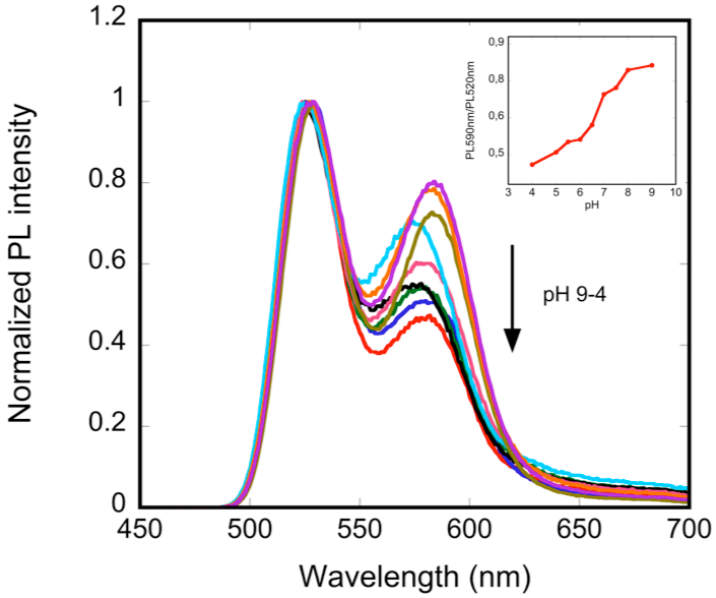

Figure 8. Comparison of normalized PL intensity of QOM with two different coloured embedded CdSe/ZnS (520 nm/ 590 nm) (core/shell) at different pH value. The inset shows the ratio between the PL intensity at 590 nm and PL intensity at 520 nm.

Figure 9 shows the comparison of a series of 2-layer QOM with two different colour QDs ($QDs_{520nm}/QDs_{520nm}/QDs_{590nm}$) at different pH values under daylight and under and UV Light. The emmited colour changes depending on the pH value because the ratio between the PL intensity at 520 and 590 nm changes. The QDs_{520nm} in the core or protected by a double silica layer, which can protect from the pH, maintain a stable signal. On the other hand, the QDs_{590nm}, which are protected by a thin silica layer, can be easily affected by pH. This makes our system useful as a ratiometric pH sensor. Furthermore, the higher 590 nm PL intensity the more red shifted emission and emited colour changes switches from green to yellow.

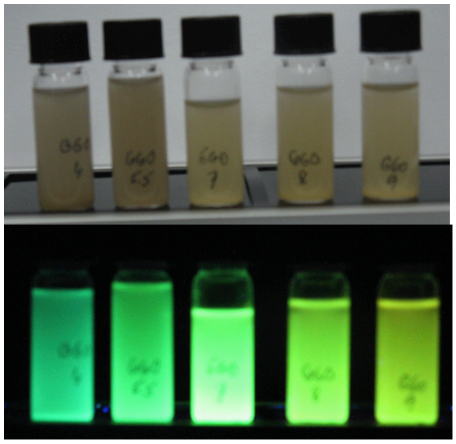

Figure 9. Photographs of a series of multiplexed optical encode silica bead based on bicolor QOM under daylight (above) and under UV light (below), respectively.

Conclusions

We have developed a new method for the preparation of stable QDs by an encapsulation method based on the formation of several silica layers. Hydrophobic QDs were first encapsulated with silica shell based on a well-established reverse microemulsion method. We went a further step and added more layers of silica with embedded QDs following the same procedure. Based on this new series of stable embedded QDs, we show that they can be used for pH sensor applications. The silica matrix used play an important role in making them water-soluble and protecting them from PL quenching, at least in the pH range useful for biological applications (between pH 4 and pH 8). The greater the silica layer thickness or higher the number of silica layers the greater the protection offered to the QDs inside. The ratio of PL intensity from two populations of QDs has been shown to correspond to the pH value in the media, making our system a potential ratiometric pH sensor. This method has a good potencial to develop a wide range of sensors by varying the functional QDs and other components either embedded or on silica surface.

References

1. Santra, S.; Zhang, P.; Wang, K.; Tapec, R.; Tan, W. Anal. Chem, 2001, 73, 4788.

2. Wang, L.; Tan, W. Nano Lett, 2006, 6, 84.

3. Rogach, A. L.; Nagesha, D.; Ostrander, J. W.; Giersig, M.; Kotov, N. A. Chem. Mater, 2000, 12, 2676.

4. Jing, L.; Yang, C.; Qiao, R.; Niu, M.; Du, M.; Wang, D.; Gao, M. Chem. Mater, 2010, 22, 420.

5. Yang, P.; Ando, M.; Murase, N. J. Colloid Interface Sci, 2007, 316, 420.

6. Chan, Y.; Zimmer, J. P.; Stroh, M.; Steckel, J. S.; Jain, R. R.; Bawendi, M. G. Adv. Mater, 2004, 16, 2092.

7. Chao, M.; Lim, K.; Woo, K. Chem. Commun, 2010, 46, 5584.

8. Ma, Q.; Castello, I; Palomares, E. Chem. Commun, 2011, 25, 7071.

9. Liu, Y. S.; Sun, Y. H.; Vernier, P. T.; Liang, C. H.; Chong, S. Y. C.; Gundersen, M. A. J. Phys. Chem. C, 2007, 11, 2872.

10. Jin, T.; Sasaki, A.; Kinjo, M.; Miyazaki, J. A. Chem. Commun, 2010, 46, 2408.

11. Snee, P. T.; Somers, R. C.; Nair, G.; Zimmer, J. P.; Bawendi, M. G. J. Am. Chem Soc, 2006, 128, 13320.

12. Aldana, J.; Wang, Y. A.; Peng, X. J. Am. Chem Soc, 2001, 112, 8844.

13. Zhu, C. Q.; Wang, P.; Wang, X.; Li, Y. Nanoscale Res. Lett, 2008, 3, 213.

14. Zong, X.; Fenf, Y.; Knoll, W.; Han, M. J. Am. Chem Soc, 2003, 125, 13559.

15. Chan, Y.; Zimmer, J. P.; Stroh, M.; Steckel, J. S.; Jain, R. R.; Bawendi, M. G. Ad Mater, 2004, 16, 2092.

16. Wolcott, A.; Gerian, D.; Visconte, M.; Sun, J.; Schwataberg, A.; Chan, S.; Zhing, J. Z. J. Phys. Chem. B, 2006, 110, 5779.

17. Bruchez, M.; Moronne, P.; Gin, P.; Weiss, J. S.; Alivisatos, A. P. Science, 1998, 281, 2013.

18. Nann, T.; Mulvaney, P. Angew. Chem, Int. Ed., 2004, 43, 5393–5396.

19. Yang, Y.; Jing, L.; Yu, X.; Yan, J.; Gao, M. Chem. Mater, 2007, 19, 4123.

20. Chang, S. Y.; Liu, L.; Asher, S. A. J. Am. Chem Soc, 1994, 116, 6739.

21. Ye, Z.; Tan, M.; Wang, G.; Yuan, J. Anal. Chem, 2004, 76, 513.

22. Zhao, X.; Bagwe, R. P.; Tan, W. Adv. Mater, 2004, 16, 173.

23. Jana, N. R.; Earhart, C.; Yin, J. Y. Chem. Mater, 2007, 19, 5074.

24. Selvan, T.; Tan, T.; Yin, J. Y. Adv. Mater, 2005, 17, 1620.

25. Gao, X.; Hu, X. ACS Nano, 2010, 4, 6080.

Chapter 3-

Chapter 4:

Layered double hydroxides as carriers for quantum dots@silica nanospheres

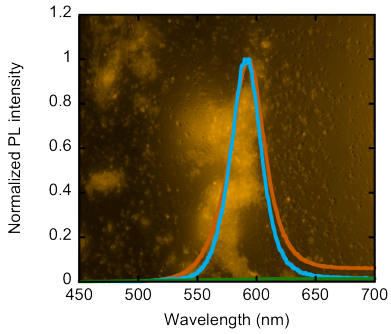

Quantum dot-hydrotalcite layered nanoplatforms were successfully prepared following a one-pot synthesis. The process is very fast and *a priori* delamination of hydrotalcite is not a prerequisite for the intercalation of quantum dots. The novel materials were extensively characterized by X-ray diffraction, thermogravimetry, infrared spectroscopy, transmission electron microscopy, true color fluorescence microscopy, photoluminescence, and nitrogen adsorption. The quantum dot-hydrotalcite nanomaterials display extremely high stability in mimicking physiological media such as saline serum (pH 5.5) and PBS (pH 7.2). Yet, quantum dot release from the solid structure is noted. In order to prevent the leaking of quantum dots we have developed a novel strategy which consists on using tailor made double layered hydrotalcites as protecting shells for quantum dots embedded into silica nanospheres without changing either the materials or the optical properties.

TABLE OF CONTENTS

Introduction

The use of theranostic medicine emerged as a new challenge with respect to the traditional concept about medicine and its application in human health. Nanoscale materials are becoming more common in the field of medicine, particularly in the field of drug delivery, since they can incorporate and also be functionalized with a wide range of biomolecules. Organic or inorganic platforms such as polymers, dendrimers, micelles, vesicles, metals, metal oxides, semiconductor nanocrystals, and nanoparticles have all been already investigated as possible multimodal imaging or simultaneous diagnosis and therapy systems.[1,2,3,4]

Well-known systems like semiconductor quantum dots (QDs) have attracted great interest in multiplexed bioassays, biotechnological applications and bioimaging.[5,6,7,8] In contrast to traditional fluorophores, QDs possess excellent optical properties, such as continuous absorption profiles, robust signal intensity, narrow emission spectra, and improved brightness with outstanding resistance to photobleaching and degradation.[9,10,11,12] Moreover, the development of QDs@ nano- or micro- silica spheres as biomolecular probes can provide new insights that overcome several limitations of individual QDs as biological markers, *i.e.*: better photostability of the embedded QDs in the bead matrix, more available surface for chemical reactions, higher binding capacity of the microspheres, less toxicity, and easier manipulation.[13,14] For example, our own group, recently prepared multicode silica nanospheres of 'onion' type with high stability in the biological pH range, *i.e.* 4-9.[15,16]

However, most inorganic nanoparticles require chemical functionalization with silane, thiol, amino and carboxy species in order to obtain desirable properties for cellular delivery, such as good biocompatibility, strong affinity between carrier and payload, cell targeting, stability and long circulation time.[17,18,19] During the past, it is apparent that layered double hydroxides (LDHs), also known as

hydrotalcite-like materials (HT) or anionic clays, form an exception to this rule. LDHs consist of layers of positively charged nanosheets with brucite-type structure neutralized by anions in the interlayer space, where water is also present.[20,21] Their anion-exchange property[20] allows the direct loading of anionic drugs/biomolecules into the interlayer galleries.[22,23,24,25,26,27] LDH are mostly well-known catalysts and ceramic precursors, catalysts, and traps for anionic pollutants.[21] The earliest application of hydrotalcites in relation to human health was their use as antiacids and antipeptic reagents,[28,29,30] whereas in the last decade nanometer-sized LDH materials were increasingly explored as drug and gene carriers and controlled release delivery systems.[22,23,25, 26,31,32,33,34-37] The capacity to incorporate drugs and other bioactive molecules (peptides, proteins, nucleic acid) in the interlayer space opened ways for their application in nanomedicine. The first obstacle for the LDH-cargo hybrid materials to be transferred into the cells is the cell membrane, which is hydrophobic and negatively charged. LDH nanoparticles, exhibiting a positive surface charge, readily achieves this without necessitating any further surface functionalization, as is the case of silica,[17,18] gold nanoparticles,[19] or carbon materials.[22] Owing to their small size they should avoid renal clearance, which translates into a long circulation time and increases their chance of crossing the blood-brain barrier. In addition, their dissolution after internalization means that no accumulative effects should be observed, making them highly biocompatible.

Most of the studies related to core-shell structures focus on magnetic, polystyrene or silica composites loaded with therapeutic and imaging agents.[38] Pioneer work includes also the magnetic core-LDH shell nanocomposites for drug delivery or catalytic applications, making use of *in situ* growth of the LDH shell or *via* the layer-by-layer technique.[39,40,41,42] Apart from the zero dimension structures, two-dimensional LDH thin films intercalated with CdTe or CdSe quantum dots were prepared by spin coating or restacking of exfoliated hydrotalcite as new light emitting devices (LEDs).[43,44] Intercalation of

anionic species in the hydrotalcite interlayer space *via* de delamination-restacking procedure led to the synthesis of interesting structures in general.[45,46,47,48,49] However, in the cases reported so far, the fabrication of multicomponent composites requires starting from all individual components in delaminated form.

Our aim in this work is to synthesize and fully characterize cost-effective nanomaterials based on the use of Mg-Al hydrotalcites containing QDs and QDs@silica shells that (a) prevent QDs leaching and (b) can be used in nanomedicine for imaging and diagnosis.

Experimental

Materials

Synthesis of hydrotalcite. Mg-Al hydrotalcite with molar Mg/Al ratio of 3 was synthesized by precipitation at constant pH 10. Briefly, aqueous solutions of $Mg(NO_3)2{\cdot}6H_2O$ (0,75 M) and $Al(NO_3)3{\cdot}9H_2O$ (0,25 M) were put in contact with the precipitating agent, *i.e.* NaOH and Na_2CO_3, 2 M each. The precipitate slurry was aged at room temperature for 12 h under mechanical stirring (500 rpm), followed by filtration, washing and drying at 60ºC for 12 h.

Delamination. A dispersion of the as-synthesized hydrotalcite in pure formamide (purity 99,5%) was prepared at a concentration of 5 g l^{-1}. The suspension was ultrasonicated six times for a period of 30 min with an interval of 60 min between treatments in order to accelerate the delamination process.

Synthesis of CdTe quantum dots. A flask with 0.02552 g Te, 0.07 g $NaBH_4$ and 1.5 mL water was mixed to prepare the NaHTe precursor. Then, another flask with 0.2283 g $CdCl_2$, 100 mL water and 132 mL mercaptopropionic acid (MPA) was mixed and ajusted to pH 11 with NaOH 1M under argon for 30 minutes and heated to 100 ºC. Then, the

tellurium precursor was added with fast injection and the synthesis was held for additional 20 min in order to achieve the desired quantum dots nanocrystals without further purification step.

Synthesis of CdSe QDs. A selenium solution was prepared by mixing 0.4 g of selenium poder, 10 mL of TOP and 0.2 mL of anhydrous toluene and stirred under argon. A mixture of 20 g of TOPO and 0.25 g of cadmium acetate dihydrate were placed in a round-bottoned flask, stirred and heated to 150ºC under argon and the temperatura was increased to 320ºC. When the mixture reached 320ºC the selenium solution was quickly injected and then cooled to 270ºC. The reaction was run for a specific time (depending on the size of the QDs that we expected to achieve). After stopping the reaction, samples were cooled and whased with etanol and acetone three times and stored in chloroform.[50]

ZnS coating of the CdSe QDs. A mixture of 5 mL of QDs in chloroform, 0.02373 of sulfur, 0.1866 g of zinc acetate dihydrate and 50 mL of paraffin oil was prepared in round-bottoned flask and heated to 80ºC for 20 minutes. When the mixture appeared homogeneous it was heated to 145ºC and kept this temperatura for 50 minutes. The solution was then removed and cooled to room temperatura. The CdSe/ZnS (core/shell) was precipitated with copious amounts of metanol and collected by centrifugation and decanting. The CdSe/ZnS was thenresuspended in chloroform. The coating procedure was repeated several times and in the final step of centrifugation and decanting the CdSe/ZnS was resuspended and stored in chloroform solution.

Synthesis of QOM nanospheres. The encapsulation of QDs into silica beads was performed following our previously reported method.[51] A mixture of 2.6 mL of Tergitol NP7 and 15 mL of cyclohexane was prepared in a flask and left to stir for 15 minutes. To this solution 800 μL

of QDs in chloroform solution and 640 μL of TEOS were added to the previous mixture and left to stir for another 30 minutes. From this moment on the reaction was conducted in the dark. 200 μL of aqueous ammonia solution (30%) were added to start the hydrolysis and left to stir for 24 hours. Acetone was added to stop the reaction and the mixture was centrifuged with ethanol 3 times at 3300 g. The samples were stored in ethanol.

Sample post-synthesis treatments

Two synthetic approaches were followed for the preparation of the composite materials, as detailed next. The first one by treating directly the as-synthesized hydrotalcite with the QDs (CdTe) aqueous solution following an anion exchange mechanism, and the second one by exfoliation-restacking, *i.e.* subjecting the hydrotalcite to delamination in formamide and subsequent treatment with the CdTe quantum dots aqueous solution or the ethanolic solution containing the CdSe/ZnS QDs@silica nanospheres. In all the cases, the concentration was kept at 5 g l^{-1}. After stirring for 1 h, the mixture was left to rest at ambient conditions for 24 h. The resulting solids were filtered, washed with deionized water, and dried at 80ºC for 12 h. When following the delamination-restacking experimental way, the resulting solid was centrifuged at 4400 rpm for 30 min and redispersed in ethanol or water, and centrifuged again at 4400 rpm for 30 min each. The washing procedure was repeated three times and the final solid was dried at 80ºC for 12 h.

Along the manuscript, the samples were designated by the codes HT*x*, where *x* refers to the approach started from the as-synthesized (HTas) or delaminated (HTd) form of hydrotalcite, respectively. The codes HT*x*-QD identify the different starting materials after treatment with the QDs aqueous solution. The code HT*x*-QDs@silica refers to the composite material obtained after contacting the QDs@silica nanospheres (where QDs are CdSe/ZnS quantum dots) with the delaminated hydrotalcite.

Samples stability tests

The HTas-QD composite nanomaterial was subjected to a stability test by immersing the composite in serum (pH 5.5) or PBS (pH 7.2) for different periods of time ranging from 2 h to 12 weeks. The aforementioned pH values were chosen with respect to the lysosomes and cytosol environments, respectively. Additionally, another HTas-QD was immersed in water for the same period of time.

Characterization techniques

Powder X-ray diffraction patterns (XRD) were measured in a Bruker AXS D8 Advance diffractometer equipped with a Cu tube, a Ge(111) incident beam monochromator, and a Vantec-1 PSD. Data were recorded in the range 5-70º 2*q* with an angular step size of 0.016º and a counting time of 6 s per step. Thermogravimetric analysis (TGA) was carried out in a Mettler Toledo TGA/SDTA851e microbalance. Analyses were performed in dry air flow of 50 cm^3 min^{-1} from ambient temperature to 900ºC using a heating rate of 5ºC min^{-1}. Fourier transform infrared (FTIR) spectroscopy was carried out in a Bruker Optics ALPHA spectrometer equipped with a ATR Platinum Diamond unit. Spectra were collected in the range 400-4000 cm^{-1} by co-addition of 32 scans at a nominal resolution of 4 cm^{-1}, taking the spectrum of the empty cell as the background. Transmission Electron Microscopy (TEM) was carried out in a JEOL JEM-1011 microscope operating at 100 kV and equipped with a SIS Megaview III CCD camera. High Resolution Transmission Electron Microscopy (HRTEM) was carried out in a JEOL JEM-2100 microscope operating at 200 kV and equipped with a INCAx-sight detector from Oxford Instruments. A few droplets of the sample suspended in ethanol were placed on a carbon-coated copper grid followed by evaporation at ambient conditions. True color fluorescence images were taken by Nikon TE2000-E confocal microscope. Photoluminescence (PL) spectra were recorded, using a 1 cm path length quartz cell in a Shimadzu UV spectrophotometer 1700 and an Aminco-Bowman Series 2 luminescence spectrometer. Nitrogen

isotherms at 77 K were measured on a Quantachrome Autosorb-1Q analyzer. Prior to the analysis, the samples were degassed in vacuum at 120ºC for 15 h. The BET method[52] was applied to calculate the total surface area, and the *t*-plot method[53] was used to discriminate between micro- and mesoporosity. The surface charge (zeta potential) of the semiconductor nanocrystals aqueous dispersion was characterized with a ZetaSizer Nano ZS (Malvern Instruments Inc, UK) utilizing dynamic light scattering (DLS) and the Smoluchowski equation.

Results and discussion

Starting hydrotalcite

The X-ray diffraction confirmed the hydrotalcite (JCPDS 22-700) as the unique crystalline phase in the precipitate as illustrated in Figure 1.

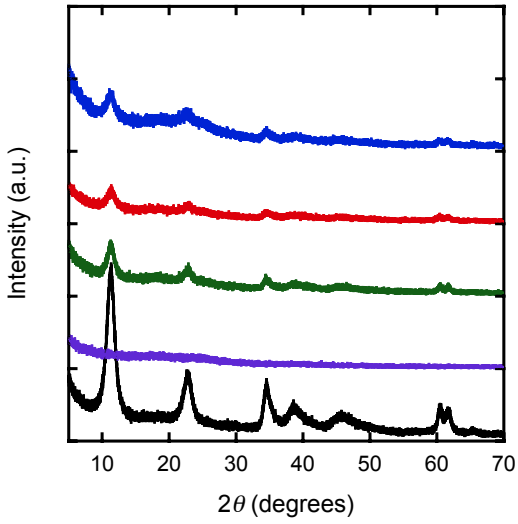

Figure 1. X-ray diffraction patterns of as-synthesized (HTas) and delaminated (HTd) hydrotalcites and the solids resulting from their treatment in CdTe QDs aqueous solution at ambient conditions. The X-ray diffraction pattern of QDs@silica-HT is also shown. Black: HTas, purple: HTd, green: HTas-QD, red: HTd-QD, blue: HTd-QDs@silica.

Thermogravimetric analysis of the as-synthesized hydrotalcite, represented by the black line in Figure 2, shows the typical two-step weight loss profile of layered double hydroxides. The first transition, attributed to the loss of interlayer water, amounts 19%. The second transition, due to the dehydroxylation of the brucite-like sheets and decarbonation, amounts to 29%.

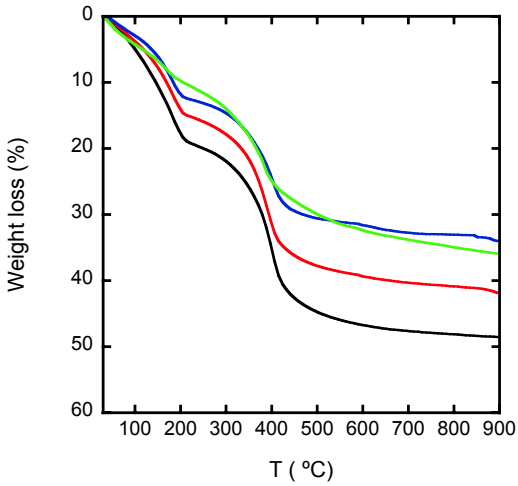

Figure 2. Thermogravimetric profiles of the solids resulting from treatment of as-synthesized (HTas) and delaminated (HTd) hydrotalcites in CdTe QDs aqueous solution at ambient conditions, as well as QDs@silica-HT. Black: HTas, red HTas-QD, blue HTd-QD, green HTd-QDs@silica.

The infrared spectrum of HTas (Figure 3) features characteristic bands of hydrotalcite: 3470 cm^{-1} (OH stretching), 1465 cm^{-1}, 1365 cm^{-1}, 1105 cm^{-1} (v_3 mode of the carbonate, antisymmetric stretching), 620 cm^{-1} (Mg-related OH translation modes, octahedral Mg), and 545 cm^{-1} (Al-O stretching vibration, octahedral Al).[54,55] The vibration at 1630 cm^{-1} is due to the bending mode of water. The appearance of the v_3 mode of the carbonate at 1365 cm^{-1} (being 1415 cm^{-1} in the 'free' carbonate anion) is related to its reorganization in the interlayer space due to electrostatic interaction with the nearby brucite-like layers. Besides, the materials

featured the platelet-like morphology characteristic of these layered materials (Figure 4a).

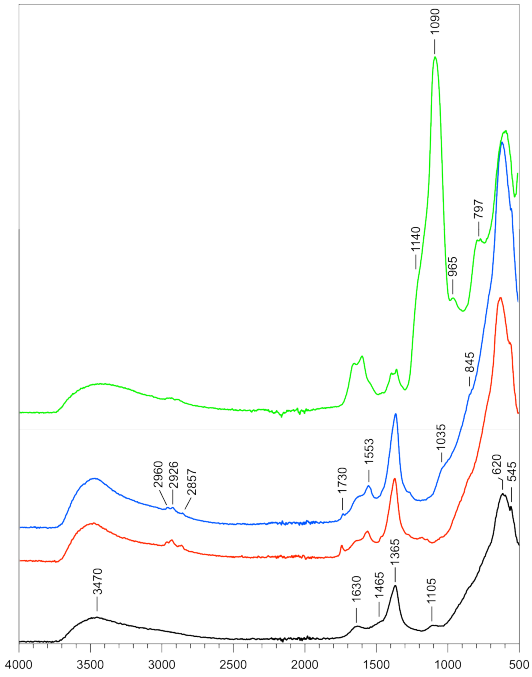

Figure 3. Infrared spectra of HTas (black), HTas-QD (red), HTd-QD (blue), and HTd-QDs@silica (green), respectively.

The textural properties of the solid were determined by adsorption of nitrogen at 77K (Figure 5). The isotherm of HTas is characteristic of the hydrotalcite clay compounds and can be classified as type IV with H1 hysteresis.[56] These fingerprints are characteristic of a purely mesoporous material with uniform pore size of 25 nm (Table 1). The total pore volume and specific surface area of HTas were 0.39 cm^3 g^{-1} and 32 m^2 g^{-1}, respectively (Table 1). The absence of microporosity was confirmed by application of the *t*-plot method.

The corresponding diffraction pattern of the exfoliated hydrotalcite evidenced the disappearance of the hydrotalcite reflections (HTd in Figure 1), proving that the delamination of LDH into positively charged brucite-like nanosheets was accomplished.[54] This was further confirmed by the transmission electron microscopy (Figure 4b) which shows the

formation of very thin particles that are almost transparent to the microscope electron beam, suggesting the presence of a few brucite-like layers.[57]

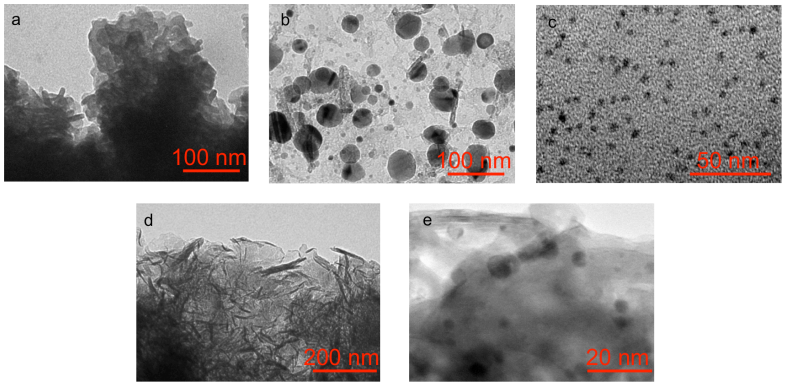

Figure 4. Transmission electron micrographs of selected samples, *i.e.* (a) HTas, (b) HTd, (c) QDs, (d) HTas-QD, (e) HRTEM image of HTas-QD, respectively. The scale bar is displayed for each micrograph.

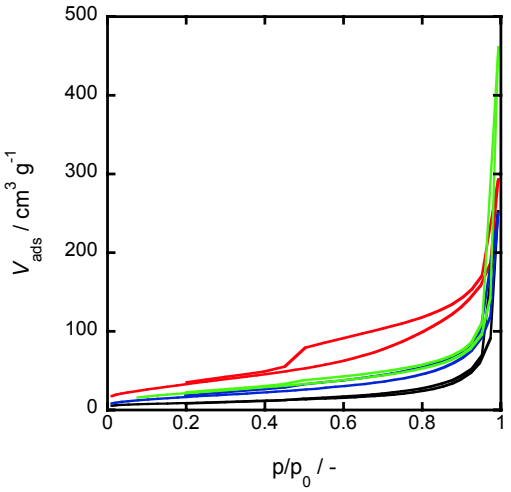

Figure 5. Nitrogen adsorption-desorption isotherms at 77 K of selected samples. Black: HTas, red HTas-QD, blue HTd-QD, green HTd-QDs@silica.

Table 1. Characterization data of selected samples.

Sample	V_{pore} ($cm^3\ g^{-1}$)	S_{BET}[a] ($m^2\ g^{-1}$)	PSD (nm)
HTas	0.39	32	24.56
HTas-QD	0.45	125	7.27
HTd-QD	0.39	63	12.4

[a] BET method.

Transformation of the hydrotalcite by anion exchange

Figure 1 illustrates the X-ray diffraction patterns of the solids resulting from treatment of HTas and HTd in CdTe QDs aqueous solution. As expected, both HTas-QD and HTd-QD displayed hydrotalcite structure after 1 day. Recovery of the hydrotalcite structure is practiced typically by chemical (treatment in aqueous solutions of $(NH_4)_2CO_3$,[58] Na_2CO_3[59] or NaCl[60,61] and ethanol[59]) or physical methods (solvent evaporation,[57] freeze-drying[60]). The d_{003} basal spacing was calculated for HTas (7.816 nm) and the derived nanocomposites and an increase was observed for HTas-QD (7.862 nm) indicating the presence of QDs in the interlayer space. In contrast, HTd-QD displayed the same basal spacing as HTas suggesting the similarity in the intercalation of QDs.

In agreement with XRD, the thermogravimetric analysis of the samples after 1 day displays the typical two-step behavior (Figure 2) during hydrotalcite decomposition with decreasing total weight loss from 48% in HTas to 42% (HTas-QD) and 34% (HTd-QD), respectively. There is an overall decrease in both the first and the second weight loss steps which is an indication of the lower amount of water, hydroxyls and carbonate groups in the interlayer space as a consequence of the anion exchange process. In other words, small negative CdTe quantum dots (4 nm, Figure 4c) with zeta potential of -33.35 mV occupy the hydrotalcite galleries at the partial expense of the original anions. The infrared spectra of the samples HTas-QD (red) and HTd-QD (green) in Figure 3 reveal new bands characteristic of the mercaptopropanoic acid (MPA), additionally to the hydrotalcite bands, in support to the thermogravimetric results. The MPA was used to make CdTe QDs

soluble in water (as detailed previously in the synthesis procedure). The most relevant bands attributed to -C=O and C-H stretching appear at 1730 cm^{-1} and 2857 cm^{-1}, 2926 cm^{-1}, and 2960 cm^{-1}, respectively.[62] No bands specific to CdTe are visible since they appear at 170 cm^{-1} and our equipment allows recording spectra in the range 400-4000 cm^{-1}.[63] Besides, the band at 1365 cm^{-1} increased in intensity in both HTas-QD and HTd-QD. This observation is a clear indication of the higher degree of reorganization as compared to HTas due to the uptake of quantum dots. Due to the loss of symmetry of the carbonate ion, the v_1 mode of the carbonate (symmetric stretching) becomes activated, thus leading to the shoulder at 1035 cm^{-1}.[64] It is evident that this effect is more pronounced in HTd-QD as a consequence of the delamination procedure. This vibration mode is inactive when the carbonate ion retains its full symmetry.[65] All the samples showed improved platelet morphology when compared to the parent hydrotalcite, selectively indicated by HTas-QD in Figure 4d, e.

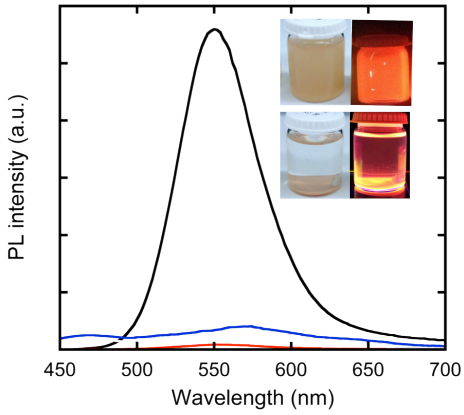

Figure 6. Photoluminescence emission spectra of CdTe QDs aqueous solution (black spectrum) and filtrates resulting from treatment of as-synthesized (HTas) and delaminated (HTd) hydrotalcites in CdTe QDs aqueous solution at ambient conditions, red and blue spectra, respectively. Inset: (top) the mixture containing CdTe QDs and HTas at *t* = 0 min under daylight (left) and UV light (right); (bottom) the mixture containing CdTe QDs and HTas at *t* = 24 h under daylight (left) and UV light (right).

The isotherm of HTas-QD in Figure 5 is characteristic of the hydrotalcite clay compounds with a significant increase of the total surface area, *i.e.* 125 m^2 g^{-1}, and total pore volume, 0.45 cm^3 g^{-1}. This is due to the interparticle mesoporosity generated by the anion exchange treatment and reorganization of hydrotalcite.[58] Additionally, the pore size distribution decreased from 25 nm in HTas to 7.27 nm in HTas-QD as a consequence of the quantum dots uptake by the hydrotalcite. Sample HTd-QD exhibits similar textural properties with HTas. The surface area doubled with respect to HTas due to the delamination-restacking process, however the total pore volume recovered the initial value, *i.e.* 63 m^2 g^{-1} and 0.39 cm^3 g^{-1}, respectively. As an aftereffect of the quantum dots take-up, the PSD of HTd-QD reached the average size of 12.4 nm.

The results above indicate that both samples, *i.e.* HTas and HTd, behave similarly after immersion in QDs. However, HTas-QD displays higher surface area after the treatment and a comparable thermogravimetric behavior with the pristine material. Accordingly, exfoliation is not certainly a prerequisite for the hydrotalcite recovery. We want to highlight herein the HTas synthetic approach, which implies only a one-pot procedure and represents a more efficient strategy towards nanocomposite formation than starting from the delaminated form of hydrotalcite by the exfoliation-restacking or layer by layer methods.

Comparative photoluminescence emission spectra of CdTe QDs aqueous solution and the filtrates resulting from treatment of HTas and HTd hydrotalcites in CdTe QDs aqueous solution at

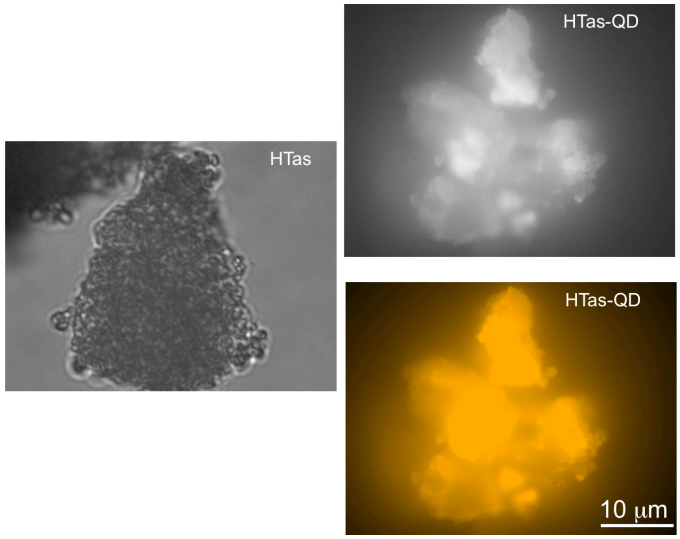

Figure 7. True color fluorescence images of HTas and HTas-QD. The scale bar is the same for all the photos.

ambient conditions are shown in Figure 6. The quantum dots luminescence in solution heavely decreased after 1 day uptake, thus evidencing a total adsorption of quantum dots by the hydrotalcite and derived materials (see inset in Figure 6).

In order to confirm this latter statement, we carried out true color fluorescence images of HTas (left) and HTas-QD (right), as depicted in Figure 7. From the picture on the left, we can clearly observe that the parent hydrotalcite (reference material) is not fluorescent. The top photo on the right illustrates HTas-QD sample as-such, without light excitation. However, after excitation with a blue laser at 488 nm, HTas-QD exhibited uniform fluorescence (bottom photo) due to the presence of quantum dots, in agreement with the photoluminescence results. In parallel, we monitored the uptake of QDs by recording the photoluminescence of the aqueous solution from 5 min up to 1 day (Figure 8A). In all the experiments, CdTe QDs and HTas were used as reference. As expected, Figure 8A shows a fast uptake of the quantum dots from the solution by the layered hydrotalcite. After 4 h, the luminescence intensity in the solution decreased by 90% indicating the

high affinity of hydrotalcite, and in particular the positive brucite-like sheets, for the negative nanoparticles. After 9 h, the PL spectrum displays the same behavior as HTas, which in turn has no emission. However, the sample was let in contact with the QDs aqueous solution for 24 h to enable the total uptake. After this time, the solid was filtered and divided in two for the stability test.

HT-QD stability

After the synthesis of HT-QDs, we moved forward to the stability studies in different conditions to evaluate the material potential in nanomedicine as per its usage as diagnostic agent in cells. In this purpose, the HTas-QD composite nanomaterial was subjected to a test by immersing the composite in saline serum (pH 5.5) or PBS (pH 7.2), respectively. The photoluminescence of the supernatant was recorded for different periods of time. The aforementioned pH values were chosen with respect to the physiologic lysosomes and cytosol environments, respectively.

Figure 8B, 8C exhibits the PL spectra in the time range 2 h – 12 weeks. In both cases, in the early times of the experiment (2 h to 9 h) (insets), we appreciated QDs leaching. Nonetheless, after 9 hours in solution a remarkable flat fluorescence spectra was recorded, indicating that there is no quantum dots leaching from the HTas-QD composite nanomaterial into the different solutions anymore (see the reference CdTe QDs spectrum for comparison). After the 12 weeks, another PL measurement was performed and no fluorescence was detected (Figure 8B) confirming the QDs confinement in the hydrotalcite structure, thus making this layered material a suitable host and carrier for the quantum dots.

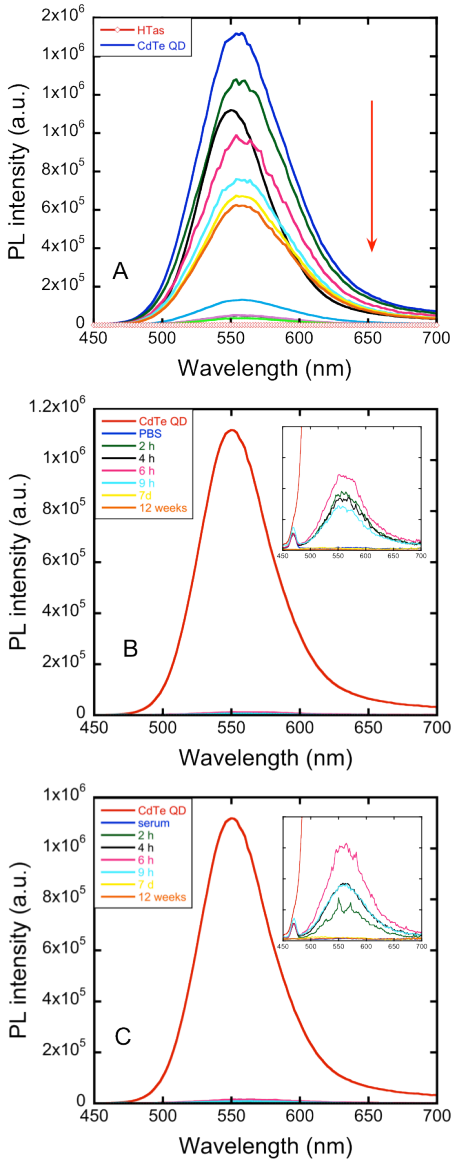

Figure 8. Photoluminescence emission spectra of (A) the CdTe QDs aqueous solution containing HTas (recorded from 5 min to 24 h), and the PBS (B) and saline serum (C) solutions containing HTas-QD (recorded from 2 h up to 12 weeks). Inset: magnification of the spectra at low PL intensity.

We would like to notice that when the solid was observed under UV light a green-yellow emission was noticed (Figure 9). This latter result indicates that there was a hypsochromic emission shift from the starting orange-emitting CdTe QDs to green-yellow -emitting QDs. This was an unexpected result, which lead us to propose three different hypotheses described below of the origin of this blue emission shift (Scheme 1).

Hypothesis 1. Solvent driven tuning of the quantum dot surface. The samples stored in PBS and serum displayed a more pronounced blue shift than the water-stored HTas-QD, green *vs.* yellow, respectively (data not shown). This indicates that phosphate and chloride anions induce higher modification of the quantum dot surface with respect to hydroxyls and carbonate ions.

Hypothesis 2. Doping the quantum dot surface by Mg^{2+} ions. The pH measurement after 12 weeks revealed a remarkable increase of the pH value from 5.5 to 8 in saline serum, and from 7.2 to 9 in the PBS solution, respectively. This result can be expected considering the higher solubility of Mg^{2+} ions with respect to Al:[66,67] $Mg(OH)_2$, DG_{diss} = -96.1 kJ mol^{-1}, $Al(OH)_3$, DG_{diss} = -46.7 kJ mol^{-1} leading to an increased concentration of magnesium in both solutions (step 1 in **Scheme 1**). Similar effects of the gradual dissolution of Mg^{2+} ions from the hydrotalcite structure were previously observed by Stoica *et al*.[58]

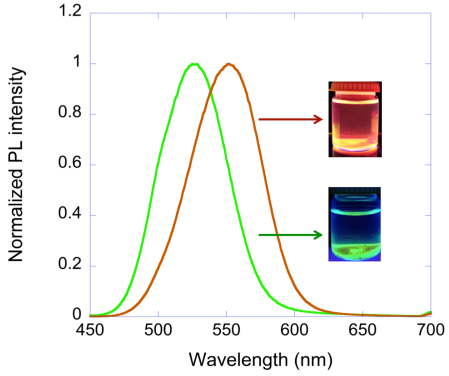

Figure 9. Photoluminescence emission spectra of HTas-QD at *t* = 0 (orange spectrum) and after 3 month (green spectrum) stability test in saline serum. Additionally, the same samples under UV light are shown.

Moreover, Xue *et al.*[68] reported that when the pH value increases, the surface of CdTe QDs can accommodate negative and positive ions charges. The same authors investigated the response of CdTe QD fluoride nanoassembly in the presence of a higher amount of anions and cations. Cl^-, Br^-, I^-, SO_4^{2-}, NO_3^-, Ac^-, HCO_3^-, HPO_4^-, NO_2^- were selected as the interferential anions and Ag^+, Mg^{2+}, Ca^{2+}, Zn^{2+}, Cu^{2+} served as the interferential cations. They concluded that the cations affected the luminescence response of quantum dots.[68] Our reaction media being rich in chloride, phosphate, carbonate and hydroxyl anions, has doped the quantum dots surface and modifies their emission properties. The high lability of magnesium to dissolve from the solid hydrotalcite structure makes it prone to further attach to the anions (step 2 in **Scheme 1**). Several studies in the field of thin films reported also the doping of CdS, CdSe and CdTe nanocrystal structures leading to $Cd_{1-x}Mg_xS(Se,Te)$ alloys.[69,70,71] Besides, pure MgTe exhibited a higher band gap. Our HTas-QD composite could undergo similar doping process, finally translated into a blue-shift emission.

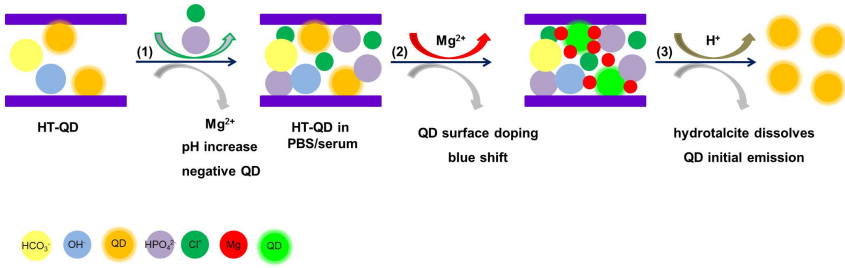

Scheme 1. Pictorial representation of the factors responsible for the blue shift of CdTe quantum dots. The quantum dot-hydrotalcite interaction, magnesium dissolution and ultimate doping at the quantum dot surface, as well as the presence of the anions induce the transient blue shift emission. Dissolution of hydrotalcite ends up in the recovering of the original fluorescence due to the optical memory effect of CdTe quantum dots.

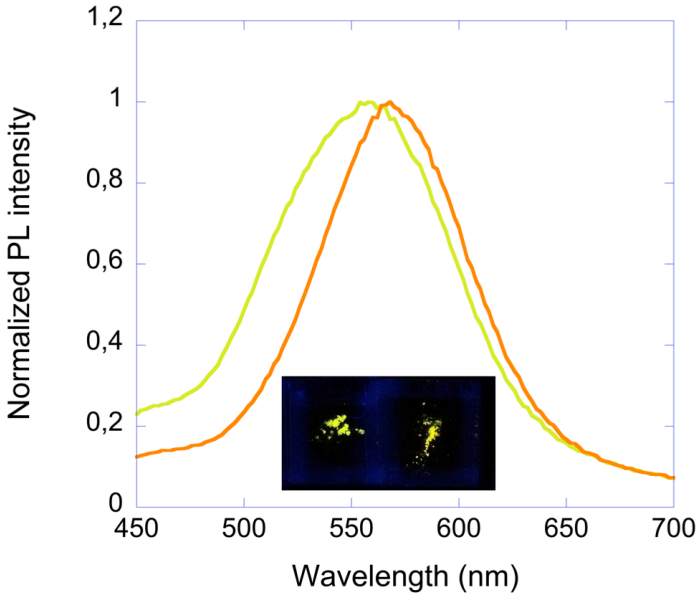

Figure 10. Photoluminescence emission spectra of the solid HTas-QD stored in PBS (yellow spectrum) and saline serum (orange spectrum), respectively, after 3 months. Below are shown the same samples under UV light (Left= in PBS, right in saline serum).

At the end of the stability test, the solids from both the PBS and saline serum solutions were washed, filtered and dried for further photoluminescence measurement. As shown in Figure 10, the emission specific to quantum dots was recovered, slightly shifting to 570 nm in the orange emission range, suggesting that the sample has a memory of the initial state (step 3 in Scheme 1). This phenomenon is known as optical memory effect of quantum dots and has been previously reported for CdSe, CdSe/CdS, InGaN, or CdTe systems.[72,73,74,75] In agreement with this observation, after excitation with a blue laser at 488 nm, HTas-QD samples exhibited uniform yellowish-orange fluorescence (Figure 10).

Hypothesis 3. Decrease of quantum dot size. Under oxidative and photolytic conditions, QD core-shell coating have been found to be labile, degrading and thus exposing potentially toxic “capping” material or intact core metalloid complexes or resulting in dissolution of the core

complex to QD core metal components (*e.g.* Cd).76 Wuister *et al.77* detected a blue shift when comparing two different CdTe QDs samples at 5 min and 20 min synthesis reaction, respectively. They attributed this change to photo-oxidation of the quantum dots as CdTe is very sensitive to oxygen. Photo-oxidation of semiconductor QDs is a well investigated process for CdS and has also been seen for CdSe.78,79,80,81 As oxidation occurs, the surface layer of the QD lattice is oxidized resulting in a smaller semiconductor particle size and thus in a blue shift in the spectrum.

Venugopal *et al.* excluded this hypothesis.43 In turn, they reported that the aggregation of semiconductor nanoparticles resulting in the delocalization of energy states might be responsible for the blue shift of LDH-DS CdSe composites. This delocalization is lost when the sample is diluted in a matrix. Thus, dilution/deaggregation itself can cause changes in optical behavior. While a very small component of the blue shift of the absorbtion maxima could be due to dilution effects, the major contribution to the observed shift comes from the host layer-nanoparticles interaction. The matrix layers appear to be strongly interacting with the nanoparticles leading to the elimination of surface defects, which decreases the density of the dissolved states.[43]

Additionally, in this particular case of QDs, the disintegration of hydrotalcites at pH lower than 5 might be accompanied by the decrease of the quantum dots PL since they are not stable in acidic media as demonstrated by previous studies.[82,83] Indeed, after the 12 weeks stability test, the saline serum and PBS solutions containing the HT-QD samples were acidified in a controlled manner until pH 5. In this way, we managed to partially dissolve the HT-QD and release the quantum dots. Under UV light, the reaction solution displayed uniform orange fluorescence indicating the release of quantum dots (right vial photo in Figure 11). Additionally, the PL measurement shown in Figure 11, indicated the presence of two QDs populations as it comes: one centered at 590 nm and another one at 520 nm, respectively. The peak

at 590 nm is attributed to the freed QDs, while the emission at 520 nm arises from the QDs intercalated with LDH. This result is the best confirmation that MgAl hydrotalcite affects the optical properties of CdTe quantum dots.

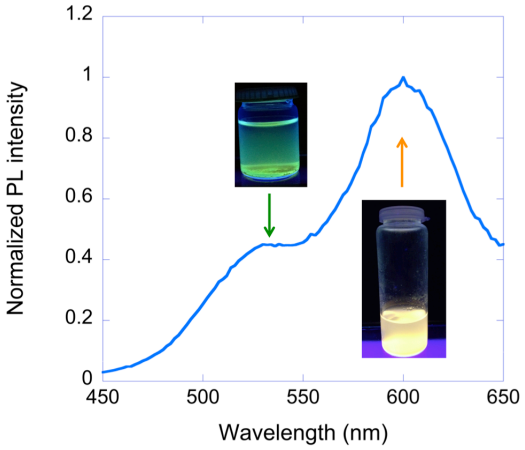

Figure 11. Photoluminescence emission spectrum of the sample HTas-QD in saline serum partially dissolved.

Based on this observation and complemented with the previous hypotheses, it can be concluded that the optical behavior of the CdTe QD is affected by the interaction LDH matrix-nanoparticles, with particular focus on magnesium, which is doping the nanocrystals surface. In other words, when hydrotalcite dissolves, the QDs recover their initial optical characteristics due to the memory effect property. Additionally, the surface doping, LDH-QD interaction, or the solvents are only transient causes for the QD photoluminescence. When these inducers are removed, the original fluorescence is recovered. Based on the same reasoning, oxidation at the QD surface is excluded.[84] If that would be the case, the final PL should be in the green-yellowish PL range and not orange as it is in our case, since quantum dot surface oxidation is an irreversible process.[85]

Hydrotalcite-coated QDs@silica by exfoliation-restacking

The possible accumulation of the metals in the cells could have negative effects at longer times if QD-embedded hydrotalcites are used for bio-medical applications. QD toxicity depends on multiple factors derived from both individual physicochemical properties and environmental conditions: QD size, charge, concentration, outer coating bioactivity (capping material, functional groups), and oxidative, photolytic, and chemical stability.[86] Cadmium and selenium, two of the most widely used constituent metals in QD core metalloid complexes are known to cause acute and chronic toxicities in vertebrates and are of considerable human health and environmental concern.[86] Cadmium, a biological carcinogen, has a biologic half-life of 15-20 years in humans, bioaccumulates, can cross the blood-brain barrier and placenta, and is systemically distributed to all body tissues, with liver and kidney being target organs of toxicity.[86] Besides, cadmium ions have been shown to bind to thiol groups on critical molecules in the mitocondria determining cell death.[87]

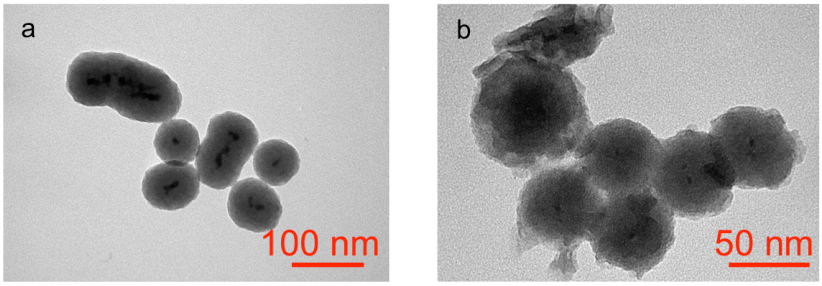

Figure 12. Transmission electron micrographs of (a) QDs@silica and (b) HTd-QDs@silica, respectively. The scale bar is displayed for each micrograph.

Addionally, some ligands themselves have proven toxic in a number of biological systems.88,89,90 Lovric *et al.*91 found that CdTe QDs coated with mercaptopropionic acid (MPA) and cysteamine were cytotoxic for a cell culture at concentrations of 10 ug/mL, higher than for uncoated CdTe QDs. They hypothesised that CdTe QDs induced cell death by

apoptosis initiated by the reactive oxygen species (ROS). In addition to MPA, also mercaptoacetic acid (MAA), both commonly used for solubilization, have been shown to be mildly cytotoxic.90 Mercaptoundecanoic acid (MUA), cysteamine and TOPO have all been shown to have the ability to damage DNA in the absence of the QD core.88 QD size was also observed to affect subcellular distribution, with smaller cationic QDs localizing to the nuclear compartment and larger cationic QDs localizing to the cytosol.86,92

Choy *et al.* proposed the cellular uptake mechanism on how LDH nanoparticles deliver their cargo into the cells.25 Once in the cell, the endocytosed LDH-cargo nanocomposites are stored in the endosomes where the LDH particles partially dissolve resulting in the subsequent buffer of the pH. This phenomenon will induce the rupture of the endosomes facilitating the release of the LDH hybrids and free the cargo into the cytoplasm.24,36 In further studies it was found that another possible release pathway could be the ion-exchange with cytoplasmic ions (*i.e.*, Cl-, PO43-, etc.) once the nanoparticles are internalized, but this seems to occur on a much slower timescale.37 Extrapolating to our system, QD-containing hydrotalcites could only undergo the endocytosis process discharging the quantum dots in the cells. The QD-chloride or QD-phosphate anion-exchange is not taking place since no fluorescence was detected in the saline serum or PBS solutions, respectively. Nevertheless, uptake of negatively charged Cl- or HPO43- by the hydrotalcite is not excluded either.

A direct way to avoid the posible toxicity of QDs or the change in optical quality, is to make them well coated to become biologically inert. The coating materials can be low or nontoxic organic molecules/polymers (e.g., PEG) or inorganic layers (e.g., ZnS and silica).87,93 The fundamental notion is that additional layers act as physical barrier to the core. Previous studies demonstrated that QD-“onion”-multicode silica nanospheres display high stability in the biological pH range, *i.e.* 4-9, while preserving the QD photoluminescence.15,16 Given that silica nanoparticles (SNP) are robust, bio-inert, and easy to control in size

and morphology, they have been employed as theranostic carriers to deliver imaging agents and therapeutic molecules.[94] In particular, mesoporous SNP is an attractive nanoscafold to build multi-task nanotools.[95]

In this purpose, similarly to the HT*x*-QD case, HTas and HTd were chosen as starting materials for the intercalation of fluorescent CdSe/ZnS QDs@silica nanoparticles. The silica spheres had a size of 50 nm and incorporated one-two quantum dots nanoparticles as a core during their *in situ* formation (Figure 12a). As expected, sample HTd-QDs@silica displayed a higher yield of QDs@silica beads coated with a thin LDH layer as the outer rim when observed by electron microscopy. This is a consequence of the bigger size of CdSe/ZnS QDs@silica nanoparticles (Figure 12b) in comparison with the CdTe QDs only, *i.e.* 4 nm *vs.* 50 nm. Besides, the interlayer space in LDH has a very limited size. Therefore, we chose to exemplify herein the exfoliation-restacking strategy to prepare the QDs@silica-LDH composite.

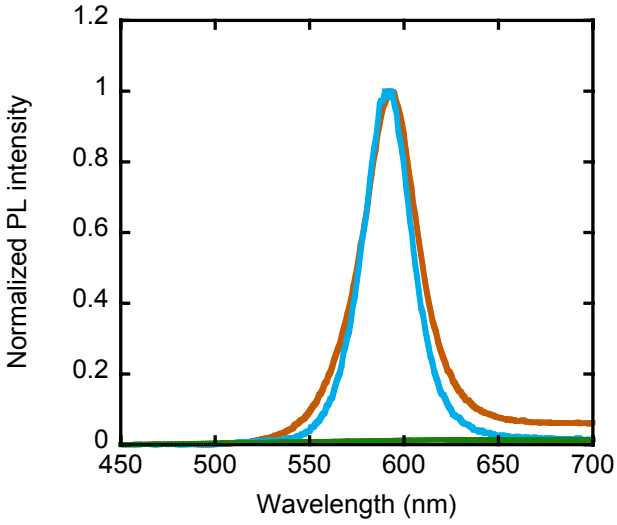

Figure 13. Photoluminescence emission spectra of CdSe QDs (orange), CdSe QDs@silica (blue), and the filtrate resulting from treatment of CdSe QDs@silica in delaminated (HTd) hydrotalcite (green).

The X-ray diffraction pattern in Figure 1 of the solid resulting from treatment of HTd with QDs@silica shows that the hydrotalcite structure was recovered after 1 day. In agreement with XRD, the thermogravimetric analysis of the sample (Figure 2) displayed the typical two-step behavior of hydrotalcite decomposition with decreasing the total weight loss from 48% in HTas to 35.5% in HTd-QDs@silica, with a significant difference in the first step (19% *vs.* 10%) attributed to the loss of water from the hydrotalcite structure. Based on these facts, our results indicate a lower amount of water in the composite material due to the formation of silanol confirmed by the infrared measurements in Figure 3. The strong vibration at 1090 cm^{-1} is assigned to the stretching mode of Si-O-Si, pointing to the formation of a carbonate LDH shell on the surface of SiO_2 core after the restacking procedure.[39] Additional bands corresponding to Si-O-Si symmetric and asymmetric vibrations observed at 1140 and 797 cm^{-1}, respectively, are specific to silica-overcoated quantum dots.[96] The band at 965 cm^{-1} is assigned to Si-OH groups and the shoulder at 2850-2960 cm^{-1} is attributed to the C-H stretching of the octyl group characteristic of TOPO (used during CdSe QDs synthesis).[97]

The morphology of the HTd-QDs@silica sample is displayed in Figure 12b. It can be seen that the surface of QDs@silica beads differs in comparison with the starting nanospeheres, with a thin LDH coating layer as the outer rim. This observation supports the thermal analysis and infrared results and represents the outcome of the chemical interaction between the positively charged LDH nanosheets and the hydroxyls groups at the silica nanospheres surface. The isotherm of HTd-QDs@silica (Figure 5) is characteristic of the layered double hydroxides with a significant increase of the total surface area, *i.e.* 81 $m^2\ g^{-1}$, and total pore volume, 0.72 $cm^3\ g^{-1}$.

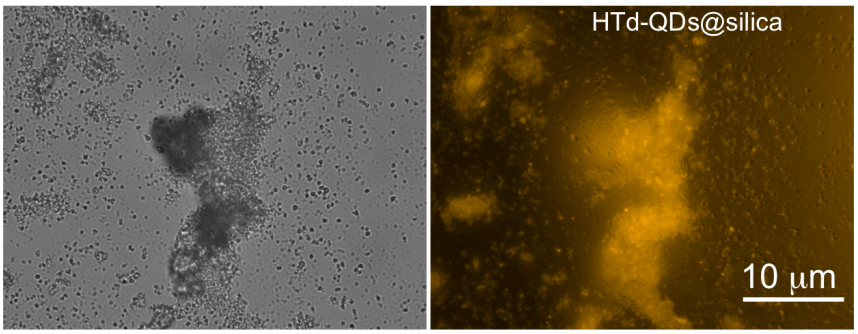

Figure 14. Overview true colour fluorescence images of HT-QDs@silica before (left) and after excitation (right). The scale bar applies for both images.

Comparative photoluminescence emission spectra of QDs@silica ethanolic solution and the filtrate resulting from treatment of delaminated hydrotalcite (HTd) in CdSe QDs@silica at ambient conditions are shown in Figure 13. The emission specific to QDs@silica significantly decreased after 1 day treatment, thus evidencing a high degree of QDs@silica incorporation into hydrotalcite. In order to confirm this latter statement, we performed true colour fluorescence and the image of HTd-QDs@silica is depicted in Figure 14. Digital picture on the left (Figure 14) illustrates the HTd-QDs@silica sample as-such, without excitation. However, after excitation with a blue laser at 488 nm, HTd-QDs@silica exhibited fluorescence arrising from the presence of quantum dots, in agreement with the photoluminescence results.

Conclusions

Layered double hydroxides intercalated with water-soluble CdTe quantum dots were successfully prepared at ambient conditions *via* a one-pot approach from the individual components without any additional treatment. The uptake of quantum dots is a very fast process, 4 h being sufficient to incorporate all the quantum dots. Additionally, delamination of hydrotalcite is not a mandatory requirement. The quantum dot-

hydrotalcite nanomaterials display extremely high stability in physiological media with different pH making them promising imaging tools for diagnostic in nanomedicine. Remarkably, the optical properties of quantum dots changed from orange to green-yellowish. This blue shift was attributed to several factors like the quantum dot-hydrotalcite interaction, magnesium dissolution and ultimate doping at the quantum dot surface, as well as the presence of chloride, phosphate, carbonate and hydroxyl anions. However, their effect is reversible upon the dissolution of the solid host. It can be concluded then that the blue shift originates from the surface changes only, while the bulk core is not affected. Besides, CdTe quantum dots display optical memory effect. The optical properties transitions were stopped when preparing QDs@silica core / LDH shell nanospheres, silica acting like a barrier between the quantum dot and hydrotalcite. This combination is reported herein for the first time and leads to efficient barrier for leaching processes of the QDs in biological alike media. In overall, we created advanced nanostructured inorganic scaffolds that will prevent cytotoxicity and will permit multimodal imaging and simultaneous diagnosis in advanced therapeutical systems.

References

1. Tu, C.; Yang, Y.; Gao, M. Nanotechnology, 2008, 19, 105601.
2. Ho, Y. P.; Leong, K. W. Nanoscale, 2010, 2, 60.
3. Ma, X.; Zhao, Y.; Liang, X. J. Acc. Chem. Res., 2011, 44, 1114.
4. Choi, K. Y.; Liu, G.; Lee, S.; Chen, X. Nanoscale, 2012, 4, 330.
5. Penn, S. G.; He, L.; Natan, M. J. Curr. Opin. Chem. Biol., 2003, 7, 609.
6. Braeckmans, K.; de Smedt, S. C.; Leblans, M.; Pawells, R.; Demeester, J. Nat. Rev. Drug Discovery, 2002, 1, 447.
7. Meza, M. B. Drug Discovery Today, 2000, 1, 38.
8. Walt, D. R. Curr. Opin. Chem. Biol., 2002, 6, 689.

9. Resch-Genger, U.; Grabolle, M.; Cavaliere-Jaricot, S.; Nitschke, R.; Nann, T. Nat. Methods, 2008, 5, 763.

10. Liu, A.; Peng, S.; Soo, J. C.; Kuang, M.; Chen, P.; Duan, J. Anal. Chem, 2011, 83, 1124.

11. Pan, J.; Wan, D.; Gong, J. Chem. Commun, 2011, 47, 3442.

12. Ma, Q.; Su, X. Analyst, 2010, 135, 1867.

13. Ma, Q.; Wang, C.; Su, X. J. Nanosci. Nanotechnol, 2008, 8, 1138.

14. Sukhanova, A.; Nabiev, I. Crit. Rev. Oncol. Hematol, 2008, 68, 39.

15. Ma, Q.; Castello, I.; Palomares, E. Chem. Commun, 2011, 47, 7071.

16. Castello, I.; Ma, Q.; Palomares, E. J. Mater. Chem, 2011, 21, 17673.

17. Kneuer, C.; Sameti, M.; Bakowsky, U.; Schiestel, T.; Schirra, H.; Schmidt, H.; Lehr, C. M. Bioconjugate Chem., 2000, 11, 926.

18. Kneuer, C.; Sameti, M.; Haltner, E. G.; Schiestel, T.; Schirra, H.; Schmidt, H.; Lehr, C. M. Int. J. Pharm., 2000, 196, 257.

19. Kulmeet, K. S.; Mcintosh, C. M.; Simard, J. M.; Smith, S. W.; Rotello, V. M. Bioconjugate Chem., 2002, 13, 3.

20. Cavani, F.; Trifiro, F.; Vaccari, A. Catal. Today, 1991, 11, 173.

21. Braterman, P. S.; Xu, Z. P.; Yarberry, F. Layered Double Hydroxides (LDHs). Handbook of Layered Materials, ed. S. M. Auerbach, K. A. Carrado and P. K. Dutta, CRC Press, New York, 2004, p. 373.

22. Xu, Z. P.; Zeng, Q. H.; Lu, G. Q.; Yu, A. B. Chem. Eng. Sci., 2005, 61, 1027.

23. Kriven, W. M.; Kwak, S. Y.; Wallig, M. A.; Choy, J. H. MRS Bull, 2004, 29, 33.

24. Xu, Z. P.; Niebert, M.; Porazik, K.; Walker, T. L.; Cooper, H. M.; Middelberg, A. P.; Gray, P. P.; Bartlett, P. F.; Lu, G. Q. J. Controlled Release, 2008, 130, 86.

25. Choy, J. H.; Kwak, S. Y.; Jeong, Y.J.; Park, J. S. Angew. Chem., Int. Ed., 2000, 39, 4042.

26. Choy, J. H.; Kwak, S. Y.; Park, J. S.; Jeong, Y. J.; Portier, J. J. Am. Chem Soc, 1999, 121, 1399.

27. Choy, J. H.; Kwak, S. Y.; Park, J. S.; Jeong, Y. J. J. Mater. Chem, 2001, 11, 1671.

28. Lin, M. S.; Sun, P.; Yu, H. Y. J. Formosan Med. Assoc, 1998, 97, 704.

29. Simoneau, G. Eur. J. Drug Metab. Pharmacokinet., 1996, 21, 351.

30. Tarnawski, A. S.; Pai, R.; Itani, R.; Wyle, F. A. Digestion, 1999, 60, 449.

31. Khan, A. I.; O'Hare, D. J. J. Mater. Chem, 2002, 12, 3191.

32. Xu, Z. P.; Lu, G. Q. Pure Appl. Chem, 2006, 78, 1771.

33. Ren, L.; Wan, L.; Duan, X. Int. J. Nanotechnol, 2006, 3, 545.

34. Leroux, F.; Taviot-Gueho, C. J. J. Mater. Chem, 2005, 15, 3628.

35. Kameshima, Y. Mater. Integr, 2007, 20, 101.

36. Choy, J. H.; Oh, J. M.; Choi, S. J. Bio-inorganic Hybrid Materials, ed. E. Ruitz-Hitzky, K. Ariga and Y. Lvov, Wiley-VCH, Weinheim, Germany, 2008, p. 401.

37. Gu, Z.; Thomas, A. C.; Xu, Z. P.; Campbell, J. H.; Lu, G. Q. (Max). Chem. Mater, 2008, 20, 3715.

38. Chaudhuri, R. G.; Paria, S. Chem. Rev., 2012, 112, 2373.

39. Li, L.; Feng, Y.; Li, Y.; Zhao, W.; Shi, J. Angew. Chem. Int. Ed., 2009, 48, 5888.

40. Pan, D.; Zhang, H.; Fan, T.; Chen, J.; Duan, X. Chem. Commun, 2011, 47, 908.

41. Mi, F.; Chen, X.; Ma, Y.; Yin, S.; Yuan, F.; Zhang, H. Chem. Commun, 2011, 47, 12804.

42. Shao, M.; Ning, F.; Zhao, J.; Wei, M.; Evans, D. G.; Duan, X. J. J. Am. Chem Soc, 2012, 134, 1071.

43. Venugopal, B. R.; Ravishankar, N.; Perrey, C. R.; Shivakumara, C.; Rajamathi, M. J. J. Phys. Chem. B, 2006, 110, 772.

44. Bendall, J. S.; Paderi, M.; Ghigliotti, F.; Pira, N. L.; Lamberyini, V.; Lesnyak, V.; Gaponik, N.; Visimberga, G.; Eychmuller, A.; Sotomayor Torres, C. M.; Welland, M. E.; Gieck, C.; Marchese, L. Adv. Funct. Mater, 2010, 20, 3298.

45. Hibino, T.; Jones, W. J. J. Mater. Chem, 2001, 11, 1321.

46. Hibino, T.; Kobayashi, M. J. Mater. Chem, 2005, 15, 653.

47. Jaubertie, C.; Holgado, M. J.; San Roman, M. S.; Rives, V. Chem. Mater, 2006, 18, 3114.

48. Venugopal, B. R.; Shivakumara, C.; Rajamathi, M. J. Colloid Interface Sci, 2006, 294, 234.

49. Hibino, T. Chem. Mater, 2004, 16, 5482.

50. Aldana, J.; Wang, Y. A.; Peng, X. J. Am. Chem Soc, 2001, 112, 8844.

51. Zhu, C. Q.; Wang, P.; Wang, X.; Li, Y. Nanoscale Res. Lett, 2008, 3, 213.

52. Brunauer, S.; Emmett, P. H.; Teller, E. J. Am. Chem Soc, 1938, 60, 309.

53. Lippens, B. C.; de Boer, J. H. J. Catal, 1965, 4, 319.

54. Kloprogge, J. T.; Frost, R. L. J. Solid State Chem, 1999, 146, 506.

55. Perez-Ramırez, J.; Mul, G.; Kapteijn, F.; Moulijn, J. A. J. Mater. Chem, 2001, 11, 821.

56. Sing, K. S. W.; Everett, D. H.; Haul, R. A. W.; Moscou, L.; Pierotti, R. A.; Rouquerol, J.; Siemieniewska, T. Pure Appl. Chem, 1985, 57, 603.

57. Gordijo, C. R.; Leopoldo Constantino, V. R.; de Oliveira Silva, D. J. Solid State Chem, 2007, 180, 1967.

58. Stoica, G.; Santiago, M.; Abello, S.; Perez-Ramırez, J. Solid State Sci, 2010, 12, 1822.

59. Wu, Q.; Olafsen, A.; Vistad, B. O.; Roots, J.; Norby, P. J. Mater. Chem, 2005, 15, 4695.

60. Leroux, F.; Adachi-Pagano, M.; Intissar, M.; Chauviere, S.; Forano, C.; Besse, J. P. J. Mater. Chem, 2001, 11, 105.

61. Adachi-Pagano, M.; Forano, C.; Besse, J. P. Chem. Commun, 2000, 91.

62. Bagaria, H. G.; Ada, E. T.; Shamsuzzoha, M.; Nikles, D. E.; Johnson, D. T. Langmuir, 2006, 22, 7732.

63. Mak, J. S. W.; Farah, A. A.; Chen, F.; Helmy, A. S. ACS Nano, 2011, 5, 3823.

64. Rives, V. Mater. Chem. Phys., 2002, 75, 19.

65. Di Cosimo, J. I.; Diez, V. K.; Xu, M.; Iglesia, E.; Apesteguia, C. R. J. Catal, 1998, 178, 499.

66. Tamura, H.; Chiba, J.; Ito, M.; Takeda, T.; Kikkawa, S.; Mawatari, Y. Tabata, M. J. Colloid Interface Sci, 2006, 300, 648.

67. Costantino, U.; Marmottini, F.; Nocchetti, M.; Vivani, R. Eur. J. Inorg. Chem, 1998, 10, 1439.

68. Xue, M.; Wang, X.; Wang, H.; Chen, D.; Tang, B. Chem. Commun, 2011, 47, 4986.

69. Reshina, I. I.; Ivanov, S. V.; Mirlin, D. N.; Sedova, I. V.; Sorokin, S. V. Semiconductors, 2005, 39, 432.

70. Hirayama, Y.; Kojima, E.; Takeyama, S.; Karczewski, G.; Wojtowicz, G.; Kossut, J. Phys. Rev. B: Condens. Matter Mater. Phys, 2009, 79, 125327.

71. Lucero, M. J.; Aguilera, I.; Diaconu, C. V.; Palacios, P.; Wahnon, P.; Scuseria, G. E. Phys. Rev. B: Condens. Matter Mater. Phys, 2011, 83, 205128.

72. Fischbein, M. D.; Drndic, M. Appl. Phys. Lett, 2005, 86, 193106.

73. Yordanov, G. G.; Gicheva, G. D.; Dushkin, C. D. Mater. Chem. Phys, 2009, 113, 507.

74. Feldmeier, C.; Abiko, M.; Schwarz, U. T.; Y. Kawakami and R. Micheletto, Opt. Express, 2009, 17, 22855.

75. Kumar, K.; Prakash, J.; Khan, M. T.; Dhawan,; Biradar, A. M. Appl. Phys. Lett, 2010, 97, 163113.

76. Derfus, A. Nano Lett, 2004, 4, 11.

77. Wuister, S. F.; van Driel, F.; Meijerink, A. Phys. Chem. Chem. Phys, 2003, 5, 1253.

78. Spanhel, L.; Haase, M.; Weller, H.; Henglein, A. J. Am. Chem Soc, 1987, 109, 5649.

79. Dunstan, D. E.; Hagfeldt, A.; Almgren, M.; Siegbahn, H. O. G.; Mukhtar, E. J. Phys. Chem., 1990, 109, 5649.

80. van Sark, W. G. J. H. M.; Frederix, P. L. T. M.; van den Heuvel, D. J.; Gerritsen, H. C.; Bol, A. A.; van Lingen, J. N. J.; de Mello Donega, C.; Meijerink, A. J. Phys. Chem. B, 2001, 105, 8281.

81. Hoyer, P.; Staudt, T.; Engelhardt, J.; Hell, S. W. Nano Lett, 2011, 11, 245.

82. Breus, V. V.; Heyes, C. D.; Tron, K.; Nienhaus, G. U. ACS Nano, 2009, 3, 2573.

83. Hu, X.; Gao, X. ACS Nano, 2010, 4, 6080.

84. Liu, L.; Peng, Q.; Li, Y. Inorg. Chem, 2008, 47, 3182.

85. Biju, V.; Ishikawa, M. Molecular Nano Dynamics, Vol. 1: Spectroscopic Methods and Nanostructures, ed. H. Fukumura, M. Irie, Y. Iwasawa, H. Masuhara and K. Uosaki, Wiley-VCH Verlag GmbH & Co. KGaA, Meinheim, Germany, 2009, p. 301.

86. Hardman, R. Environ. Health Perspect, 2006, 114, 165.

87. Walling, M. A.; Novak, J. A.; Shepard, J. R. E. Int. J. Mol. Sci, 2009, 10, 441.

88. Hoshino, A.; Fujioka, K.; Oku, V.; Suga, M.; Sasaki, Y. F.; Ohta, T.; Yasuhara, M.; Suzuki, K.; Yamamoto, K. Nano Lett, 2004, 4, 2163.

89. Hoshino, A.; Hanaki, K.; Suzuki, K.; Yamamoto, K. Biochem. Biophys. Res. Commun, 2004, 314, 46.

90. Kirchner, C.; Liedl, T.; Kudera, S.; Pellegrino, T.; Munoz Javier, A.; Gaub, H. E.; Stolzle, S.; Fertig, N.; Parak, W. J. Nano Lett, 2005, 5, 331.

91. Lovric, J.; Bazzi, H. S.; Cuie, Y.; Fortin, G. R. A.; Winnik, F. M.; Maysinger, D. J. Mol. Med, 2005, 83, 377.

92. Maysinger, D.; Behrendt, M.; Przybytkowski, E. NanoPharmaceuticals, 2006, 1, 1.

93. Mazumder, S.; Dey, R.; Mitra, M. K.; Mukherjee, S.; Das, G. C.; J. Nanomater, 2009, 2009, 1.

94. Cotı, K. K.; Liong, M. E.; Ambrogio, M. W.; Lau, Y. A.; Khatib, H. A.; Zink, J. I.; Khashab, N. M.; Stoddart, J. F. Nanoscale, 2009, 1, 16.

95. Lee, J. E.; Lee, N.; Kim, T.; Kim, J.; Hyeon, T. Acc. Chem. Res., 2011, 44, 893.

96. Yang, H.; Holloway, P. H.; Santra, S. J. Chem. Phys., 2004, 121, 7421.

97. Frasco, M. F.; Vamvakaki, V.; Chaniotakis, N. J. Nanopart. Res, 2010, 12, 1449.

Chapter 5:

Photoluminescent CdSe@CdS/2D as potential biocompatible materials

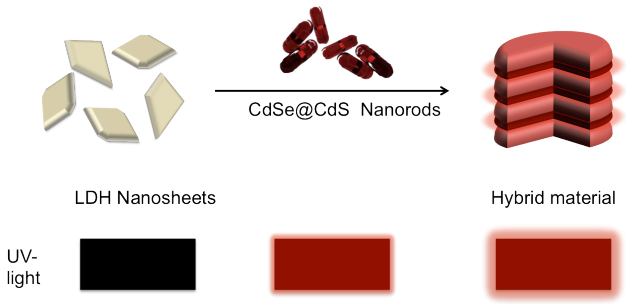

We have successfully fabricated herein a complex hybrid nanostructure composed of 1D CdSe@CdS nanorods and 2D Mg-Al brucite-like nanosheets. The novel material exhibits enhanced photoluminescence when compared to as-prepared CdSe@CdS rods. The results show that the two different starting materials can be heterogeneously integrated as functional components, being the nanorods aligned in parallel to the hydrotalcite crystals. Of particular interest are the changes in the fluorescence emission lifetime of the nanorods depending on the starting form of the host hydrotalcite (as-such or delaminated). The material enhanced photoluminescence reduces the need of higher concentration of CdSe@CdS nanorods, a requisite for their biological use as markers.

TABLE OF CONTENTS

Introduction

The field of photonic nanomaterials has increased exponentially in the last decade with already several applications in the market.[1] Moreover, novel hybrid materials showing properties that none of the individual parts can display are attracting very much interest.[2] For example, several groups have recently reported the use of hydrotalcites as host materials for CdTe or CdSe quantum dots (QD), QDs@silica-LDH core-shell nanostructures as new light emitting devices or for biological applications.[3-5] In particular, our own group explored CdSe nanocrystals embedded in silica shells (CdSe@silica) where the luminescence properties of the CdSe were tuned by the chemical composition of the hydrotalcite to display photoluminescence emission at different wavelength without changing the CdSe size.[3] The original characteristics of hybrid materials based on layered double hydroxides and colloidal quantum nanorods, combining the unique optical properties of the inorganic moiety with the processability of the host matrix (together with stabilization and protection of the CdSe nanocrystals) are highly appealing in view of their technological impact on the development of biological markers. Since quantum dots are well-known sensors and imaging tools,[6-8] other authors have highlighted the potential of nanorods in multicomponent biosensing.[9,10]

Two-dimensional (2D) nanosheets obtained *via* exfoliation of layered compounds have also attracted intensive research in recent years, opening up new fields in the design and synthesis of 2D materials.[11-14] Exploring the use of 2D materials started with the layered double hydroxides and intensified as a result of emerging progress in graphene and novel functionalities offered by the oxide nanosheets.[11,12,15] In particular, layered double hydroxides (LDH) or hydrotalcite-like compunds (HTlc) have raised much interest with potential application in areas raging from catalysis to medical science.[16,17] The structure of this class of compounds is based on that of a natural mineral called hydrotalcite ($Mg_6Al_2(OH)_{16}CO_3{\cdot}4H_2O$), a derivative of brucite $Mg(OH)_2$ where Mg^{2+} ions were replaced by Al^{3+}.[16] From the medical point of view,

many interesting chemical variations of HTlc have been reported since hydrotalcite interlayer space can accommodate a variety of drugs and biomolecules by either anion exchange or delamination-restacking procedure.[16,18,19]

Hydrotalcites are expected to have lower phonon energies due to the lower stretching vibration of Mg-O and Al-O (< 600 cm^{-1}), which might be used to host optically active ions displaying higher phonon energy.[20] So far, only fluorescent molecules alike chromophores, dyes, lanthanide-based complexes, or quantum nanocrystals were impregnated or intercalated between the hydrotalcite layers.[21-24] Nevertheless, the chromophore or QD guest species provide optical functions such as color, fluorescence, and nonlinear (dyes) or a mixture of linear and nonlinear (QD) optical properties.[25-28] Unlike spherical nanoparticles, elongated and rod-shaped direct-band semiconductor nanocrystals, such as CdS, CdSe, or core-shell CdSe@CdS nanorods, possess high photoluminescence quantum efficiency,[29] suppressed Auger recombination,[30] stimulated emission,[31] fast carrier relaxation,[32] and increased Stokes shift in photoluminescence.[33] Besides, their photoemission is highly anisotropic and maximized in the plane perpendicular to the long axis, even at room temperature.[34] Based on these characteristics, semiconductor nanorods became very attractive for applications in solar cells, LEDs, lasers, or cell labeling.[9,35-37] In particular, CdSe@CdS rods present the striking features of strong and tunable light emission from green to red wavelengths with high fluorescence intensity.

Owing to the exceptional biocompatibility property of hydrotalcite-like materials related to the human health and the high luminescence of quantum nanorods, these nanomaterials are excellent candidates in the field of biodetection. To the best of our knowledge, this is the first time that a nanocomposite material prepared by incorporating CdSe@CdS core-shell nanorods in an inorganic layered matrix is proposed and experimentally demonstrated.

Experimental

Materials

Layered double hydrotalcite. Mg-Al hydrotalcite with molar Mg/Al ratio of 3 was synthesized by precipitation at constant pH 10. Briefly, aqueous solutions of $Mg(NO_3)2{\cdot}6H_2O$ (0,75 M) and $Al(NO_3)3{\cdot}9H_2O$ (0,25 M) were put in contact with the precipitating agent, *i.e.* NaOH and Na_2CO_3, 2 M each. The precipitate slurry was aged at room temperature for 12 h under mechanical stirring (500 rpm), followed by filtration, washing and drying at 60ºC for 12 h.

Synthesis of CdSe@CdS quantum nanorods. CdSe@CdS core-shell nanorods have been prepared by following a published seeded-growth method in which a rod-like CdS shell is grown over CdSe quantum dots, the latter acting as seeds, in the presence of an appropriate mixture of phosphonic acids.[34]

Synthesis of CdSe seeds. TOPO (3.0 g), ODPA (0.280 g) and CdO (0.060 g) were mixed in a 50 mL flask, heated to *ca.* 150°C and exposed to vacuum for *ca.* 1 h. Then, under nitrogen, the solution was heated to 320°C to dissolve the CdO until it turned optically clear and colorless. When the solution became optically clear, 1.5 g of TOP was injected in the flask and the temperature was set to 380°C. When this temperature was reached, 0.058 g Se dissolved in 0.360 g TOP were injected into the flask. The heating mantle was immediately removed after injection. The reaction flask was cooled to 100°C and 2 mL of degased toluene were injected into the flask. The nanocrystals were precipitated with methanol, washed by repeated redissolution in toluene and precipitation with the addition of methanol, and finally dissolved in TOP.

Synthesis of CdSe@CdS nanorods. CdSe@CdS nanorods were prepared *via* seeded growth. 0.060 g CdO were mixed in a flask together with 3 g TOPO,

0.290 g ODPA and 0.080 g HPA. After pumping the flask to vacuum for about 1 h at 150°C, the resulting solution was heated to 320°C under nitrogen until the solution became optically clear. Then, 1.5 g of TOP was injected, after which the temperature was set to 370°C. In parallel, a solution containing 0.120 g of elemental S, 400 mL of the previously prepared CdSe Seeds-TOP solution (197 mM) and 1.5 g TOP was prepared in a glass vial. The resulting solution was quickly injected in the flask at 370°C. After injection, the temperature droped to 270-300°C and it recovered within 2 min to the pre-injection temperature. The nanocrystals were allowed to grow for about 8 min after the injection, after which the heating mantle was removed. The nanorods were washed following the same procedure described for CdSe seeds.

Treatments

Two synthetic approaches were followed for the preparation of the composite materials, as detailed next. The first one by treating directly the as-synthesized hydrotalcite with the CdSe@CdS quantum nanorods toluene solution following an anion exchange mechanism, and the second one by exfoliation-restacking, *i.e.* subjecting the hydrotalcite to delamination in formamide and subsequent treatment with the CdSe@CdS quantum nanorods toluene solution. After stirring for 3 days, the mixture was left to rest at ambient conditions for another 3 days. The resulting solid was centrifuged at 4400 rpm for 30 min and redispersed in toluene, and centrifuged again at 4400 rpm for 30 min each. The washing procedure was repeated three times and the final solid was dried at 80ºC for 12 h.

Along the manuscript, the samples were designated by the codes NR (CdSe@CdS quantum nanorods), and HT*x*-NR, where *x* identifies the different starting materials such as parent or as-synthesized (HTas-NR) and delaminated (HTd-NR), respectively. HTas-QD and HTd-QD were labeled according to ref. 1.

Characterization techniques

Powder X-ray diffraction patterns (XRD) were measured in a Bruker AXS D8 Advance diffractometer equipped with a Cu tube, a Ge(111) incident beam

monochromator, and a Vantec-1 PSD. Data were recorded in the range 5-70º 2*q* with an angular step size of 0.016º and a counting time of 6 s per step. Fourier transform infrared (FTIR) spectroscopy was carried out in a Bruker Optics ALPHA spectrometer equipped with a ATR Platinum Diamond unit. Spectra were collected in the range 400-4000 cm^{-1} by co-addition of 32 scans at a nominal resolution of 4 cm^{-1}, taking the spectrum of the empty cell as the background. Transmission Electron Microscopy (TEM) was carried out in a JEOL JEM-1011 microscope operating at 100 kV and equipped with a SIS Megaview III CCD camera. High Resolution Transmission Electron Microscopy (HRTEM) was carried out in a JEOL JEM-2100 microscope operating at 200 kV and equipped with a INCAx-sight detector from Oxford Instruments. A few droplets of the sample suspended in ethanol were placed on a carbon-coated copper grids followed by evaporation at ambient conditions. True color fluorescence images were taken by Nikon TE2000-E CCD microscope. Photoluminescence (PL) spectra were recorded, using a 1 cm path length quartz cell in a Shimadzu UV spectrophotometer 1700 and an Aminco-Bowman Series 2 luminescence spectrometer. Time Correlated Single Photon Counting experiments were carried out with Lifespec picosecond fluorescence lifetime spectrophotometer from Edinburgh Instruments. As excitation source a diode laser with 405 nominal wavelength was used. The instrument response measure at the FWHM was below 350 ps. The laser power was 5 mW.

Results and discusion

Pristine hydrotalcite

The X-ray diffraction (Fig. 1) and infrared (Fig. 2) analyses confirmed hydrotalcite as the unique crystalline phase in the precipitate (JCPDS 22-700) in agreement with previous studies.[38,39] Besides, the materials featured the platelet-like morphology characteristic of these layered materials (HTas in Fig. S1 in Supplementary Information).

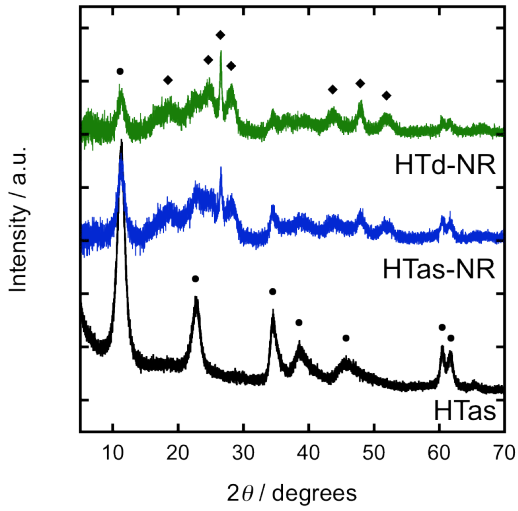

Figure 1. X-ray diffraction patterns of as-synthesized hydrotalcite (HTas) and derived solids. Black: HTas, blue: HTas-NR, green: HTd-NR. Symbols: (•) Hydrotalcite, JCPDS 22-700, (◆) wurtzite, JCPDS 41-1049.

The corresponding diffraction pattern of the exfoliated hydrotalcite evidenced the disappearance of the hydrotalcite reflections, proving the delamination of LDH into positively charged brucite-like nanosheets.[3] This was further confirmed by transmission electron microscopy.[3,40]

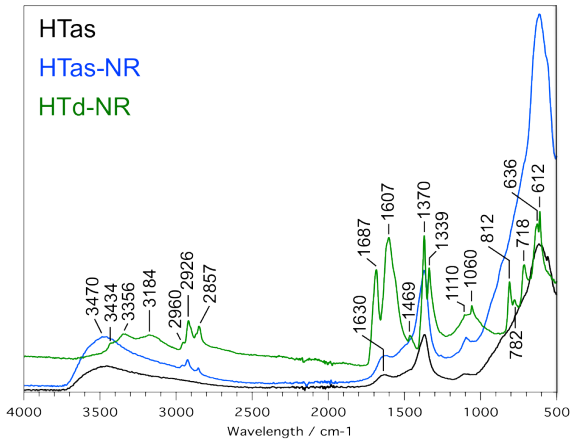

Figure 2. Infrared spectra of HTas (black), HTas-NR (blue), and

HTd-NR (green), respectively.

CdSe@CdS quantum nanorods

The growth of the CdS shell over the previously prepared CdSe seeds led to nanorod structures with an average length of 43 nm and 4 nm in diameter as determined by transmission electron microscopy (Fig. 3). This is translated into a high aspect ratio (rod length/ rod diameter, AR) of *ca.* 11:1. This is was somehow expected since we employed herein the seeded-growth approach[34] which allows to achieve much higher AR values for CdSe@CdS core-shell nanorods than the traditional synthesis reported by Talapin *et al.*[41] for which the maximum AR was 4:1.

Two populations of CdSe@CdS quantum nanorods were used for the experiments carried out in this research, *i.e.* CdSe@CdS_1 and CdSe@CdS_2, respectively. The optical spectra of these samples are shown in Fig. 4. Both the absorbance profile and the FWHM value of the emission peak are in agreement with what can be expected and indicate the quality and homogeneity of the sample.[34] CdSe@CdS_1 nanorods were employed when starting from HTas, meanwhile CdSe@CdS_2 were used for the delamination-restacking approach. In the absorbance spectrum, the peaks/bands from 500 nm to the blue correspond mainly to the CdS shell while the peaks at 598 nm and 618 nm correspond to the CdSe seed and are the only one leading to photoluminescence at 606 nm and 626 nm, respectively.

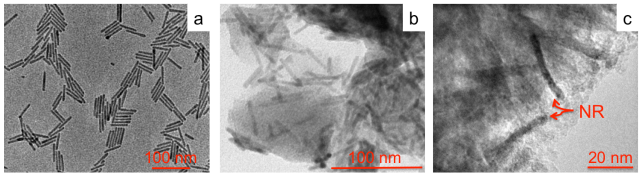

Figure 3. Transmission electron micrographs of selected samples, *i.e.* (a) NR, (b) HTd-NR, and (c) HRTEM HTd-NR, respectively. The scale bar is displayed for each micrograph.

Quantum nanorods – layered double hydroxide composites

Fig. 1 shows the X-ray diffraction patterns of the solids resulting from treatment of HTas and HTd in CdSe@CdS nanorods toluene solution. Interestingly, the hydrotalcite structure was displayed irrespective of the starting material, with hydrotalcite reflections more pronounced in HTas-NR. Likewise, this is the first time that recovery of the hydrotalcite structure was successfully carried out in toluene. So far, toluene was only employed as exfoliation agent of SDS-intercalated hydrotalcite, alone or in combination with CCl_4.[42,43]

As displayed by the XRD patterns of HTas-NR and HTd-NR in Fig. 1, additional reflections can be observed at 2*q* 18º, 25º, 26.5º, 28º, 43º, 47.8º, and 52º, respectively. These reflections correspond to the CdS phase of the CdSe@CdS nanorods.[44] The structure based on the XRD pattern is consistent with predominantly hexagonal CdS, *i.e.* JCPDS 41-1049. The (100), (002), (101), (102), (103) and (112) planes of wurtzite are clearly distinguishable.[45] The reflections of hydrotalcite are still visible although with less intensity and with a slight shift in the basal reflection peak ((003) at 2*q* 11.3º). This suggests the structural similarity between the initial MgAl-LDH host materials and their nanorod intercalation derivatives.[46] The decrease in the intensity of the (003) reflection peak was observed for both HTas-NR and HTd-NR composites, which may be ascribed to the disorder in the stacked structure. The d_{003} basal spacing was calculated for HTas (7.816 nm) and the derived nanocomposites, and an increase was observed, *i.e.* 7.857 nm for HTas-NR and 7.821 nm for HTd-NR. This change may be attributed both to the confinement of LDH crystallites, and to the resultantly weakened electrostatic interaction between the brucite-like sheets and the interlayer species.[44]

In agreement with XRD, the infrared spectra of the samples HTas-NR (blue) and HTd-NR (green) in Fig. 2 reveal both new bands at 2850-2960 cm^{-1} attributed to the C-H stretching of the

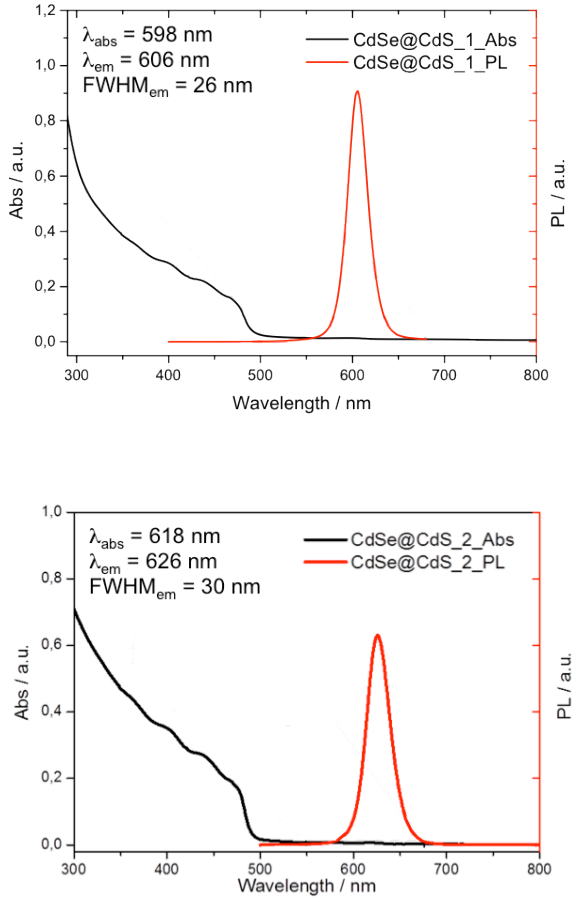

Figure 4. Photoluminescence absorption and emission spectra of CdSe@CdS nanorods in toluene.

octyl group characteristic of TOPO (used during the synthesis of CdSe and CdS seeds).[47] These bands are poorly represented in HTas-NR, where the vibration bands specific to hydrotalcite are predominant indicating a low uptake of nanorods by the layered material (Fig. 2). In contrast, HTd-NR displays significant vibration bands associated with the CdSe@CdS highlighting a more pronounced nanorods intake as a consequence of the delamination procedure. The bands at 2857, 2926, and 29608 cm^{-1}, respectively, specific to the C-H stretching of the octyl group in TOPO

become higher in intensity. Accordingly, more bands characteristic of TOPO became visible at 1060 and 1110 cm^{-1}, respectively, and correspond to the P=O group of the capping ligand.[47] These latter vibrations overlap however with antisymmetric stretching v_3 mode of the carbonate in hydrotalcite at 1105 cm^{-1}. The P=O stretching vibrations shifted to a lower wavenumber with respect to the corresponding vibration for pure TOPO at 1146 cm^{-1}.[47] The P=O stretching vibration peak has also broadened into two peaks as has been observed previously for TOPO-capped CdSe quantum dots.[47] This broadening is attributed to a variety of differing coordination environments that are present on the CdS surface. The absence of the P=O stretch absorption of uncoordinated TOPO indicates that all TOPO present in the sample is coordinated to the CdS surface. The bands at 1469 and 1370 cm^{-1}, respectively, belong to the $d(CH_2)$ and $d(CH_3)$ in-plane deformations,[47,48] while the one at 718 cm^{-1} indicates the presence of $d(CH_2)$ out-of-plane.[47]

Additional bands in the range 3184-3434 cm^{-1} were attributed to symmetric NH stretching vibration in formamide or even possible coupling modes.[49,50] These bands overlap with the OH stretching mode of hydrotalcite. Formamide may be still present in the composite since the delamination step. Furthermore, the band at 1687 cm^{-1} corresponds to the formamide carbonyl C=O stretching band,[51] and is visible at lower wavelengths than in pure formamide, *i.e.* 1755 cm^{-1}.[49,50] This shift may be due to the possible reaction of formamide with toluene during the restacking process. Indeed, the bands at 782-812 cm^{-1} are related to aromatic substitutions like 1,4-disubstituted benzene ring (812 cm^{-1}) and 1,2-disubstituted benzene ring (782 cm^{-1}).[52] The band at 1607 cm^{-1} corresponding to the C=C benzene ring vibration[53] is overlapping with the formamide in-plane NH_2 bending vibration.[50] Although these observations do not represent the main purpose of our work, we would like to shortly give a possible explanation. It is known that formamide-derived compounds are good formylating agents of toluene in the presence of Lewis acid.[54,55] Therefore, it might be possible that following a similar mechanism, metallic CdSe@CdS quantum nanorods act as Lewis acid/base sites which will allow aromatic substitutions. As indicated by the infrared bands intensity, the *para* substitution is favored over *ortho* where the steric hindrance is more

pronounced. On one hand, it is well known that zeolites acid-catalyzed alkylation of toluene with methanol led to the formation of ring alkylated products.[56] On the other hand, several authors reported a photoluminescence (PL) enhancement properties of both single CdSe nanocrystals or nanoparticle-polymer composite in the presence of gaseous amines such as NH_3, CH_3NH_2, $(CH_3)_2NH$, $(CH_3)_3N$, $(CH_3CH_2)_3N$.[57-59] They correlated the PL enhancement with the intrinsic basicity of the amines as an evidence for the acid-base adducts formation between the amine molecules and the atoms at the surface of the semiconducting crystal. Based on these facts, we hypothesize herein that the Lewis acidic characteristics of the metal chalcogenide (surface Cd^{2+} in the CdSe@CdS quantum nanorods) would activate toluene in our system leading to subsequent substitutions with formamide at the benzene ring. Formamide is an amphoteric solvent where the acid or base approaching the basic or acidic site of the molecule leads to reaching the equilibrium.[60]

Both HTas-NR and HTd-NR displayed the typical hydrotalcite platelet morphology. For the sake of conciseness we show HTd-NR in Fig. 3. High-resolution microscopy of this sample clearly indicates the presence of the quantum nanorods together with the layered double hydroxide. Photoluminescence (PL) emission spectra of HTas-NR and HTd-NR are shown in Fig. 5. The optical properties of the nanostructures, and consequently of the quantum nanorods, are very well preserved in combination with the hydrotalcite matrix (see Fig. 4 for comparison purpose) unlike the reported blue shift of quantum dots-layered double hydroxide composites.[3,4] The emission specific to the quantum nanorods is of higher intensity in HTd-NR in comparison with that in HTas-NR. Noteworthy mentioning that the same volume was used for the PL measurement of each sample. The remarkable intensity of HTd-NR indicates a higher uptake of nanorods when the hydrotalcite was previously exfoliated. Therefore, the synthetic strategy involving hydrotalcite delamination is more reactive

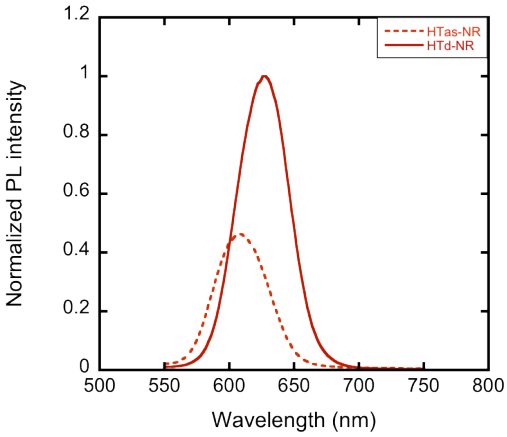

Figure 5. Photoluminescence emission spectra of solid HTas-NR and HTd-NR, respectively.

towards quantum nanorods incorporation, most probably due to the big size of the nanocrystals, 43 nm length and 4 nm diameter *versus* the narrow interlayer space size of the hydrotalcite, *i.e.* 7.816 nm. Keeping this in mind, we propose an arrangement of the quantum nanorods parallel to the layered hydrotalcite whiskers. Similar distribution was observed by electron microscopy in the case of NiAl-layered double hydroxide/graphene or LDH/carbon nanotubes where the NiAl-LDH platelets are predominately oriented face-on (*i.e.*, with *ab* faces parallel) with respect to the substrate.[46,61] In order to confirm the PL measurement, true color fluorescence was carried out and the results are depicted for HTd-NR in Fig. 6. The first image on the left illustrates HTd-NR without excitation, followed by the same sample with excitation (without color in the middle and with color on the right). It can be seen that the light emitted (blue laser at 488 nm) from the clusters is similar in intensity in the whole sample. This indicates a successful uptake of the quantum nanorods around the edges as well as in the center. HTas-NR also showed uniform fluorescence (Fig. S2 in Supplementary Information).

Photoluminescence lifetime of the quantum nanorods – LDH composites

Picosecond-to-nanosecond time-correlated single photon counting (Fig. 7) was used to measure (at the emission peak maximum) the luminescence decay of both the composite materials as well as the individual components, *i.e.* HTas and CdSe@CdS quantum nanorods.

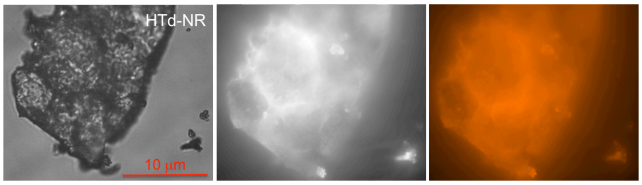

Figure 6. True color fluorescence images of HTd-NR. Left image: HTd-NR without excitation, middle: HTd-NR with excitation (without color), right image: HTd-NR (with color). The samples were excited with a blue laser at 488 nm. The scale bar is the same for all the photos.

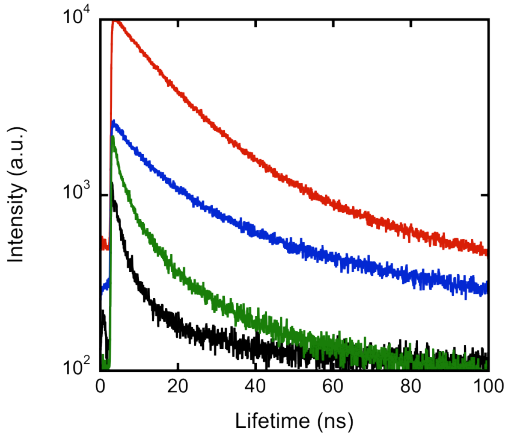

Figure 7. Typical PL decay curves. HTas (black), CdSe@CdS NR (red), HTas-NR (blue), and HTd-NR (green), respectively.

The decay curve of HTas (black curve) can be fitted to a biexponential model described in Chapter 2:

The fitting parameters B_1, τ_1, B_2, τ_2, and τ are summarized in Table 1.

The HTas material has the fastest luminescence lifetime (4.9 ns). On the contrary, the average lifetime of CdSe@CdS is 18.3 ns (red curve) and displays a typical quantum nanorod PL decay spectrum, which consists of two time-decay components with time constants of several nanoseconds and several tens of nanoseconds (Table 1), respectively. The fast decay component is dominant over the slow one in the first 40 ns (Fig. 7). Similar observations were reported by Wang *et al.*,[63] attributing the dominant rapid decay to transitions between electronic bands, and the weak long time-decay to processes involving electronic traps on the surface.[64,65] The PL decays of HTas-NR and HTd-NR are multi-exponentials with the shorter-lived contribution being predominant. The observed bi-exponential decay is the result of a distribution of emission lifetimes caused by different environments surrounding the 1D nanocrystals. As shown in Fig. 7, HTas-NR and HTd-NR exhibit PL decay spectra intermediates between those of HTas and CdSe@CdS, thus confirming the presence of two different environments in the hybrid nanomaterials. Analogous behavior was observed when fluorescent molecules alike chromophores[21-23] or lanthanide-based complexes[20,24] were impregnated or intercalated between the hydrotalcite layers.

The mean luminescence lifetime of HTas-NR (blue curve) and HTd-NR (green curve) are 16.6 and 15.8 ns, respectively. These tendencies are ascribed to the surface modification of the CdSe@CdS quantum nanorods as a consequence of their intercalation between the hydrotalcite layers. The slightly faster lifetime of HTd-NR in comparison with HTas-NR could arise from the differences in the nanorods uptake by the layered material. In other words, hydrotalcite exercises a more pronounced influence on the quantum nanorods in HTd-NR as an outcome of the higher concentration of nanocrystals surrounded by the LDH. While in HTas-NR, the intake is lower as demonstrated by the previous characterization techniques; it could also be that nanorods are partially segregated from the LDH. Thus the surface is

affected in a minor extent. The LDHs are expected to have weaker phonon energies due to lesser stretching vibration of Mg-O (620 cm^{-1}) and Al-O (545 cm^{-1}), which is utilized to host optically active ions displaying higher phonon energy.[20] The phonon energy corresponds to the highest energy stretching vibration bond.

Table 1. Time constants τ_1 and τ_2, components B_1 and B_2, and average lifetime τ of HTas, CdSe@CdS quantum nanorods (NR), CdTe quantum dots (QD), HTas-NR, HTd-NR, HTas-QD, and HTd-QD, respectively.

Sample	B_1 (%)	τ_1 (ns)	B_2 (%)	τ_2 (ns)	τ (ns)
HTas	59.19	2.03	40.81	8.92	4.84
NR	21.96	8.94	78.04	20.95	18.31
QD	12.11	3.42	87.89	28.11	25.12
HTas-NR	43.57	5.66	56.43	25.12	16.64
HTd-NR	35.79	4.54	64.21	22.10	15.81
HTas-QD	65.53	2.77	34.46	13.31	6.40
HTd-QD	45.29	2.53	54.71	21.97	13.17

A similar trend was observed also with the HT-QD-derived materials, in the as-synthesized as well as delaminated form. The PL lifetime of CdTe quantum dots shortened from 25.12 ns to 6.40 ns in HTas-QD and 13.17 ns in HTd-QD, respectively. The spectra display the typical bi-exponential decay where the fast and slow components can be clearly identified (Table 1). Contrarily to the LDH-quantum nanorods series, it is HTas-QD that displays significantly reduced lifetime, very close to HTas. This effect could be the result of quantum dot surface traps doping process induced by the presence of the anionic interlayer species as well as magnesium. In a previous study, we observed a blue shift of CdTe quantum dots in the presence of chloride, phosphate, carbonate and hydroxyl anions, in addition to magnesium.[3] Due to the CdS coating, quantum nanorods display less traps on the surface. When they are embedded into the hydrotalcite, the interlayer environment less affects their lifespan.

Conclusions

Layered double hydroxides intercalated with highly luminescent CdSe@CdS quantum nanorods were successfully prepared at ambient conditions. As expected, the delamination approach proved to be more successful owing to the large-sized nanorods. Due to the same characteristic, a parallel alignment of the nanorods with respect to the hydrotalcite whiskers is proposed. The lifetime decay of the embedded nanorods changed depending on the starting form of the hydrotalcite (as-synthesized or delaminated), but in a lower extent than that observed for quantum dots. Additionally, nanorods preserve their initial optical properties. Therefore, quantum nanorods-hydrotalcite nanostructures exhibit higher luminescence and longer lifetime than with quantum dots, an advantage and prerequisite for the long-term *in vivo* observation associated with the fluorescence microscopy, detection, diagnostic, and bioimaging. In consequence, a lower amount of nanoparticles and less excitation are required when this system is used as biomarker. Implicitly and the most important, lower toxicity/damage will be applied to the cells. The present results highlight the combination of the two fields of optic and nanomaterials as a powerful tool for biodetection.

References

1. Thomas, K. G. Current Trends in Science – Platinum Jubilee Special (ed. N. Mukunda), Indian Academy of Sciences, 2009, 53.

2. Ariga, K.; Mao, L.; Richards, G. J.; Hill, J. P. J. Nanosci. Nanotechnol. 2011, 11, 1.

3. Stoica, G.; Castello, I.; Figuerola, A.; Ugarte, I.; Pacios, R.; Palomares, E. Nanoscale 2012, 4, 5409.

4. Venugopal, B. R.; Ravishankar, N.; Perrey, C. R.; Shivakumara, C.; Rajamathi, M. J. J. Phys. Chem. B 2006, 110, 772.

5. Bendall, J. S.; Paderi, M.; Ghigliotti, F.; Pira, N. L.; Lamberyini, V.; Lesnyak, V.; Gaponik, N.; Visimberga, G.; Eychmüller, A.; Sotomayor Torres, C. M.; Welland, M.; Gieck, C.; Marchese, L. Adv. Funct. Mater. 2010, 20, 3298.

6. Zhang, F.; Lees, E.; Amin, F.; Rivera-Gil, P.; Yang, F.; Mulvaney, P.; Parak, W. J. Small 2011, 22, 3113.

7. Hötzer, B.; Medintz, I. L.; Hildebrandt, N. Small 2012, 8, 2297.

8. Jin, Z.; Hildebrandt, N. Trends Biotechnol. 2012, 30, 394.

9. Artemyev, M.; Kisiel, D.; Abmiotko, S.; Antipina, M. N.; Khomutov, G. B.; Kislov, V. V.; Rakhnyanskaya, A. A. J. Am. Chem Soc, 2004, 126, 10594.

10. O'Sullivan, C.; Crilly, S.; Laffir, F. R.; Singh, A.; Magner, E.; Ryan, K. M. Chem. Commun. 2011, 47, 2655.

11. Geim, A. K.; Novoselov, K. S. Nature Mater. 2007, 6, 183.

12. Osada, M.; Sasaki, T. J. Mater. Chem. 2009, 19, 2503.

13. Ma, R. Z.; Sasaki, T. Adv. Mater. 2010, 22, 5082.

14. Golberg, D. Nature Nanotech. 2011, 6, 200.

15. Leroux, F.; Adachi-Pagano, M.; Intissar, M.; Chauviere, S.; Forano, C.; Besse, J. P. J. Mater. Chem. 2001, 11, 105.

16. Cavani, F.; Trifiro, F.; Vaccari, A. Catal. Today 1991, 11, 173.

17. Braterman, P. S.; Xu, Z. P.; Yarberry, F. Layered Double Hydroxides (LDHs). Handbook of Layered Materials (eds. S. M. Auerbach, K. A. Carrado, P. K. Dutta), CRC Press (New York), 2004, 373.

18. Rives, V.; Ulibarri, M. A. Coord. Chem. Rev. 1999, 181, 61.

19. Hibino, T. Chem. Mater. 2004, 16, 5482.

20. Chen, H.; Zhang, W. G. J. Am. Chem Soc, 2010, 93, 2305.

21. Aloisi, G. G.; Costantino, U.; Elisei, F.; Latterini, L.; Natalia, C.; Nocchetti, M. J. Mater. Chem. 2002, 12, 3316.

22. Costantino, U.; Coletti, N.; Nocchetti, M.; Aloisi, G. G.; Elisei, F.; Latterini, L. Langmuir 2000, 16, 10351.

23. Wagner, B. D. Molecules 2009, 14, 210.

24. Chen, H.; Zhang, W. G. Sci. China Chem. 2010, 53, 1273.

25. Bauer, J.; Behrens, P.; Speckbacher, M.; Langhals, H. Adv. Funct. Mater. 2003, 13, 241.

26. Mackowski, S. Thin Solid Films 2002, 412, 96.

27. Maikhuri, D.; Purohit, S. P.; Mathur, K. C. AIP ADVANCES 2012, 2, 012160-1.

28. Fragnito, H. L.; Rios, J. M. M.; Duarte, A. S.; Palange, E.; Medeiros Neto, J. A.; Cesar, C. L.; Barbosa, L. C.; Alves, O. L.; Brito Cruz, C. H. J. Phys.: Condens. Matter. 1993, 5, A179.

29. Peng, X. G.; Manna, L.; Yang, W.; Wickham, J.; Scher, E.; Kadavanich, A.; Alivisatos, A. P. Nature 2000, 404, 59.

30. Htoon, H.; Hollingsworth, J. A.; Dickerson, R.; Klimov, V. I. Phys. Rev. Lett. 2003, 91, 227401.

31. Kazes, M.; Lewis, D. Y.; Ebenstein, Y.; Mokari, T.; Banin, U. Adv. Mater. 2002, 14, 317.

32. Mohamed, M. B.; Burda, C.; El-Sayed, M. A. Nano Lett. 2001, 1, 589.

33. Hu, J.; Li, L. S.; Yang, W.; Manna, L.; Wang, L. W.; Alivisatos, A. P. Science, 2001, 292, 2060.

34. Carbone, L.; Nobile, C.; De Giorgi, M.; Della Sala, F.; Morello, G.; Pompa, P.; Hytch, M.; Snoeck, E.; Fiore, A.; Franchini, I. R.; Nadasan, M.; Silvestre, A. F.; Chiodo, L.; Kudera, S.; Cingolani, R.; Krahne, R.; Manna, L. Nano Lett. 2007, 7, 2942.

35. Huynh, W. U.; Dittmer, J. J.; Alivisatos, A. P. Science 2002, 295, 2425.

36. Ezhov, A. A.; Shandryuk, G. A.; Bondarenko, G. N.; Merekalov, A. S.; Abramchuk, S. S.; Shatalova, A. M.; Manna, P.; Zubarev, E. R.; Talroze, R. V. Langmuir 2011, 27, 13353.

37. Yuan, Y.; Krüger, M. Polymers 2012, 4, 1.

38. Kloprogge, J. T.; Frost, R. L. J. Solid State Chem. 1999, 146, 506.

39. Pérez-Ramírez, J.; Mul, G.; Kapteijn, F.; Moulijn, J. A. J. Mater. Chem. 2001, 11, 821.

40. Gordijo, C. R.; Leopoldo Constantino, V. R.; de Oliveira Silva, D. J. Solid State Chem. 2007, 180, 1967.

41. Talapin, D. V.; Koeppe, R.; Gotzinger, S.; Kornowski, A.; Lupton, J. M.; Rogach, A. L.; Benson, O.; Feldmann, J.; Weller, H. Nano Lett. 2003, 3, 1677.

42. Jobbagy, M.; Regazzoni, A. E. J. Colloid. Interface Sci. 2004, 275, 345.

43. She, C.; Demortiere, A.; Shevchenko, E. V.; Pelton, M. J. Phys. Chem. Lett. 2011, 2, 1469.

44. Palache, C.; Berman, H.; Frondel, C. Dana's system of mineralogy 1944 (7th edition), vol. I, 228.

45. Chen, S.; Zhang, X.; Zhang, Q.; Tan, W. Nanoscale Res. Lett. 2009, 4, 1159.

46. Li, M.; Zhu, J. E.; Zhang, L.; Chen, X.; Zhang, H.; Zhang, F.; Xu, S.; Evans, D. G. Nanoscale 2011, 3, 4240.

47. Young, A. G.; Al-Salim, N.; Green, D. P.; McQuillan, A. J. Langmuir 2008, 24, 3841.

48. Trindade, T.; O'Brien, P. Chem. Mater. 1997, 9, 523.

49. McNaughton, D.; Evans, C. J.; Lane, S.; Nielsen, C. J. J. Molec. Spectroscopy 1999, 193, 104.

50. Brummel, C. L.; Shen, M.; Hewett, K. B.; Philips, L. A. J. Opt. Soc Am B 1994, 11, 176.

51. Huang, G.; Ma, S.; Zhao, X.; Yang, X.; Ooi, K. Chem. Mater. 2010, 22, 1870.

52. Mayo, D. W.; Miller, F. A.; Hannah, R. W. Course Notes on the Interpretation of Infrared and Raman Spectra, John Wiley & Sons, Inc. (New Jersey), 2003, 126.

53. Farhadyar, N.; Rahimi, A.; Langroudi, A. E. Iranian Polym. J. 2005, 14, 155.

54. Sood, D. S.; Sherman, S. C.; Iretskii, A. V.; Kenvin, J. C.; Schiraldi, D. A.; White, M. G. J. Catal. 2001, 199, 149.

55. Bagno, A.; Kantlehner, W.; Scherr, O.; Vetter, J.; Ziegler, G. Eur. J. Org. Chem. 2001, 15, 2947.

56. Kiwi-Minsker, L.; Bulushev, D. A.; Rainone, F.; Renken, A. J. Molec. Catal. A: Chem. 2002, 184, 223.

57. Meyer, G. J.; Lisensky, G. C.; Ellis, A. B.; J. Am. Chem Soc, 1988, 110, 4914.

58. Yao, Q.; Brock, S. L. Nanotechnol. 2010, 21, 115502-1.

59. Nazzal, A. Y.; Qu, L.; Peng, X. G.; Xiao, M. Nano Lett. 2003, 3, 819.

60. Szatyłowicz, J.; Krygowski, T. M.; Palusiak, M. Struct. Chem. 2012, DOI 10.1007/s11224-012-9973-6.

61. Wang, H.; Xiang, X.; Li, F. J. Mater. Chem. 2010, 20, 3944.

62. Zeng, Q.; Kong, X.; Sun, Y.; Zhang, Y.; Tu, L.; Zhao, J.; Zhang, H. J. Phys. Chem. C 2008, 112, 8587.

63. Wang, X. Y.; Zhang, J. Y.; Nazzal, A.; Darragh, M.; Xiao, M. Appl. Phys. Lett. 2002, 81, 4829.

64. Bawendi, P. C.; Wilson, W. L.; Brus, L. J. Chem. Phys. 1992, 96, 946.

65. Nirmal, M.; Norris, D.; Kuno, M.; Bawendi, M.; Efros, A.; Rosen, M. Phys. Rev. Lett. 1995, 75, 3728.

Chapter 6:
Application of layered double hydroxides-quantum nanocrystals composite nanomaterials in cell bioimaging

The use of hybrid materials, where layered double hydroxides (LDH) act as carriers for the fluorescent semiconductor nanoparticles (QDs, QOM, and nanorods) is described herein. Hydrotalcites are highly compatible with cell membranes, thus allowing the nanoparticles to enter the cell. Differences were observed depending on the nanoparticles delivered.

TABLE OF CONTENTS

Introduction

Understanding how cellular components located at the plasma membrane are able to sense changes in the extracellular environment, transmit signals into the cell, and carry out the uptake of essential molecules is one of the most important problems in the field of cell biology. Endocytic membrane traffic in mammalian cells has an essential role in delivering membrane components, receptor-associated ligands and solute molecules to various intracelular destinations. There are several mechanisms for internalizing molecules from the cell surface. (Figure 1) The most well understood endocytic process – receptor-mediated endocitosis- involves internalization of receptors and their ligands by clathrin-coated pits.[1] Subsequently, the receptor–ligand complexes are endocytosed and delivered to endosomal compartments for degradation or recycling back to the plasma membrane (Figure 2).[2, 3]

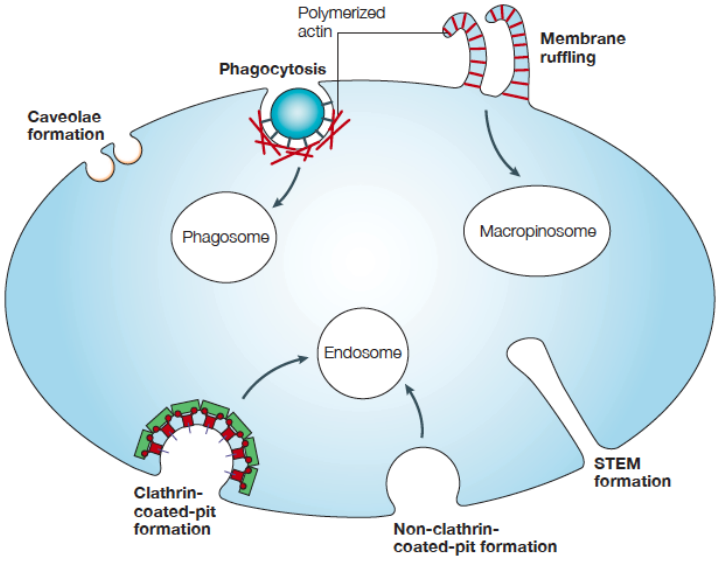

Figure 1. Models of internalization. Several types of plasma-membrane deformation give rise to the formation of sealed endocytic compartments, and the most well known of these begins with clathrin-coated pit formation.

A schematic diagram of endocytic membrane transport pathways that occur after receptor-mediated endocitosis in non-polarized cells is shown in Figure 2. It should be noted that several of the non-clathrin-coated pit internalization pathways fuse with these pathways.[4-6]

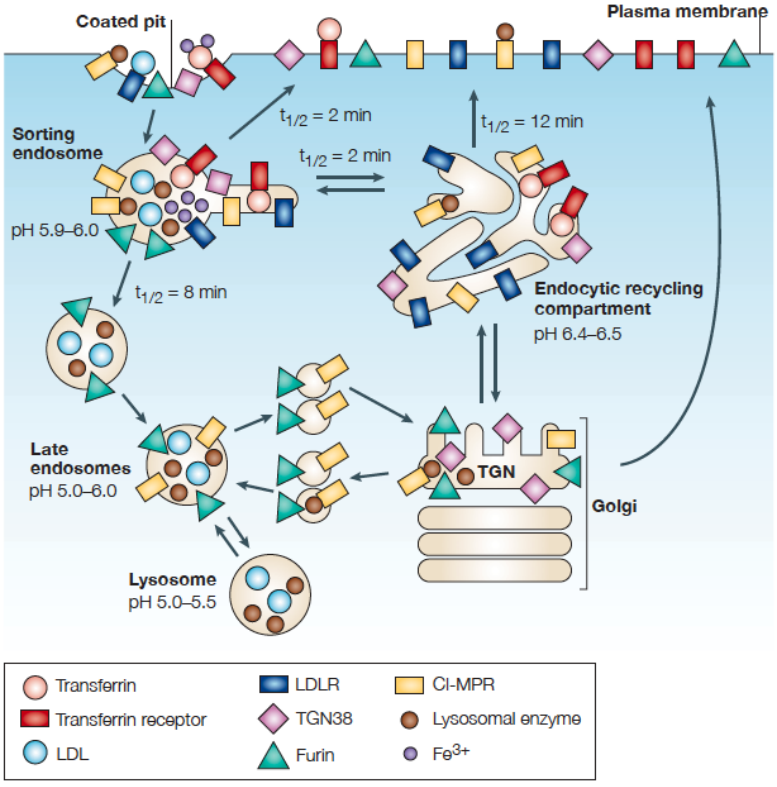

Figure 2. Endocytic recycling pathways. LDLR: Low-density lipoprotein receptor; LDL: low-density lipoprotein; CI-MPR: Cation independent mannose-6-phosphate receptor; TGN: trans-Golgi network.

The development of new QD-based bioimaging technologies is essential to further our understanding of the regulation of receptor-mediated endocytic pathways in cells and tissues.

Because of their brightness and photostability, water-stabilized QDs have been used to track many receptor-mediated endocytic trafficking events in live cells using fluorescence microscopy.[7]

There are several advantages in using QDs versus organic dyes to track membrane receptor dynamics. First, QD–ligand conjugates provide measurements of single or small quantities of ligand-bound receptors, allowing for development of SPT methods.[8-11] Second, QD-based SPT has been used to determine the diffusion characteristics of individual receptors as well as their subcellular localization over time.[10, 12, 13] Third, individual or small assemblies of QD–ligand receptor complexes can be tracked for long periods of time in live cells.[13, 14] In the future, QDs will be used to further advance receptor imaging technology, bringing together the ability to follow individually multiple membrane receptors over long periods of time with three-dimensional resolution[15] and biosensor, multiplexing, and tissue imaging technology. For example, the detailed analysis of QD blinking dynamics may be used in a wide range of biosensing applications.[16] Furthermore, the QD's narrow emission spectra permits the efficient co-tracking of membrane receptors together with one or more regulatory proteins.[8]

The delivery of molecules to mammalian cells with the aim of transferring them across the cell membrane into the cytoplasm is an area of research with increasing importance to medicine. Direct delivery is generally inefficient and suffers from problems such as enzymatic degradation, por bioability, por stability, undesirable accumulative effects of the carrier, and many others. In recent years, it has become apparent that layered double hydroxides (LDH), also known as hydrotalcite or anionic clays form the exception to the rule. Their properties have been explained in previous chapters. Although the intercalation of molecules by anionic exchange decreases their usually positive surface charge, thay remain sufficiently positively charged to facilitate celular uptake.[17]

At present, the most widely accepted mechanism of how LDH delivers its cargo to cells is as follows: 1) ion-exchange of interlayer anions with negatively charged biomolecules facilitates the formation of LDH-bio-nanohybrids; 2) the positive surface charge of the nanoparticles attracts them to the cell surface owing to electrostatic interaction; 3) the LDH-bio-nanohybrids are then taken up by means the receptor-mediated endocytosis; and 4) owing the lower pH in the endosome, the LDH particles dissolve, whereby they buffer the endosomal pH and subsequently facilitate the escape of the LDH-biomolecule hybrids into the cytoplasm by endosome rupture. This mechanism, hypothesized by Choy et al.,[18] is illustrated in Figure 3.

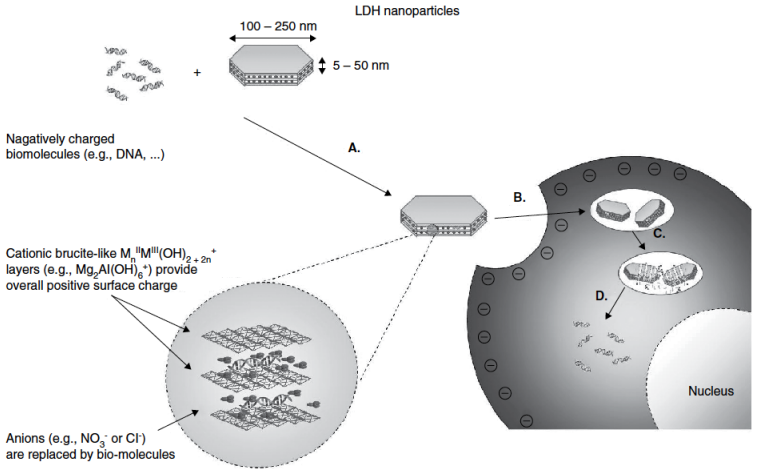

Figure 3. Currently accepted mechanism for LDH-mediated transfection of mammalian cells with DNA. A) Anion exhange between interlayer anions and negatively charged biomolecules (DNA) leads to the formation of LDH-nanohybrids. B) Uptake via receptor-mediated endocytosis. C) Acidification of the endosome causes LDH particles to dissolve slowly, thereby buffering the endosomal pH ("proton-sponge effect") and releasing the biomolecule. D) Further influx of H+ into the endosome and disolution of LDH particles leads to an increase in ionic strength inside the endosome and causes the endosomal membrane to rupture, which liberates the payload (and undissolved particles).

Xu et al.[19] cofirmed that the uptake is by clathrin-mediated endocytosis, together with a minor portion of caveole-mediated endocytosis. In this study it was further shown that endocytosed particles are subsequently stored in slowly acidifying vesicles of the endosomal pathway. Other groups recently came to similar conclusions.[20] However, it is not only able to confirm the uptake of LDH hybrids carrying dye-labelled siRNA molecules by means of endocytosis, but also their perinuclear localization after release into the cytoplasm was identified and the buffering of the endosomal pH using pH-sensitive probe was verified.[21] In further studies it was found that another posible reléase pathway could be ion-exchange with cytoplasmic anions once the nanoparticles are internalized, but this seems to occur on a much slower timescale.[22, 23]

It has been reported that the LDH can be used as host matrix for luminescent dyes[21] but also for nanoparticles (QD, QOM, nanorods and lanthanides), enhancing their photoluminescence and stability.[24-29]
Herein, hydrotalcite-like materials encapsulating luminescent nanoparticles (QDs, QOM and nanorods) were employed for the first time for cell-imaging. The preliminary results obtained from the interaction of these nanoparticles with granulocytes cell culture will be shown. The differences depending on the nature of the nanoparticles will be discussed as well.

Experimental

Materials. CdTe-LDH (QD-LDH), CdSe@silica-LDH (QOM-LDH), and CdSe@CdS-LDH (NR-LDH) composite nanostructures, prepared as detailed in the previous chapters, were employed.

Cell culture. Human granolocytes cell culture, also called polymorphonuclear (PMNs) were provided by the Centre for Innovation Competence - Humoral Immune Reactions in Cardiovascular Diseases (ZIK HIKE), University of Greifswald, Germany.

Cell interaction. First, the hybrid materials were suspended in 1 mL PBS buffer pH 7.2 and sonicated briefly. The incubation was carried out in RPMI media with 10% FCS and PS (antibiotics) for 60 min at 37ºC in a cell culture incubator with 100,000 cells per 1 mL of media and 50 μL of the nanoparticles suspended in the PBS buffer were added. The images were obtained by fluorescence microscopy using a LEICA SP5. Cells were imaged alive after the incubation period. Oregon Green DHPE and DRAQ5 were used for membrane and nucleus labeling, respectively.

Results and discussion

Figure 4-top shows the cell culture in normal light (left) and under excitation (right) making use of QD-LDH hybrid material. As shown by the image on the left, the background is pretty clean, indicating a good uptake by the cells. In Figure 4-bottom,, from left to right, different labelled components of the cells can be observed depending on the channel opened: red for QD-LDH, green for the cell membrane, and in blue the nucleus.

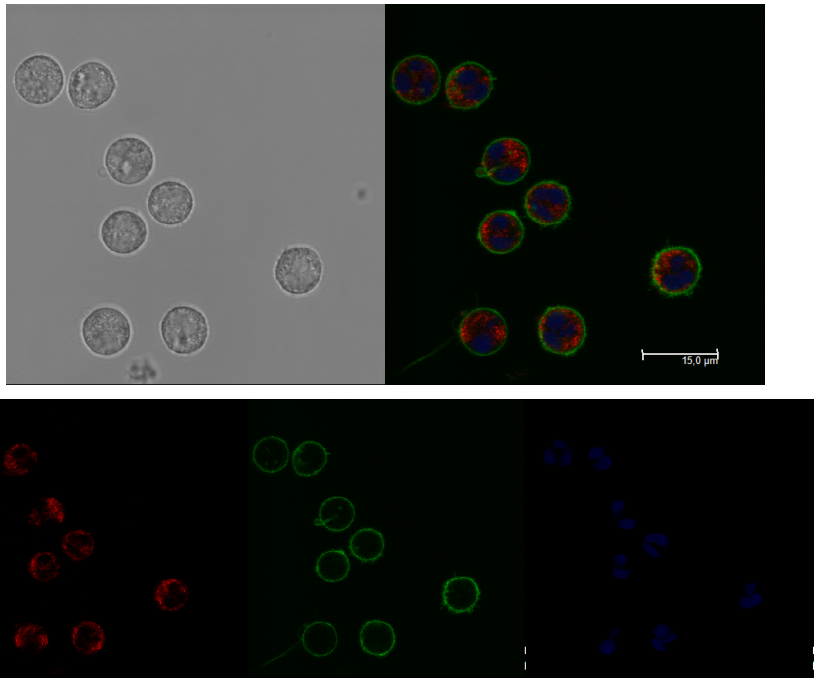

Figure 4. Confocal microscopy pictures of a cell culture of human granulocytes incubated with QD-LDH. Red: LDH-CdTe QDs; Green: Oregon Green DHPE; Blue: DRAQ5.

When using QOM-LDH (Figure 5), the sample became aggregated as indicated by the background scenario. Aggregation is a known phenomenon in the case of silica. Besides, the size of the QOM-LDH (more than 50 nm as demonstrated in the previous chapters) is bigger

when compared to the QD-LDH. Nevertheless, the nanoparticles were still able to pass the membrane barrier as indicated by the red fluorescence inside the cells.

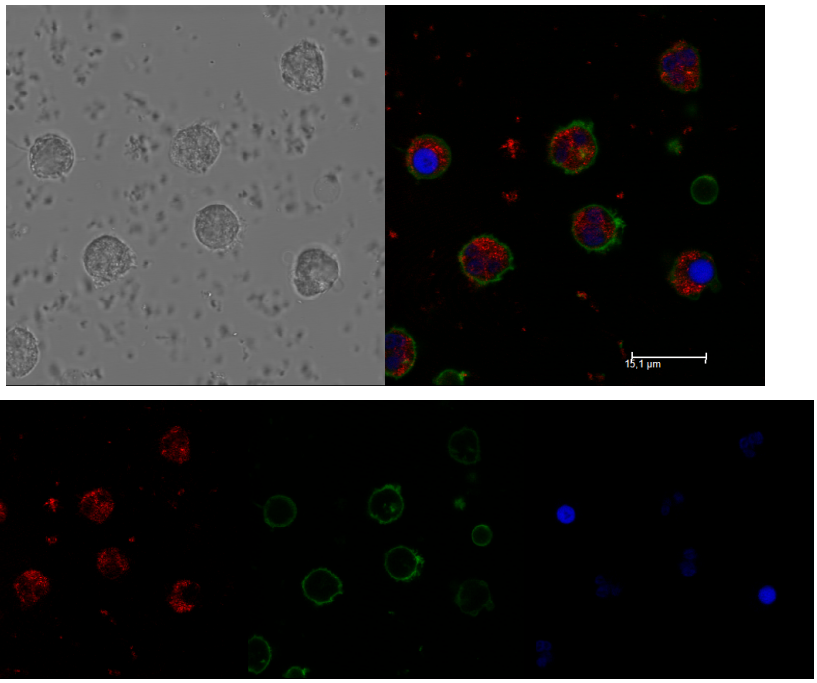

Figure 5. Confocal microscopy pictures of a cell culture of human granulocytes incubated with QOM-LDH. Red: LDH-QOM nanospheres; Green: Oregon Green DHPE; Blue: DRAQ5.

Interaction of the hydrotalcite-nanorod material (NR-LDH) with the cells occured similar to the QD-LDH, with a high uptake by the granulocytes (Figure 6). Due to the similar CdSe@CdS quantum nanorod diameters (4 nm) versus quantum dot size (3-4 nm), and in addition to their parallel arrangement to the hydrotalcite planes (Chapter 5), the two materials display analogous morphology and size. These characteristics finally led also to comparable cell uptakes.

The results are in good agreement with Experimental studies on targeted drug delivery into cells which have identified particle size as an important factor in cellular uptake of nanomaterials. It has been shown

that particles with radii <50 nm exhibit significantly greater uptake compared with particles >50 nm.[28, 29] Aoyama and coworkers[30-32] made a specific investigation of the size effects and receptor contributions in glycoviral gene delivery by excluding potential complications arising from the charge effects. They concluded that receptor-mediated endocytosis is strongly size-dependent and that there is an optimal size, ≈25 nm.

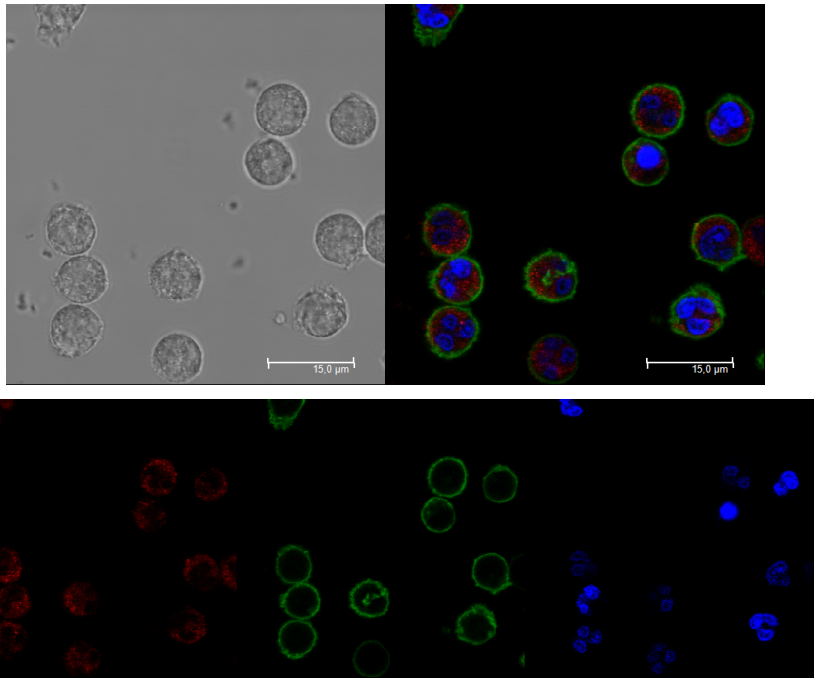

Figure 6. Confocal microscopy pictures of a cell culture of human granulocytes incubated with NR-LDH. Red: LDH-CdSe@CdS nanorods; Green: Oregon Green DHPE; Blue: DRAQ5.

Conclusions

We demonstrated herein the potential application of core-shell quantum nanocrystals-hydrotalcite or quantum nanorods-hydrotalcite for bioimaging. The quick uptake is due to the attractive interactions between positively charged double layered hydroxide particles and the negatively charged cell membrane. Cell viability was not affected by the nanocomposite addition. The efficiency of the luminescent composites uptake by the cells, granulocytes in this particular case, seems to be material size- or shape-dependent. Despite the difference in length, CdTe QDs and CdSe@CdS NRs have similar diameter, thus behaving comparable when their corresponding hydrotalcite hybrids interact with the cells. Their penetration into the cells is easy and almost no particle aggregation is observed neither in the media nor the outer part of the cell membrane. On the other hand, when spherical QOM were used, some aggregation was observed in the media or in the outer part of the cells. So far, only hybridized rod-like or sheet-like LDH nanoparticles were studied with respect to the cell interactions. Accordingly, uptake of spherical LDH nanocomposite structures should also be taken into account. Besides, QOM are essentially nontoxic to cells and animals when compared to bare QDs or quantum nanorods.

Most probably as expected from the hydrotalcite cell uptake mechanism, the nanocomposites after 60 min incubation time are still in the endosomes. Therefore, longer time studies are in progress to monitor the ‘fate’ of the particles inside the cell, as well as that of the cells itselves. That is, if they will be released to the cytosol or totally discharged from the cell, if their presence influences the cytosolic pH, etc.

References

1. Mukherjee, S.; Gosh, R. N.; Maxfield, F. R. Physiol. Rev. 1997, 77, 759.

2. Maxfield, F. R.; McGraw, T. E. Nat. Rev. Mol. Cell. Biol. 2004, 5, 121.

3. von Sorkin, A.; Zastrow, M. Nat Rev Mol Cell Biol, 2009, 10, 609.

4. Sandvig, K.; van Deurs, FEBS Lett, 2002, 529, 49.

5. Sabharanjak, S.; Sharma, P.; Parton, R. G.; Mayor, S. Dev Cell 2002, 2, 411.

6. Sharma, D. K. J Biol Chem 2003, 278, 7564.

7. Resch-Genger, U.; Grabolle, M.; Cavaliere-Jaricot, S. Nitchske R.; Nann, T. Nat Methods, 2008, 5, 763.

8. Alcor, D.; Gouzer, G. Triller, A. 2009, Eur J Neurosci, 30, 987.

9. Chang, Y. P.; Pineaud, F.; Antelman, J. Weiss, S. J Biophotonics, 2008, 1, 287.

10. Groc, L.; Heine, M.; Cognet, L.; Brickley, K.; Stephenson, F. A.; Lounis, B.; Choquet, D. Nat Neurosci 2004, 7, 695.

11. Serge, A.; Bertaux, N.; Rigneault, H.; Marguet, D. Nat Methods, 2008, 5, 687.

12. Bats, C.; Groc, L.; Choquet, D. Neuron 2007, 53, 719.

13. Groc, L.; Lafoucarde, m.; Heine, M.; Renner, M.; Racine, V.; Sibarita, J. B.; Lounis, B.; Choquet, D.; Cognet, L. J Neurosci 2007, 27, 12433.

14. Gralle M.; Botelho, M. G.; Wouter, F. S. J Biol Chem 2009, 284, 15016.

15. Ram, S.; Prabhat, P.; Chao, J.; Ward, E. S.; Ober, R. J. Biophys J 2008, 95, 6025.

16. Lee, S. F.; Osborne, M. A. Chemphyschem 2009, 10, 2174.

17. Xu, Z. P.; Zeng, Q. H.; Lu, G. Q.; Yu, A. B. Chem Eng Sci 2005, 61 (3) 1027.

18. Choy, J. H. ; Hwak, S. Y.; Jeong, Y. J.; Park, J. S. Angwe Chemie Int Ed, 2000, 39 (22), 4042.

19. Xu, Z. P.; Niebert, M.; Porazaik, K. J Control Release, 2008, 130 (1), 86.

20. Choy, J. H.; Oh, J. M.; Choi, S. J. Bio-inorganic conjugates for drug and gene delivery. Bio-inorganic hybrid materials (ed. E. Ruitz-Hitzky, K. Ariga, Y. Lvov) Whiley-VCh (Weinheim, Germany), 2008, p401-418.

21. Ladewig, K.; Niebert, M.; Xu, Z. P. Biomaterials 2009, 7, 1821.

22. Gu, Z.; Thomas, A. C.; Xu, Z. P. Chem Mater, 2008, 20 (11), 3715.

23. Kim, J. Y.; Choi, S. J.; Oh, J. M. J Nanosci Nanotechnol, 2007, 7 (11), 3700.

24. Koean, B. Chem REv, 2009m 109, 4283.

25. Stoica, G.; Castello Serrano, I.; Figuerola, A.; Ugarte, I.; Pacios, R.; Palomares, E. Nanoscale 2012, 4, 5409.

26. Castello Serrano, I.; Stoica, G.; Figuerola, A.; Palomares, E. J Mater Chem B. 2013, 1, 793.

27. Cho, S.; Jung, S.; Jeong, S.; Bang, J.; Park, J.; Park, Y.; Kim, S. Langmuir, 2013, 29 (1), 441.

28. Desai, M. P.; Labhasetwar, V.; Walter, E.; Levy, R. J.; Amidon, G. L. Pharma Res, 1997, 14, 1568.

29. Prahba, S.; Zhou, W. Z.; Panyam, J.; Labhasetwar, V. Int J Pharmacol, 2002, 244, 105.

30. Aoyama, Y.; Kanamori, T.; Nakai, T.; Sasaki, T.; Horiuchi, S.; Sando, S.; Niidome, T. J Am Chem Soc, 2003, 125, 3455.

31. Nakai, T.; Kanamori, T.; Sando. S.; Aoyama, Y. J. Am. Chem Soc, 2003, 125, 8465.

32. Osaki, F.; Kanamori, T.; Sando, S.; Sera, T.; Aoyama, Y. J. Am. Chem Soc, 2004, 126, 6520.

Chapter 7:
Two color encoded silica nanospheres as biomarkers for the ratiometric detection of trypsin enzymatic activity: a model for cystic fribrosis detection

We present herein a two colour encoded silica nanospheres (2nanoSi) using quantum dots with fluorescence emission at λ = 540 nm and λ = 660 nm for the ratiometric detection of trypsin enzymatic activity using fluorescence emission spectroscopy. Upon light excitation, the Förster Resonance Energy Transfer (FRET) process between the 2nanoSi and an organic dye (TAMRA), with fluorescence at λ = 575 nm, attached to the end of a short peptide, occurs. The enzyme proteolytic activity avoids the FRET process leading to quantitative determination of trypsin enzymatic activity by measuring the 2nanoSi fluorescence emission changes. The 2nanoSi proved to be a very sensitive system, allowing trypsin detection below 25 ppb. The fluorescence emission signal at λ = 660 nm of the 2nanoSi remained constant as internal reference for the enzymatic activity ratiometric quantification, while the photoluminescence signal at λ = 540 nm increases with a concomitant decrease of the emission of the TAMRA molecules at λ = 575 nm. The use of the quantum dot based 2nanoSi assay allows the determination of a wide range concentration of trypsin enzyme (25-350 μg/L). As trypsin is directly related to the development of cystic fibrosis (CF), we can use our assay to determine different phenotypes according to the presence of different trypsin concentration, *i.e.* normal (160-340 μg/L), CF homozygotic (0-90 μg/L), and CF heterozygotic (89-349 μg/L) patients, respectively.

TABLE OF CONTENTS

Introduction

The use of fluorescent biomarkers, based on organic dyes, has dominated over the past years in molecular biology helping researchers to study and analyse gene expression,[1] cell division[2] and enzymatic activity.[3] While much of the former experiments use green fluorescence protein (GFP) expression and measure its fluorescence emission,[4, 5] the latter, the analysis of enzyme activity, is still measured in many cases by the use of organic dyes as markers in antibody or antigen biomolecules that bind selectively to the target enzyme or molecule. Among several proteolytic enzymes, trypsin has attracted much attention, as it is a target in the study of several human diseases including, for example, cystic fibrosis (CF). Recent advances based on the evaluation of enzyme proteolytic processes through genomic and proteomic approaches have taken advantage of the use of short peptide substrates[6, 7] that can be cleaved specifically by trypsin[8] allowing an easy, high sensitive and low-cost route to analyze and trace enzyme activity and, therefore, its concentration in human serum, blood or tissues. Of particular interest, in these bio-analytical systems, is the use of Förster fluorescence resonance energy transfer (FRET),[9, 10] a process based on two fluorophores where initially one of the flourophore can transfer energy to the second one. This pair of fluorophores is known as energy donor and energy acceptor pair, respectively. The efficiency of this energy transfer process is inversely proportional to the sixth power of the distance between donor and acceptor making FRET extremely sensitive to short distances between the two fluorophores.[11]

In the work reported herein, a short peptide substrate previously marked with TAMRA, a Rhodamine-derived (carboxytetramethylrhodamine) dye with fluorescence emission at λ = 575 nm, (see **Scheme 1**) is anchored to the surface of a silica nanosphere containing two types of CdSe quantum dot nanocrystals with different fluorescence emission wavelengths.

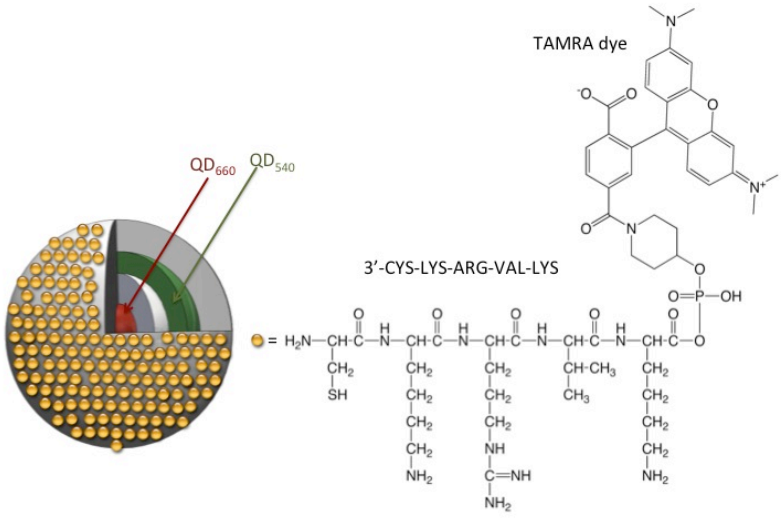

Scheme 1. Pictorial description of the 2nanoSi with the QD_{660} in red at the nanosilica sphere core, the QD_{540}, green color, at the silica coating layer and the attached small labeled peptide.

In brief, the 2nanoSi system consists of a 77 nm silica nanospheres with a core of CdSe nanocrystals ($CdSe_{660}$), with luminescence emission maxima at λ = 660 nm, and a second shell of silica embedding the second type of CdSe nanocrystals with luminescence emission maxima at λ = 540 nm ($CdSe_{540}$). Upon light excitation at λ = 400 nm, both types of CdSe quantum dots undergo fluorescence emission. Moreover, due to the FRET process between the $CdSe_{540}$@2nanoSi, as energy donor, and the TAMRA dye, as energy acceptor, it is possible to register TAMRA fluorescence emission at λ = 575 nm. Control experiments show negligible emission of TAMRA upon excitation at λ = 400 nm (see Figure 1 Annex I).

In the presence of trypsin, the proteolytic activity of the enzyme leads to the cleavage of the peptide and the FRET process is disrupted. Thus, by measuring the signal increase at λ = 540 nm, that corresponds to the $CdSe_{540}$@2nanoSi, it is possible to correlate the changes in the emission intensity with the enzyme activity using an internal reference,

which fluorescence emission remains constant through the proteolytic process. In this case, the internal reference are the $CdSe_{660}$@2nanoSi with fluorescence emission at $\lambda = 660$ nm. Hence, the ratiometric 2nanoSi system has the advantage of not being influenced by the TAMRA concentration and the excitation intensity as it occurs with simple fluorescence intensity based measurements.

Pioneering work by other research groups have focussed on QD-QD[12], QD-dye[13], QD-dye-dye (in a two-step FRET process[14, 15] or dual-donor FRET[16] systems), rare earth-QD-dye,[17] or QD-plasmonic nanoparticles[18] were reported in the literature. Besides, the use of peptide-conjugated quantum dots proved to be successful for proteolytic enzyme assays.[14] We took this approach one step further by protecting the quantum dots by silica shells, thus upgrading the properties of the system from sensing to non-toxic and ratiometric, which will allow direct enzymatic assay in vivo. Yet, to the best of our knowledge, this is the first time that labelled peptide-functionalized dual colour quantum dot@silica ratiometric nanosensors are employed to measure enzyme activity. Due to the properties of quantum dots and the efficiency of the FRET process, our system can be used as an excellent probe for high-throughput trypsin assay as alternative for the traditional approaches of CF diagnosis and other pancreatic-related diseases.

Experimental

Materials

Synthesis of CdSe QD. The procedure to obtain CdSe QDs was using TOPO-TOP as capping ligand.[19] A selenium solution was prepared by mixing 0.4 g of selenium poder, 10 mL of TOP and 0.2 mL of anhydrous toluene and stirred under argon. A mixture of 20 g of TOPO and 0.25 g of cadmium acetate dihydrate were placed in a round-bottoned flask, stirred and heated to 150ºC under argon and the temperatura was

increased to 320ºC. When the mixture reached 320ºC the selenium solution was quickly injected and then cooled to 270ºC. The reaction was run for a specific time (depending on the size of the QDs that we expected to achieve). After stopping the reaction, samples were cooled and whased with etanol and acetone three times and stored in chloroform.

Synthesis of QD@silica nanospheres. The experiments were performed using CdSe core quantum dots with emission wavelength at 540 nm (green (2,7 nm)) and 660 nm (red (5,6 nm)). Next, single and two colors quantum dots embedded silica nanospheres, *i.e.* QD_{540}@silica and QD_{660}@silica@QD_{540}@silica, respectively, were prepared by the reverse microemulsion method as detailed elsewhere.[20, 21] An amine functionalization was done adding 30 mL of APMS and 80 mL of THPM to the reaction and leaving to stir for 24 hours at room temperature.

Peptide-functionalization of QD@silica nanospheres. The positive surface of the QD_{540}@silica nanospheres (given by APMS and THPM) was functionalized with two different TAMRA-labelled peptides:
Pro-active: NH_2-Cys-Lys-Arg-Val-Lys-TAMRA
In-active: NH_2-Cys-Lys-Pro-Val-Lys-TAMRA
The two different sequences TAMRA-labelled peptides were particularly designed for our study by BIOTREND. Glutaraldehyde was used to bind the amine functional groups of the peptides with the hydroxyl groups of the silica nanospheres surface as described in the following methodology. 2 mL of QD_{540}@silica-APMS in PBS and 0.25 mL of glutaraldehyde (0.25 mg/mL) were mixed and shaked for 4 h at 37 ºC. Then the solution was centrifuged to remove the unreacted glutaraldehyde and finally the pellet was resuspended in PBS. A determined amount of TAMRA-labelled peptides was added and shaked for 20 hours at 4ºC. After this time, the solution was centrifuged to remove the unbound peptides. In the end, the TAMRA-labelled

peptide-functionalized QD@silica nanospheres were resuspended in 5 mL and stored in PBS.

Enzymatic digestion. A determined concentration of trypsin between 25-350 μg/L was added to the labelled peptides-nanospheres and mixed for a period of time: from 30 sec to 120 min, at 37 ºC. After this time, the mixture was heated up to 70ºC and held for 1 h in order to denaturalize the enzyme and stop the reaction. If not measured immediately after the enzymatic digestion, it is recommended to keep the samples in the freezer until the analysis.

Characterization. The formation of the QDs@silica nanospheres was directly visualized by transmission electron microscopy (TEM) using a JEOL 1011 microscope. The UV-Visible and fluorescence spectra were recorded using a 1 cm path length quartz cell in a Shimadzu UV Spectrophotometer 1700 and an Aminco-Bowman Series 2 luminescence spectrometer.

Results and discussion

Transmission Electron Microscopy (TEM) confirmed the formation of 2nanoSi spheres. For a typical single color synthesis, the QD_{540}@silica beads displayed a diameter of 38 nm (Figure 1A). [20, 21] When the beads were coated with a second QDs/silica layer to obtain the 2nanoSi spheres, *i.e.* QD_{660}@silica@QD_{540}@silica, the size increased to 77 nm (Figure 1B). The silica layer thickness was *ca.* 16.5 nm. For details, see Figure 2 Annex I.

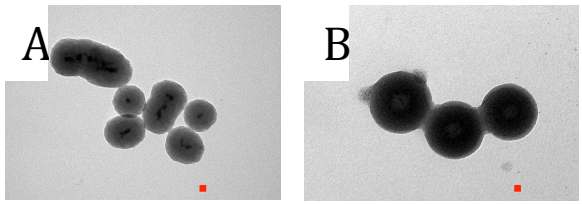

Figure 1. TEM image of (A) QD_{540}@silica and (B) QD_{660}@silica@QD_{540}@silica nanospheres. The scale bar corresponds to 100 nm.

Analysis of trypsin activity using single colour quantum dot@silica-FRET nanosensors (1nanoSi): Proof-of-concept.

Figure 2 shows the photoluminescence (PL) absorption-emission profiles of QD_{540}@silica nanospheres and the TAMRA dye. There is a blue shift in the PL of QD@silica in comparison to the pristine QDs in solution, *i.e.* 520 nm versus 540 nm, as observed previously, [20-22] yet the original fluorescence is recovered after the trypsin digestion as shown later on this work. The TAMRA dye displays fluorescence emission at 575 nm. As it can be seen in **Figure 2**, the fluorescence emission from the QD_{540}@silica nanospheres (without any further surface functionalization at the silica nanosphere) overlaps with the absorption peak of TAMRA thus allowing the FRET process.[23]

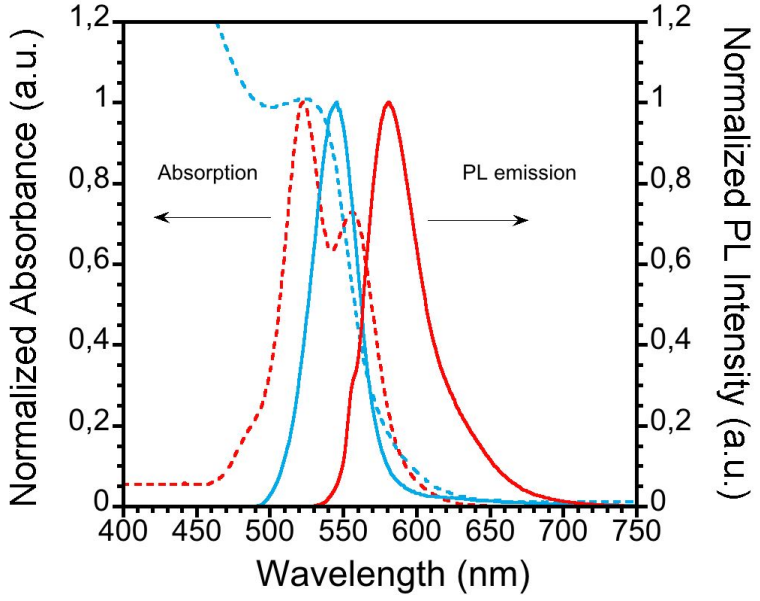

Figure 2. Absorption (dash line) and emission spectra (straight line) of QD_{540}@silica nanospheres (blue) and 5'-TAMRA (red).

Once the overlap between the QD_{540}@silica nanospheres and the fluorescent dye was confirmed, we carried out the assembling between the QD@silica nanospheres and the TAMRA-labelled peptide. Thereafter, we performed the enzyme digestion using trypsin and read-

out the emission of the 1nanoSi system. We used two different labelled peptides in order to obtain a control sample for our experiments. On one hand, the "*pro-active*" labelled peptide has the following sequence: 3'-NH_2-Cys-Lys-Arg-Val-Lys-TAMRA-5'. Trypsin proteolytic activity is highly specific to the Lys-Arg-Val sequence and the enzyme digestions will cleave the peptide. On the other hand, our control sample, the "*in-active*" labelled peptide has the same chemical nature except for a change by Proline (Pro) instead of Arginine (Arg). Needless to say that trypsin cannot digest the small "*in-active*" peptide and the 1nanoSi fluorescence emission properties will remain the same.

Figure 3 displays the emission spectra of the 1nanoSi nanospheres functionalized with different concentrations of the "*pro-active*" TAMRA-labelled peptide in order to see how the amount of dye affects the emission of QDs. We would like to emphasize that increasing the amount of TAMRA-labelled peptides at the QD_{540}@silica nanospheres leads to a decrease in the emission intensity between λ = 500 nm and 550 nm range, which corresponds to the fluorescence emission wavelength of the quantum dots, as mentioned above. The emission intensity drop is a direct evidence of efficient FRET between the QD_{540}@silica nanospheres and the TAMRA dye in the 1nanoSi system, as reported previously in analogous FRET systems. [24, 25]

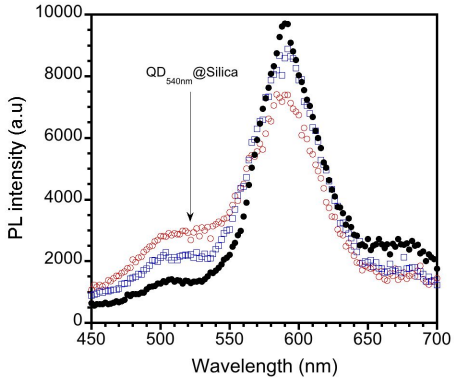

Figure 3. Emission spectra of "*pro-active*" 1nanoSi system increasing the amount of TAMRA-labelled peptide at the surface of the nanosphere, (○) 400μg/L, (□) 800μg/L, and (•) 1200μg/L of labelled peptide, respectively.

The 1nanoSi system was incubated with trypsin for the peptide digestion, and the recorded emission spectra are shown in Figure 4. The spectroscopic profiles further demonstrated the existence of FRET processes between the QD_{540}@silica nanospheres and the "*pro-active*" TAMRA-labelled peptide (Figure 4a). Moreover, our control sample with the "*in-active*" 1nanoSi system, as expected, does not show any significant change in the fluorescence emission spectra (Figure 4b).

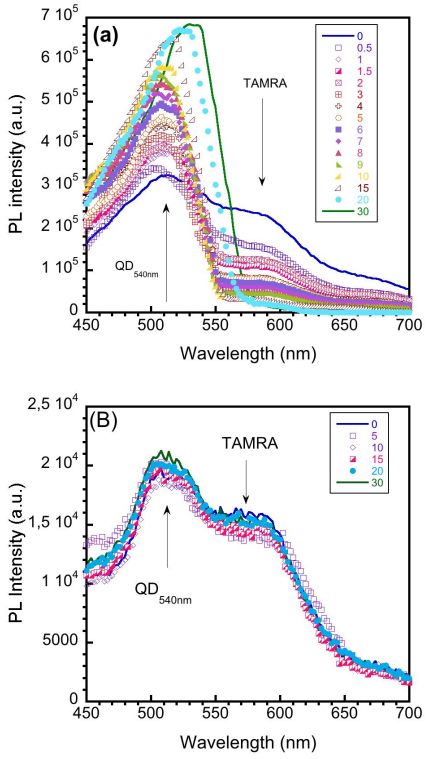

Figure 4. Emission spectra of 5'TAMRA-labelled peptide-functionalized QD_{540}@silica nanospheres after trypsin digestion (a) the "*pro-active*" 1nanoSi and (b) the "*in-active*" 1nanoSi. The 1nanoSi system was incubated with trypsin (250 μg/mL) and the figure legends correspond to the enzymatic digestion time in minutes (0-30 min).

Quantitative detection of trypsin activity using two colours quantum dots@silica nanosensors as ratiometric sensor (2nanoSi).

The use of a single quantum dot fluorophore (1nanoSi) allowed us for the qualitative analysis of the trypsin proteolytic activity. However, our aim is to be able to quantify the enzymatic activity and, thus, the need of an internal reference in our fluorescence system is required. As mentioned above, we added a second population of QDs at the core of the silica nanospheres with fluorescence emission at l = 660 nm (Figure 5).

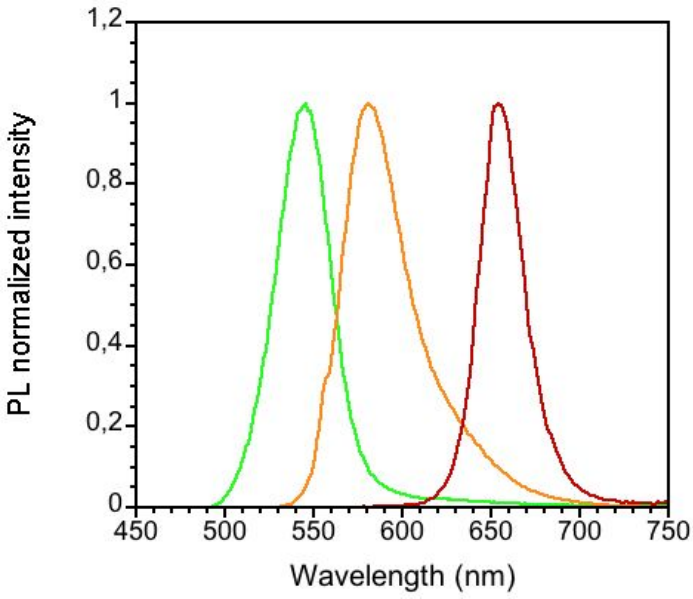

Figure 5. Emission spectra of QD_{540} (green), 5'-TAMRA (orange) and QD_{660} (red).

Thus, the use of two QDs fluorophores with distinguishable emission spectra allows us to establish a measurable ratio, namely, I_{540}/I_{660}. Moreover, the emission intensity at l = 660 nm remains constant as the QD_{660nm} at the silica nanospheres does not influence the FRET process. The key feature in our 2nanoSi is that, due to the absorption properties

of the nanocrystal quantum dots, both fluorophores can be excited at the same wavelength (l = 400 nm), but only the nanocrystals in the outlayer emitting at 540 nm undergo FRET with the TAMRA dye. Despite the small overlapping between the emission of QD_{660} and the absorption of TAMRA, the distance between them however is around 38 nm thus holding off the energy transfer, meanwhile the distance and the overlapping between QD540 and the dye allow the FRET to occur. Using TCSPC and steady-state emission spectroscopy, we correlate that the distance between the QD_{540} and the TAMRA dye is 14.6 nm for an efficiency of 0.5238. The calculated R_0 (distance at which the efficiency of FRET is 50%) is 7.79 nm, and the distance between CdSe540 and TAMRA dye (r) is 7.657 calculated from the fluorescence. This is in good agreement with the value obtained from the lifetime measurements (Figure 3 Table 1 in Annex I), *i.e.* 7.665 nm (for complete calculations, check the Annex I). In conclusion, all the prerequisites for a quantitative nanosensor are accomplished.

Figure 6 illustrates the changes in the fluorescence emission of the 2nanoSi in the presence of two different trypsin concentrations, 25 µg/L (Figure 6a) *versus* 350 µg/L (Figure 6b). As expected, increasing the enzyme concentration leads to faster recovery of the original emission at 540 nm (Figure 6b). The complete enzyme concentrations study can be found in Figure 4 Annex I.

Taking into account the values of trypsin in the different phenotypes of patients with cystic fibrosis (CF),[26] *i.e.* homozygotic (0-90 mg/L), normal (160-340 mg/L), and heterozygotic (89-349 mg/L), and considering the specificity of the 2nanoSi, we performed the study of the enzymatic digestion using the "*pro-active*" labelled peptide in a wide range of trypsin concentrations (25-350 mg/L) that fall in the values found for CF patients mentioned above. Figure 7 shows the ratio between the PL emission peaks of both QD_{540} and QD_{660} (I_{540}/I_{660}) during enzymatic digestion for 120 minutes in different enzyme concentrations. As expected, there is a direct relationship between the enzymatic digestion rate and the enzyme concentration that allowed us to unequivocally

differentiate between the different enzyme concentrations used. In other words, the higher the trypsin concentration the shorter the time we need to reach a plateau in our kinetic measurements. Hence, analysing the trypsin activity at early digestion times using our 2nanoSi ratiometric system (for example 10 minutes) we can differentiate between the different trypsin concentrations as shown in Figure 8.

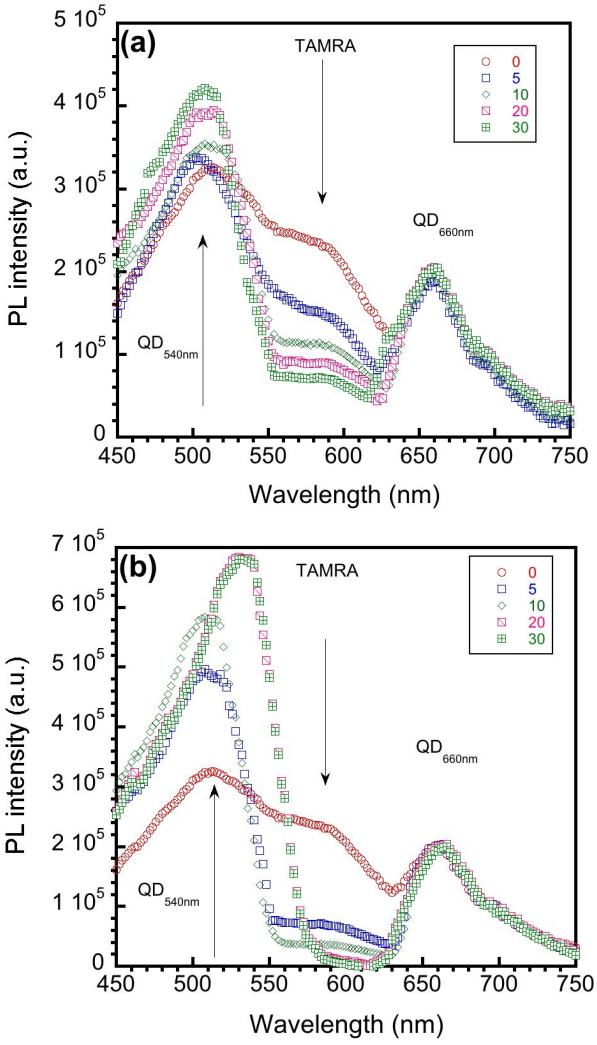

Figure 6. 2nanoSi emission spectra (a) after digestion with 25µg/L of trypsin, and (b) after digestion with 350µg/L. The figure legends correspond to the enzymatic digestion time in minutes (0-30 min).

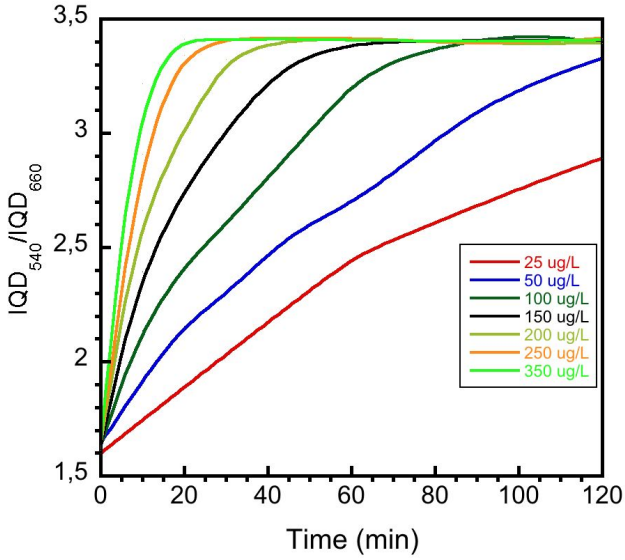

Figure 7. Kinetics of the enzymatic digestion as a function of trypsin concentration using the ratio between PL emission peaks of both QD_{540} and QD_{660} at the 2nanoSi system.

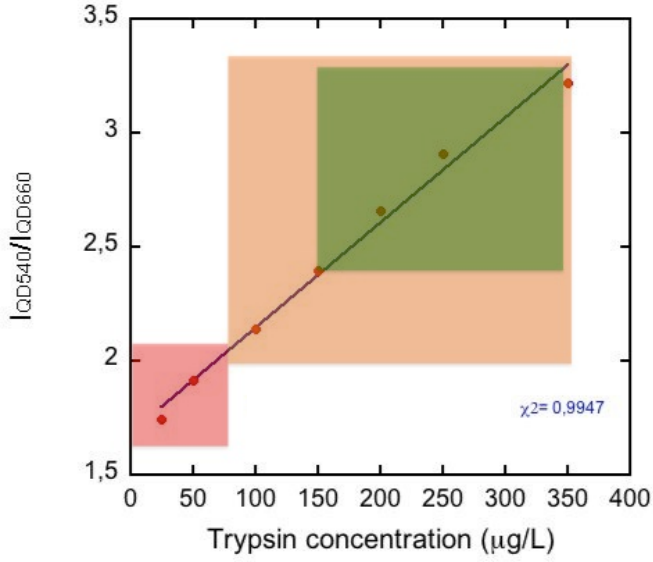

Figure 8. Calibration curve resulting from fitting the fluorescence I_{540}/I_{660} experimental values from Figure 7 at the enzyme digestion time of 10 minutes. Red, orange and green correspond to CF homozygotic, CF heterozygotic and normal, respectively.

As it can be seen, the calibration curve proved to be highly linear (χ^2=0.9947) and allowed us to determine the trypsin concentration at levels that are clinically relevant for the cystic fibrosis prognosis, *i.e.* CF homozygotic (0-90 μg/L), CF heterozygotic (89-349 μg/L) and normal (160-340 μg/L), respectively. These ranges correspond to the 2nanoSi system fluorescence I_{540}/I_{660} values of 1.68-2.09, 2.10-3.30 and 2.42-3.25, respectively.

The overall results shown herein permit us to propose the 2nanoSi system as a ratiometric fluorescence sensor for the trypsin tool test, as it is easy-to-use, fast, and non-invasive for the diagnostic of cystic fibrosis and other pancreas-related diseases.

Conclusions

By combining the specificity of biomolecular interactions with tunability of quantum dot and organic dye optical properties, we have developed for the first time an *in vitro* detection system capable of cystic fibrosis prognoses, both qualitatively (1nanoSi) and quantitatively (2nanoSi). The trypsin enzymatic activity was reported via FRET process, which mediates changes in the quantum dot emission spectra, between the organic dye TAMRA (λ = 575 nm) and green CdSe QDs (**λ** = 540 nm). Cross-reactivity and signal overlap were avoided by designing enzyme-specific peptidic sequences, *i.e.* NH_2-Cys-Lys-Pro-Val-Lys (*in-active*) and NH_2-Cys-Lys-Arg-Val-Lys (*pro-active*), respectively, for attachment to the QD@silica nanospheres surface. Trypsin specifically recognizes the *pro-active* peptide.

The combination TAMRA-QD_{540} (1nanoSi) proved to be a suitable tool for the qualitative detection of cystic fibrosis markers. However, when this system was upgraded with a second QD population (**λ** = 660 nm) as the core of the previous nanostructure leading to 2nanoSi, we were able to perform quantitative enzymatic studies based on the ratiometric sensor I_{540}/I_{660}, considering the red QD as reference. The detection was fast, 10 min being sufficient to withdraw a highly accurate calibration

curve (χ^2=0.9947). The latter result allowed us to determine the trypsin concentration at levels that are clinically relevant for the cystic fibrosis prognosis, *i.e.* CF homozygotic (0-90 µg /L), CF heterozygotic (89-349 µg /L), and normal (160-340 µg/L), respectively.

Our newly developed system displays many advantages, including simplicity, low cost, fast detection, high specificity and sensitivity, in addition of being noninvasive. The biomarker has been shown to provide significant prognostic information, and hence represents a promising system for proof-of-concept demonstration of our proposed approach.

References

1. Steuerwald, N.; Cohen, J.; Herrera, R. J.; Brenner, C. A.; Mol. Hum Reprod. 1999, 11, 1034.

2. Murray, A. W.; Kirschner, M. N. Nature, 1989, 339, 575.

3. Henning, A.; Bakirci, H.; Nau, W. M. Nature Methods, 2007, 4, 629.

4. Mahajan NP, Harrison-Shostak DC, Michaux J, Herman B. Chem Biol. 1999; 6:401-9.

5. Methods of biochemical analysis, green fluorescent protein: properties, applications and protocols (ed: Martin Chelfie, Stven R. Kain).

6. Schilling O., Overall, C.M. Nat Biotechnol. 2008; 26:685.

7. Thomas, D. A.; Francis, P.; Smith, C.; Ratcliffe, S.; Ede, N. J.; Kay, C. Proteomics. 2006; 6:2112-20.

8. Sapsford, K. E.; Farre, D. I; Sun, S.; Rasooly, A.; Mattoussi, H.; Medintz, I. Sensors and Actuators B: Chemical, 2009, 139, 13.

9. Medintz, I.; Tetsuo Uyeda, H.; Goldman E. R.; Mattoussi, H. Nat. Mater, 2006, 4, 435.

10. Medintz, I.; Mattoussi, H. Phys Chem Phys Chem, 2009, 11 (1), 17.

11. Lakowicz, J. R. Principles of Fluorescence Spectroscopy 2nd ed (Kluwer Academic/Plenum, 1999).

12. Chen, C. Y.; Cheng, C.T.; Lai, C. W.; Wu, P. W.; Wu, K.C.; Chou, P.T.; Chou, Y. H.; Chiu, H. Y. Chem Comm, 2006, 263.

13. Kim, G. B.; Kim, Y. P. Therasnostics, 2012, 2 (2), 127.

14. Medintz, I.; Clapp, A.R.; Mattoussi, H.; Goldman, E. R.; Fisher, B.; Mauro, J. M, Nat. Mater, 2003, 2 (9), 630.

15. Chen, H. H.; Ho, Y. P.; Jiang, X.; Mao, H. Q.; Wang, T. H.; Leong, K. W. Nano Today, 2009, 4 (2), 125.

16. Zhang, H.; Zhou, D. Chem Comm, 2012, 48, 5097.

17. Algar, W. R.; Malanoski, A. P.; Susumu, K.; Stwewart, M. H.; Hildebrandt, N.; Medintz, I. Anal Chem 2012, 84 (22), 10136.

18. Lowe, S. B.; Dick, J. A. G.; Cohen, B. E.; Stevens, M. M. ACS Nano, 2012, 6, 851.

19. Aldana, J.; Wang, Y. A.; Peng, X. J. Am Chem Soc, 2001, 112, 8844.

20. Castello, I.; Ma, Q.; Palomares, E. J. Mater Chem 2011, 21, 17673.

21. Ma, Q.; Castello, I.; Palomares, E. Chem Comm, 2011, 47, 7071.

22. Wang, S. P.; Mamedova, N.; Kotov, N. A.; Chen, W.; Studer, J. Nano Lett, 2002, 2, 817.

23. Clegg, R. Förster resonance energy transfer – FRET: what is it, why do it, and how it's done. In Gadella, Theodorus W. J. FRET and FLIM techniques. Laboratories tecniques in biochemistry and molecular biology, 2009, volumr 33, Elsevier. Pp 1-57.

24. Somers, R. C.; Lanning, R. M.; Snee, P. T.; Greytak, A. B.; Jain, R. K.; Bawendi, M. G.; Nocera, D. G. Chem Sci 2012, 3, 2980.

25. Dennis, A. M.; Rhee, W. J.; Sotto, D.; Dublin, S. N. Bao, G. ACS Nano 2012, 2917.

26. Dandona, P.; Hodson, M. E.; Batten, J. C. J Clin Pathol, 1983, 36, 790.

Annex I

Figure 1 Annex I. Emission spectra of control samples excited at 400 nm: $CdSe_{540}$@silica (green), $CdSe_{660}$@silica-TAMRA (orange) and TAMRA (red), respectively. All the samples were measured at the same concentration and window aperture conditions.

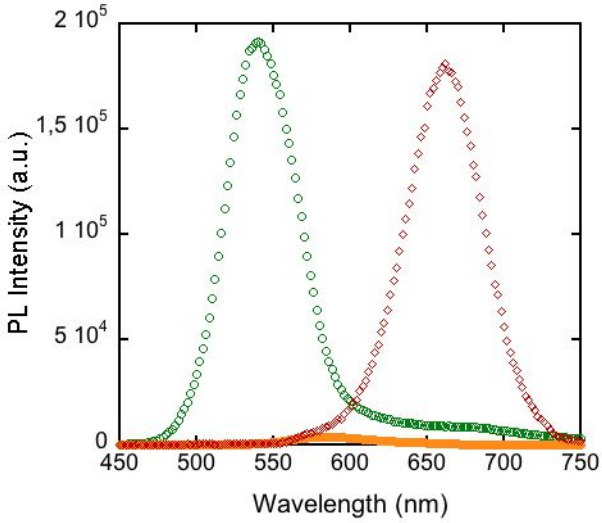

Figure 2 Annex I. Scheme of 2nanoSi with the corresponding distances between the different components. Distances are given in Angstroms (A).

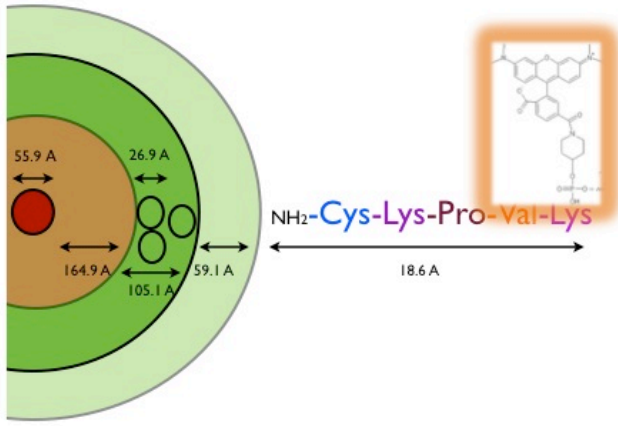

Figure 3 Annex I. Lifetime decay of $CdSe_{540}@SiO_2$ (blue), the TAMRA (red) dye and CdSe540@SiO2-TAMRA (green).

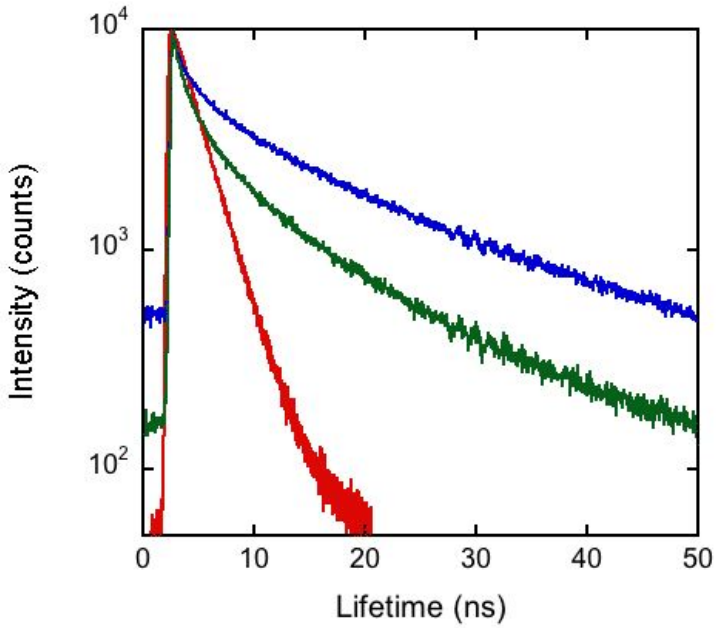

Table 1 Annex I. Time constants t_1 and t_2, components B_1 and B_2, and average lifetime of $CdSe_{540}@SiO2$, TAMRA dye and 2nanoSi.

	t1 (ns)	*B1* (%)	*t2* (ns)	*B2* (%)	*p* (ns)
$CdSe_{540}@SiO2$	4.28	48.12	25.88	51.88	15.48
2nanoSi	1.82	58.79	17.17	41.21	8.14
TAMRA	2.47	100.00	-	-	2.47

Calculations.

The FRET efficiency (E) is the quantum yield of the energy transfer transition, *i.e.* the fraction of energy transfer event occurring per donor excitation event.
The experimental efficiency, E is defined by the following equation:

$$E = (F_D - F_{DA})/F_D$$

where F_D and F_{DA} are the fluorescence intensities of the donor alone and the donor in the presence of acceptor[1], respectively.
The FRET efficiency relates to the quantum yield and the fluorescence lifetime of the donor molecule as follows:[2]

$$E = 1 - t'_D/t_D$$

where t'_D and t_D are the donor fluorescence lifetimes in the presence and absence of an acceptor, respectively.

Based on the lifetime measurements, we obtained an efficiency E = 0.5258, which matches well with the efficiency resulted by fluorescence, *i.e.* E = 0.5238.

Estimates of the QD donor–dye acceptor separation distance *r* were calculated via the Förster formalism by fitting the above experimental FRET efficiencies E using the expression:

$$E = 1/(1+(r/R_0)^6$$

Where R_0 is the Förster distance designating the donor–acceptor separation at 50% energy transfer efficiency. R_0 is expressed as:[3]

$$R_0 = 9.78 \times 10^3 (\kappa^2 n_D^{-4} Q_D J(l))^{1/6}$$

where n_D is the refractive index of the medium, Q_D is the donor quantum yield in the absence of acceptor, J **(***I***)** is the spectral overlap integral, and κ^2 is the dipole orientation factor. We use $\kappa^2 = 2/3$ corresponding to a random dipole orientation shown to be appropriate for our self-assembled QD–protein/peptide–dye conjugates, as detailed in reported previous studies.[1] This is based on the assumption that in a self assembled QD–peptide/protein–dye pair it is impossible to control the relative orientation of the dipoles. Each time a dye-labeled protein it is added to the conjugate, that dye will have a dipole orientation that does not correlate with the existing QD and dyes.

For our system, we obtained a $R_0 = 7.79$ nm and r = 7,657 nm by fluorescence, which is in very good agreement with the value calculated from lifetime, *i.e.* r = 7.665, respectively.

Figure 4 Annex I. Emission spectra of 5'TAMRA-labelled 2nanoSi nanospheres. Enzymatic digestion with different trypsin concentration: a) 250 μg/L, b) 200 μg/L, c) 100 μg/L, d) 50 μg/L and e) 25 μg/L, respectively.

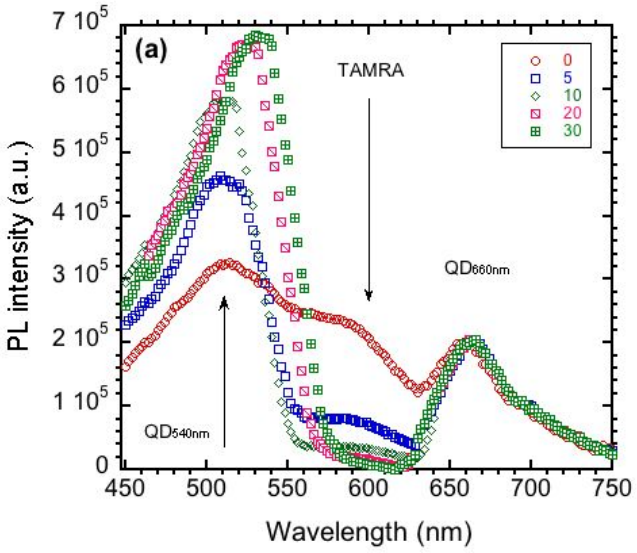

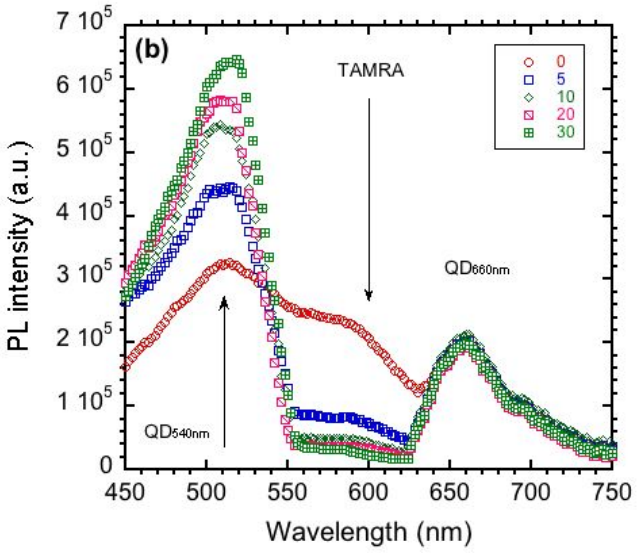
(b)
TAMRA
QD660nm
QD540nm
0
5
10
20
30
PL intensity (a.u.)
Wavelength (nm)
7 10^5
6 10^5
5 10^5
4 10^5
3 10^5
2 10^5
1 10^5
0
450
500
550
600
650
700
750

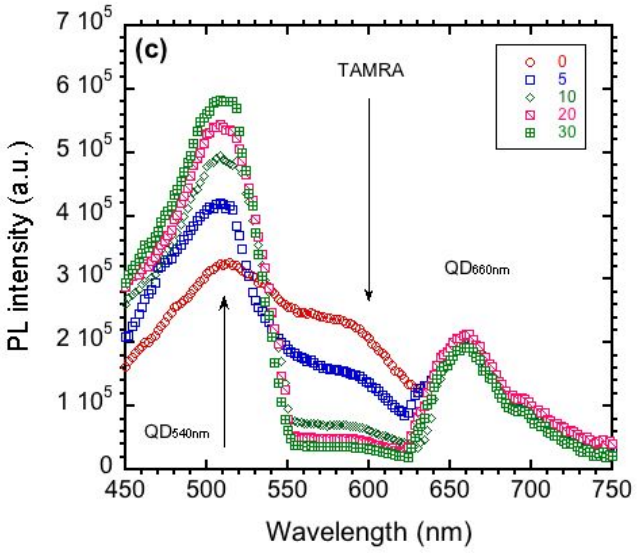
(c)
TAMRA
QD660nm
QD540nm
0
5
10
20
30
PL intensity (a.u.)
Wavelength (nm)
7 10^5
6 10^5
5 10^5
4 10^5
3 10^5
2 10^5
1 10^5
0
450
500
550
600
650
700
750

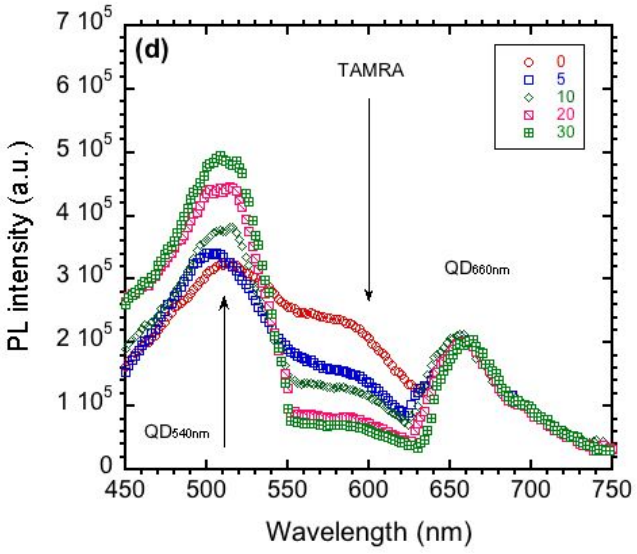

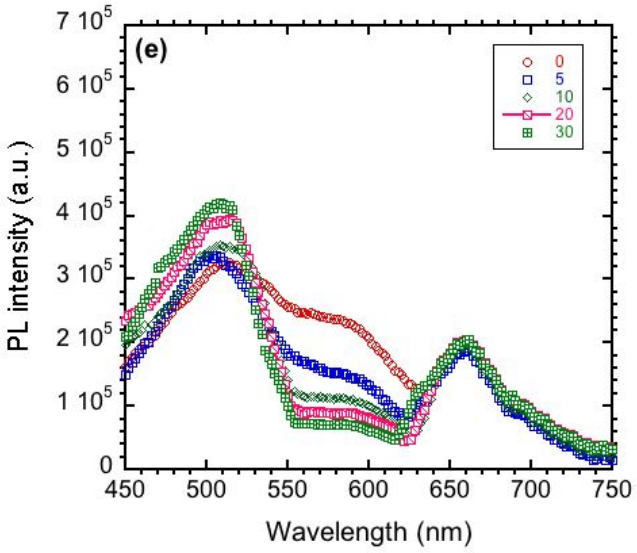

References

1. Clapp, A. R. J. Am. Chem. Soc. 2004, 126, 301.

2. Majoul, I.; Jia, Y.; Duden, R. (2006). "Practical Fluorescence Resonance Energy Transfer or Molecular Nanobioscopy of Living

Cells". In Pawley, James B.. *Handbook Of Biological Confocal Microscopy* (3rd ed.). New York, NY: Springer. pp. 788–808.

3. Lakowicz, J. R. Principles of Fluorescence Spectroscopy 2nd ed. (Kluwer Academic/Plenum, 1999).

Chapter 8:

Summary and Outlook

Advances in semiconductor nanocolloids have provided a new set of materials with unique optical and electrical properties, which recently have grabbed biologists and biomedical engineers' attention for applications such as biolabels, biosensors and image-contrast agents. These nanosemiconductors have also been used to fabricate drug delivery and medical therapeutic tools. In this thesis, I studied the fabrication of fluorescent materials based on semiconductor luminescent nanocrystals to be further used as: Quantum-"Onion"-Multicode (QOM) pH ratiometric sensor; hybrid fluorescent materials combining the layered double hydroxides as inorganic scaffold to bear luminescent nanoparticles (QDs, QOM or nanorods) and their use as bioimaging agents in cell cultures; and finally, QOM were used as ratiometric sensor based on FRET to study the enzymatic activity.

TABLE OF CONTENTS

Summary

Quantum dots (QDs) are inorganic semiconductor nanoparticles that exhibit size-dependent optical and electronic properties. Due to the typical dimension in the range of 1-100 nm, the surface-to-volume ratios of the materials become large and their electronic states become discrete. Moreover, due to the fact that the size of the nanocrystal is smaller than the size of the exciton, charge carriers become spatially confined, which raises their energy and it is called quantum confinement. Thus the size-dependent optoelectronic properties are attributed to the quantum confinement effect and light emission from these semiconductor nanoparticles can be tuned.

QDs have very stable fluorescence compared to organic dyes that show photobleaching after some minutes. Furthermore and contrary to organic dyes, these nanocrystals have broad excitation and narrow emission which make them extremely applicable to multicolor imaging. Tuning the emission wavelength of the QDs is simply a case of tuning their size. For all these reasons explained in Chapter 1, QDs have displaced organic dyes as method for imaging in the last 5 years.

However, these QDs are toxic, so it is needed to encapsulate them to prevent heavy metal poisoning when using them for bioapplications. Previous work in our lab, detailed in Chapter 2, found a layer-by-layer synthesis to obtain “nano-onions”, which are comprised of several layers of silica embedded with different quantum dots. This arrangement is very useful to have different colors, like having different vials, confined in few nanometers.

The silica matrix used plays an important role in making the QDs water-soluble and protecting them from photoluminescence quenching, at least in the pH range useful for biological applications. The greater the silica layer thickness or higher the number of silica layers the greater the protection offered to the QDs inside. Based on this principle, we showed that these “nano-onions”, which we call Quantum-“Onion”-Multicode (QOM), can be used for pH sensor applications, as detailed

in Chapter 3. The ratio of photoluminescence intensity from two populations of QDs has been shown to correspond to the pH value in the media, making our system a potential ratiometric pH sensor.

Moreover, the development of QDs@silica spheres as biomolecular probes can provide new insights that overcome several limitations of individual QDs as biological markers, *i.e.*: better photostability of the embedded QDs in the bead matrix, more available surface for chemical reactions, higher binding capacity of the spheres, less toxicity, and easier manipulation.

However, most inorganic nanoparticles require chemical functionalization with silane, thiol, amino, carboxy and other species in order to obtain desirable properties for celular delivery, such as good compatibility, strong affinity between carrier and payload, cell targeting, stability and long circulation time.

In the past, it became apparent that layered double hydroxides (LDH), also known as hydrotalcite-like materials (HT) or anio(χ^2=0.9947)nic clays, form an exception to this rule. LDHs constist of layers of positively charged nanosheets with the brucite-type structure neutralized by anions in the interlayer space. From a medical point of view, many interesting chemical variations of HT have been reported since hydrotalcite interlayer space can accommodate a variety of drugs and biomolecules by either anion exchange or a delamination-restacking process. This kind of material has been used as a carrier for CdTe water-soluble QDs (Chapter 4) or Nanorods (Chapter 5).

On the one hand, LDH intercalated water-soluble CdTe with very fast uptake. Additionally, delamination of hydrotalcite is not a mandatory requirement. The hybrid material displays extremely high stability in physiological media with different pH, making them a potential imaging tool for diagnostics in nanomedicine. Remarkably, the optical properties of QDs were blue-shifted, attributed to several factors, as detailed in Chapter 4. However, this effect is reversible upon the dissolution of the solid host (HT). Besides, CdTe QDs display an optical memory effect. These optical transitions were stopped when surrounding the QDs with

silica, leading to QDs@silica core/LDH shell nanospheres (silica acting like a barrier between the QDs and hydrotalcite). This combination leads to an efficient barrier for leaching processes of the QDs in biological media, being a nanostrucutured inorganic scaffold that prevents citotoxicity and will permit multimodal imaging and simultaneous diagnosis in advanced therapeutical systems.

On the other hand, LDH intercalated with highly luminescent CdSe@CdS quantum nanorods were succesfully prepared under ambient conditions, being the delamination approach more successful owing to the large-sized nanorods, as detailed in Chapter 5. This hybrid nanomaterial showed higher luminescence and longer lifetime than QDs, an advantatge and prerequisite for the long-term *in vivo* observation. In consequence, a lower amount of nanoparticles and less excitation are required, which means an implicit, and most important, lower toxicity or damage will be applied to the cells. With these results we highlight the combination of the two fields of optic and nanomaterials as a powerful tool for bioapplications.

In Chapter 6, the incubation of blood cell cultures with the nanocomposites detailed in both Chapter 4 and Chapter 5, was used to demonstrate the usefulness of these materials as bioimaging agents. We observed a dependency of diameter of the nanoparticles used and the good quality of the samples as labelling tool. Further studies are required to clarify if this correlation is true or other reasons like the structure of the carrier material are involved.

Finally, in Chapter 7 I detailed how, combining the specificity of biomolecular interactions with tunability of quantum dot and organic dye optical properties, we have developed for the first time an *in vitro* detection system capable of cystic fibrosis prognoses, both qualitatively (1nanoSi) and quantitatively (2nanoSi). The trypsin enzymatic activity was reported via FRET process, which mediates changes in the quantum dot emission spectra, between the organic dye TAMRA (λ = 575 nm) and green CdSe QDs ($\boldsymbol{\lambda}$ = 540 nm). Cross-reactivity and signal overlap were avoided by designing enzyme-specific peptidic

sequences, *i.e.* NH_2-Cys-Lys-Pro-Val-Lys (*in-active*) and NH_2-Cys-Lys-Arg-Val-Lys (*pro-active*), respectively, for attachment to the QD@silica nanospheres surface. Trypsin specifically recognizes the *pro-active* peptide.

The combination TAMRA-QD_{540} (1nanoSi) proved to be a suitable tool for the qualitative detection of cystic fibrosis markers. However, when this system was upgraded with a second QD population (**λ** = 660 nm) as the core of the previous nanostructure leading to 2nanoSi, we were able to perform quantitative enzymatic studies based on the ratiometric sensor I_{540}/I_{660}, considering the red QD as reference. The detection was fast, 10 min being sufficient to withdraw a highly accurate calibration curve (χ^2=0.9947). The latter result allowed us to determine the trypsin concentration at levels that are clinically relevant for the cystic fibrosis prognosis, *i.e.* CF homozygotic (0-90 μg /L), CF heterozygotic (89-349 μg /L), and normal (160-340 μg/L), respectively.

Our newly developed system displays many advantages, including simplicity, low cost, fast detection, high specificity and sensitivity, in addition of being noninvasive. The biomarker has been shown to provide significant prognostic information, and hence represents a promising system for proof-of-concept demonstration of our proposed approach.

Outlook

I will try to summarize here the future research plan focused on the use of the QOM in multiplexed assays for the study of proteins involved in some specific diseases, such as Schizophrenia or Dilated Cardiomyopathy. In the case of Schizophrenia, a tyrosin kinase receptor has been associated with this disease. This tyrosin kinase is the Discoidin Domain Receptor 1 (DDR1), which interacts with collagen to trigger a signal cascade in the cell to promote the differentiation. The problem is that there is a lack of collagen in the brain and we will try to figure out which is the ligand of DDR1 in the brain using our QOMs for multiplexed assays. For the Dilated Cardiomiopathy, it has been reported that is an autoimmune disease where many antibodies and proteins are involved. We will use our QOMs to study the interaction of antibody-protein across the time to figure out if they are acting at the same time or there is a sequence of events.

Mentioning the toxicity of the QDs due to cadmium, other materials have been studied to develop imaging and biomedicine tools, based on rare earths (also called lanthanides) what opens a new area for further studies. We referred to these materials as “cadmium-free” and they have some properties as the possibility of up-conversion (a process in which the sequential absorption of two or more photons leads to the emission of light at shorter wavelength than the excitation wavelength), which is very promising because they can be excited at near-infrared wavelengths able to penetrate the skin without causing any damage to the cells and emit in the visible.

Annexes

Contributions to the Scientific Community

Publications related to this thesis:

Multiplexed color encoded silica nanospheres prepared by stepwise encapsulating quantum dot/SiO2 multilayers. Q. Ma; I. Castello Serrano; E. Palomares. *Chem. Comm*, **2011**, 47 (25), 7071.

QD-"Onion"-Multicode silica nanospheres with remarkable stability as pH sensors. I. Castelló Serrano; Q. Ma; E. Palomares. *J. Mater. Chem*, **2011**, 21 (44), 17673.

Layered double hydroxides as carriers for quantum dots@silica nanospheres. G. Stoica; I. Castelló Serrano; A. Figuerola; I. Ugarte; R. Pacios; E. Palomares. *Nanoscal*e, **2012**, 4, 5409.

Photoluminescent CdSe@CdS/2D as potential biocompatible materials. I. Castelló Serrano; G. Stoica; A. Figuerola; E. Palomares. *J. Mater. Chem. B*, **2013**, 1, 793.

Two color encoded silica nanospheres as biomarkers for the ratiometric detection of trypsin enzymatic activity: a model for cystic fibrosis detection. I. Castelló Serrano; G. Stoica; E. Palomares. Submitted.

Publications not related to this thesis:

Quantum Dots as a light indicator for emitting diodes and biological coding. I. Ugarte; I. Castelló Serrano; E. Palomares; R. Pacios. *Quantum Dots- A variety of new applications. Chapter 6*. **2012.** Dr. Ameenah Al-Ahmadi (Ed.)

Conferences:

I. Castelló Serrano; Q. Ma; E. Palomares. QDs-"Onion"-Multicode silica nanospheres with remarkable stability.
Poster presentation
Frontiers in organic, dye-sensitised and Hybrid solar cells. VII International Summer School of Krutyn, Poland 2011.

La llum com a font d'energia. Del laboratory al món industrial.

Attendance

Summer School at Universitat Rovira i Virgili, Tarragona, Spain 2011.

I. Castelló Serrano; Q. Ma; G. Stoica; E. Palomares.

Smart QD-"Onion"-Multicode silica nanospheres as ratiometric sensor in the biological range of pH.

Poster presentation

Nanomaterials for biomedical technologies, Frankfurt am Main, Germany 2012.

I. Castelló Serrano.

FRET process between QDs and dye to detect Cystic Fibrosis.

Oral presentation.

ICIQ Young Seminar. 2012 ICIQ seminar programme, Tarragona, Spain 2012.

Magnetic nanocontainers for combined hyperthermia and controlled drug release.

Attendance

Final International Workshop of the European Project MAGNIFYCO, Barcelona, Spain 2013.

Acknowledgements

This project would not have been possible without the inestimable help and support of many people, who I will mention here briefly.

First of all, I would like to thank my supervisor, Dr. Emilio Palomares Gil, not only for his support, encouragement, and sometimes lots of patience during this work, but also for trusting me when I joined his research group. These years have been very stimulating and instructive, with nice discussions and ideas, in and out of the workplace.

I would like to thank Georgiana Stoica for her helpful discussions and advices. She has been invaluable on both in academic and in personal level. I also want to thank Qiang Ma for sharing with me his wisedoom and treaks that do not appear in the papers.

I have to mention specially Josep Albero for his patience the whole time, eventhough during our running sessions and some train trips; Núria for this talks during “coffee” breaks at work and good friendship outdoors; James and John for making me

realize that I have had too much of Irish people for the rest of my life. I cannot forget the other partners in the group, either first generation with Eugenia, Amparo, Anna, Miquel, Eva, Bea, Toni Sanchez, Margherita, …, or the second one with Laia, Lydia, Aurelien, Taye, Toni… or the last one with the people of Malaga, Alba and Beloqui, and the Bollywood King, Vijay, who have given me more than expected in my last year. Some of them have left and others remain in the group, but thank you all for your help and such a fiendly environment in the lab. That was of great fun, loyalty and friendship.

I am also thankful to Dr. Fernando Bozoglian for asking always because it made me realice I was wrong in some aspects, as well as for the photophysycal characterization advices. And the whole group of Servei de microscopia at University Rovira i Virgili, specially Rita Marimon, for all the invested time on my samples and for the good results.

Of course I want to thank my family for all the support and encourgement, specially to my parents for being the only ones that did not ask me everytime “what exactely are you doing?” and tried to understand me

and my job. To my friends, for those parties that relaxed me from time to time.

And the last, but not least, I am extremely grateful to my sister Tamara, thank you for being yourself all the time and for all these laughs that you only could provoke.

About the author

Iván Castelló Serrano was born on the 21st August, 1984 in Valencia, Spain. He finalized high-school in 2002 at the Institute of Secondary School Blasco Ibañez, in Cullera, Spain and followed his studies in Biochemistry and Biology at University of Valencia, Spain, graduating in 2008 and 2009, respectively. During his bachelor studies he did different interships in several research groups: at the Institute Principe Felipe (Valencia, Spain) investigating Multiple Sclerosis and at the Hospital de la Ribera (Alzira, Spain) in the unit of Molecular Diagnostics.

In 2009 he started the Master in Nanoscience and Nanotechnology at University Rovira i Virgili in Tarragona, Spain and, after this, he started his PhD Project at the Institute of Chemical Research of Catalonia (ICIQ) in Tarragona under the supervisión of Prof. Dr. Emilio Palomares Gil. The main focus was the synthesis of luminescent semiconductor nanoparticles and their bioapplications such as labelling agents, sensors or diagnostic tools. The most important results acquired during this research are enclosed in the present thesis. The autor is thankful for financial support of this Project offered by European Research Council Starting Grants

(ERCstg), Ministerio de Ciencia e Innovacion and IKERLAN.

During his PhD period he made a short stay at ZIK HIKE Institute in Greifswald, Germany to study alternative non-toxic materials based on lanthanides or rare-earths for imaging in cell cultures.